UNIVERSITÀ
POLITECNICA
DELLE MARCHE

Scuola di Dottorato di Ricerca in Scienze dell'Ingegneria
Corso di dottorato in ingegneria industriale

Surface Modification of Fabric Reinforcements for FRCM Systems: Effect on the Mechanical Properties and Durability

Candidate:
Francesca Bompadre

Advisor:
Prof. Ing. Valeria Corinaldesi

Coadvisor:
Dot. Ing. Jacopo Donnini

Ph.D. Course coordinator:
Prof. Giovanni Di Nicola

XXXIII edition - 19° new series

UNIVERSITÀ
POLITECNICA
DELLE MARCHE

Scuola di Dottorato di Ricerca in Scienze dell'Ingegneria
Corso di dottorato in ingegneria industriale

Surface Modification of Fabric Reinforcements for FRCM Systems: Effect on the Mechanical Properties and Durability

Candidate:
Francesca Bompadre

Advisor:
Prof. Ing. Valeria Corinaldesi

Coadvisor:
Dot. Ing. Jacopo Donnini

Ph.D. Course coordinator:
Prof. Giovanni Di Nicola

XXXIII edition - 19° new series

Università Politecnica delle Marche
Dipartimento di Scienze dei Materiali dell'Ambiente e dell'Urbanistica
Via Brecce Bianche – 60131 Ancona (AN), Italy

Acknowledgments

Looking back at these years I realized how much this research project has also been a part of my life project, in the good and bad times. There are so many people who have direct or indirect contributed to this work, supporting me in my professional formation as well as in my private life.

I miei ringraziamenti vanno in particolare alla mia coordinatrice prof. Valeria Corinaldesi per aver tirato fuori tutta la grinta e determinazione necessarie a portare a termine questo progetto. Ringrazio Diego Mingarelli, per aver cofinanziato il mio dottorato, ma sopratutto per avermi fatto capire cosa mi aspetto da un lavoro che rispecchi i miei valori e le mie aspettative professionali. Ringrazio Jacopo Donnini a cui devo molto della mia crescita professionale. I miei più sinceri ringraziamenti vanno a tutto il personale tecnico del SIMAU che mi ha aiutata a portare avanti il mio lavoro sperimentale. Ringrazio Adriano di Cristoforo per la costante disponibilità ad analizzare i miei campioni, Carla Conti senza la quale non sarei riuscita a dare un nome ai coating sulle mie fibre. Gianpaolo Giuliani senza il cui aiuto non avrei mai potuto preparare i miei campioni, Mirco Marcellini per le analisi all'IC e i litri d'acqua distillata, Orlando Favoni per la costante assistenza e disponibilità. Il mio lavoro all'università e in azienda non sarebbe stato lo stesso senza i colleghi e le colleghe che ho incontrato in questi anni. Un particolare ringraziamento va a Silvia Palmieri e Chiara Tribuiani per il costante supporto morale e per il proficuo scambio di idee e conoscenze. Un grazie speciale anche a Chiara Giosuè la cui passione lavorativa e spirito di collaborazione mi sono stati di ispirazione nei momenti più bui del mio dottorato.

Ein großer Teil meines Forschungsprojektes ist entstanden während meines Aufenthaltes als Gastwissenschaftlerin am Leibniz-Institut für Polymerforschung. Ich möchte mich ganz herzlich bedanken bei allen Mitarbeiterinnen und Mitarbeitern am IPF. An erster Stelle gilt mein Dank Frau Dr.-Ing. Christina Scheffler für ihre wissenschaftliche Unterstützung. Vieles das ich gelernt habe verdanke ich ihren konstruktiven Korrekturen so wie ihrer inspirierenden Doktorarbeit. Ganz besonders möchte ich Steffi Preßler und Alma Rote danken, ohne deren Unterstützung das Kapitel über die mikromechanischen Tests gar nicht möglich gewesen wäre. Ich danke Janett Hiller und Matthias Krüger, die es noch rechtzeitig vor der Pandemie geschafft haben für mich die Glasfasern zu spinnen und zu beschichten. Ich danke Mikhail Malanin, Regine Boldt und Sabine Krause, die mir geholfen haben meine

Proben zu charakterisieren. Ich danke Andreas Leuteritz und Ivonne Hasselhorst für die Schichtsilikate und dafür, dass ich in ihrem Labor arbeiten dürfte. Ich danke Robert Backes und Enrico Wölfel für die wertvollen Tipps sowie die konstruktive und angenehme Zusammenarbeit.

Ringrazio la mia famiglia per avermi sempre supportato lungo tutto il mio percorso accademico. Mio padre per essermi stato sempre da irraggiungibile modello. Mia mamma la cui grinta mi è sempre stata di inspirazione e dalla quale ho imparato a fare il pane con la farina che ho. Ringrazio Emiliano Poeta senza la cui comprensione e supporto non avrei mai raggiunto tanti importanti traguardi nella mia vita.

Ich danke Paul Krahmer, ohne dessen Unterstützung ich viele große Veränderung im meinem Leben nicht verkraftet hätte. Ich bin froh, dass ich dich habe.

Ancona, Maggio 2021

Francesca Bompadre

Abstract

Over the last decades Fabric Reinforced Cementitious Matrix (FRCM) systems have gained great interest as a promising technique for the reinforcement and rehabilitation of concrete and masonry structures. However, due to the lack of anecdotal information or documented long-term performance, at present relatively few is known about the durability of these materials under different environmental exposure.

Therefore, a comprehensive understating of the different mechanisms responsible for the deterioration of FRCM systems over time is still an issue. This is due to the different kind of environmental stress that the composite may have to withstand during its life, and on the great varieties of materials (cementitious matrices and fabrics) that can be employed. Moreover, when textile are modified with some kind of coatings, as it has been proposed by different studies to improve the mechanical properties of the composite, the overall performance of the composite over time will also be affected by the different kind of coatings possibly applied.

The primary aim of this work is to understand how different techniques, proposed in the literature for the modification of FRCM reinforcements, influence the ability of the composite to withstand environmental exposures. Secondary, different coatings based on a Carboxylated Styrene Butadiene (SB) polymer formulated with increasing percentage of nanoclay were investigated as modification technique to obtain a composite with improved mechanical properties and durability.

Chemically stable carbon fibers as well as AR-glass fibers, which are known to undergo chemical degradation in alkaline environments, have been used. Carbon fibers have been modified with an oxidative solution, a nanosilica coating and an epoxy coating. The experimental nanoclay-SB coatings were applied on AR-glass fibers specifically spun for this project at the Leibniz Institut für Polymerforschung Dresden (IPF), where part of this work has been conducted. Durability test on commercially available reinforcements were also conducted using a Styrene Butadiene preimpregnated AR-glass fabric.

Aging protocols adopted include immersion in saltwater and alkaline solution and freeze–thaw cycles. Tests were performed on both the composite material and its components. Compressive and three point bending test were employed to evaluate the change in the matrix properties after environmental exposure. Ionic chromatography and X-ray diffraction (XRD) were used to investigate possible change in the chemical composition of the matrix. Tensile test on single yarn and pull-out test were respectively employed to evaluate the effect of different coatings on the durability of the reinforcement and the composite. Characterization of the composite

based on the AR-Glass commercial fabric were performed on FRCM coupons. For the IPF fibers single fiber tensile test and quasi-static single fiber pull-out test were also performed. FTIR, TGA, DSC, XRD, SEM-EDX and AFM analysis were employed for the characterization of the coatings as well as the surfaces of the modified fibers.

In general, it could be observed that the chemical stability of the reinforcement plays a minor role on the durability of the composites, and that no conclusion on the ability of the composite to withstand different environmental exposure can be drawn on the base of the components' behavior. Epoxy resin and nanosilica coatings were both found to improve the interaction of the reinforcement with the matrix and simultaneously preserve the mechanical properties of the composite over time. For the nanoclay coatings an increase in the pull-out load was observed for high amount of nanoclay. However, the best results in terms of polymer-matrix interaction and durability were obtained with the addition of 5% of nanoclay in the polymeric coating.

Sommario

L'utilizzo di sistemi FRCM si sta progressivamente affermando in campo ingegneristico come promettente tecnica per il rinforzo e la riabilitazione di strutture in cemento e in muratura. Tuttavia, a causa della mancanza di documentate informazione sulle prestazioni nel tempo di questi materiali compositi, ad oggi poco è noto della loro capacità di resistere all'esposizione a diversi ambienti potenzialmente aggressivi.

La complessità nello studiare i diversi meccanismi responsabili per il deterioramento di questi sistemi nel tempo è data dai diversi tipi di stress ambientale a cui il materiale può essere esposto durante la sua vita di servizio, così come dall'ampia varietà di materiali che possono essere impiegati. Inoltre, per rinforzi modificati con coating organici o inorganici, spesso proposti in letteratura per aumentare le capacità di carico del composito, le performance complessive del sistema saranno influenzate dal tipo di coating applicato.

Lo scopo principale di questo studio è verificare come diverse tecniche, proposte in letteratura per la modifica dei rinforzi in rete, influenzino la capacità degli FRCM di mantenere inalterate le proprie proprietà meccaniche a seguito dell'esposizione a diversi ambienti. Inoltre, al fine di ottimizzare sia le proprietà meccaniche che la durabilità del composito, è stato studiata l'efficacia di coating a base stirene-butadiene contenenti diverse percentuali di nano argille.

I rinforzi in fibra presi in considerazione in questo studio comprendono sia fibre in carbonio che in vetro, le prime note per godere di un ottima stabilità chimica, le seconde soggette a corrosione in ambiente alcalino. Le fibre in carbonio sono state modificate con una soluzione ossidativa, un coating epossidico e un a base di nano silice. L'efficacia dei coating con nano argille è stata studiata su fibre in vetro alcalino resistente appositamente filate per questo progetto al Leibniz Institute für Polymerforschung (IPF) di Dresda, dove è stato condotto parte di questo lavoro. Come caso studio di sistemi commercialmente disponibili si è fatto uso di un rinforzo in fibra di vetro preapprettato con coating stirene-butadiene.

I protocolli d'invecchiamento accelerato adottati comprendo: immersione dei provini in soluzioni alcaline e saline ed esposizione a cicli gelo-disgelo. I test sono stati eseguiti sia sul materiale composito che su i suoi componenti (matrice e rete in fibra). L'effetto dei vari ambienti di esposizione sulla matrice cementizia è stato studiato tramite test a flessione e compressione abbinati a cromatografia ionica e diffrazioni a raggi X. Tensil test e pull-out test sono stati eseguiti su singoli yarn al fine di valutare l'effetto dei caoting sulle proprietà meccaniche e la durabilità del rinforzo e del materiale composito. La caratterizzazione del sistema ottenuto con la

rete preapprettata è stato eseguito tramite tensile test. Per le fibre realizzate all'IPF sono stati effettuati anche test micro meccanici su filamenti singoli. Analisi FTIR, TGA, DSC, XRD, SEM-EDX e AFM sono state effettuate per la caratterizzazione dei coating e della superficie delle fibre.

In generale si è potuto constatare che la stabilità chimica del rinforzo svolge un ruolo secondario nella durabilità del composito, e che sulla base del comportamento delle singole componenti non si possono trarre conclusioni sulla capacità del composito di sottostare l'esposizione a diversi ambienti. Il coating epossidico e quello a base di nano silice sono in grado sia di aumentare l'interazione delle fibre in carbonio con la matrice, che di preservare le proprietà del composito nel tempo. Per i coating contenenti nano argille, un aumento delle capacità di carico è stato osservato nelle prove di pull-out al crescere della percentuale di nano argille. Tuttavia i migliori risultati in termine d'interazione coating-matrice e durabilità del composito si ottengono per un quantitativo di nano argille pari al 5%.

Contents

List of Figures

List of Tables

List of Abbreviations

AMEO	Aminopropyltriethoxysilane
AFM	Atomic Force Microscopy
ARG, AR-glass	Alkali-Resistant Glass
ASR	Alkali Silica Reaction
ASTM	American Society for Testing Materials
C2S	Dicalcium silicate
C3S	Tricalcium silicate
CH	Calcium Hydroxide
COV	Cofficient of Variation
CSH	Calcium Silicate Hydrated
CSLP	Consiglio Superiore dei Lavori Pubblici
DSC	Differential Scanning Calorimetry
FRCM	Fabric Reinforced Cementitious Matrix
FRP	Fiber Reinforced Polymer
FTIR	Furier Transformed Infrared Spectroscopy
GFRC	Glass fibers Reinforced Concrete
IFFS	Interfacial shear strength
ITZ	Interfacial Transition Zone
MMT	Montomorillonite
OPC	Orindary Portland Cement
PAN	Polyacrylonitrile
PBO	Polyparaphenylenebenzobisoxazole
PTIMO	N-Propyltrimethoxysilane
QSFPO	Quasi-static Single Fiber Pull-Out
SB	Styrene-butadiene
SEM	Scanning Elcttron Microscopy
SEM-EDX	Scanning Electron Microscopy coupled with Energy Dispersive X-Ray
TEOS	Tetraethyl orthosilicate
TGA	Thermogravimetric Analysis
TRC	Textile Reinforced Concrete
XRD	X-Ray Diffraction

List of Symbols

A	Cross sectional area
At%	Atomic percentage
E	Elastic modulus
$\mathbf{F}_{max}$	Maximum measured force
m	Weibull modulus
N	Number of samples
$\mathbf{P}_{\sigma}$	Probability of failure
Wt%	Weight percentage
ε_u	Ultimate strain
$\sigma_{0,i}$ i=1,2	Weibull scale parameter for distribution I and II
σ_c	Compressive strength
σ_f	Flexural Strength
σ_{max}	Maximum tensile strength
τ_e	Shear stress

Chapter 1

Introduction and aim of the work

1.1 Introduction

Over the last decades Fabric Reinforced Cementitious Matrix (FRCM) systems have gain great interest as a promising technique for the reinforcement and rehabilitation of concrete and masonry structures. This relatively new class of composite basically consist in a multi-filament reinforcement in form of open meshes applied on concrete or masonry structural members by means of a cementitious matrix. Although a rich literature is available about the mechanical properties of this class of composites and their applicability for the strengthening of existing building elements, at present relatively few is known about the durability of these materials under different environmental exposure. This is mainly due to the lack of anecdotal information or documented long-term performance available for this relatively new class of composites. In order to partially address this issue different aging protocols have been proposed in experimental studies and some guidelines. However, the comparison of results is often difficult due to differences in the materials used, tests performed and conditioning protocols adopted. Moreover, the limit of the available information also concern the kind of fibers employed and the environmental exposure investigated. Indeed, the majority of the durability studies conducted on FRCM systems make use of glass or basalt reinforcements, since those materials are reported to be affected by alkali-attack, but very few works have been conducted on fibers with a high chemical stability, such as carbon fibers. Because investigation on the alkali resistance of glass and basalt fibers dominated the literature concerning the long-term behavior of fiber reinforced composite, the aging protocols adopted mainly consist in immersion of the fibers in alkaline solution, or accelerate aging of the composites in chamber fog. Therefore, very little is known about the effect of other environmental exposure, such freeze-thaw cycles and salt penetration. Beside, the difference in the kind of fibers that can be employed as reinforcement, the durability of the composite can be significantly influenced by the application of some kind of coating on the reinforcement surface, which has been proposed in different studies in order to enhance the mechanical properties of the composites. However, modification of the reinforcement should also be design in order to ensure high performance level of the composite over time.

1.2 Aim of the work

The primary aim of this work is to investigate how the modification of the fiber-matrix interface can influence the durability of FRCM systems exposed to different aggressive environments. In order to elucidate the role of each component as well as that of the fiber-matrix interface on the long term behavior of the composite, durability tests will be conducted on the cementitious matrix, on the fabric (before and after modification) and the composite. Since the present literature mainly focuses on exposure of fibers to alkaline attack, further aging protocols will be taken in consideration.

In the first part of this work aging test will be conducted using a commercial available preimpregnated AR-glass fabric. In this part the study will focus on the effect of different aggressive environments on the mechanical properties of the composites as well as of its components.

In the second part carbon fibers will be modified with different techniques described in the literature. All the systems obtained will than be subjected to the same aging protocols and the results will be compared in order to evaluate how the modification of the fiber matrix-interface influences the durability of the composite.

In the third part of this work Carboxylated Styrene Butadiene (SB) coatings, formulated with increasing percentage of nanoclay, were investigated as modification technique to obtain a composite with improved mechanical properties and durability. In order to investigate the effect of nanoclay on the interaction of the fiber with the cementitious matrix single fiber pull-out test will be performed. Successively, the most promising nanoclay-coating formulation will be employed for the realization of multi-filament rovings. These will than be used to evaluate the effect of the coatings on the composite long-term performance.

Chapter 2

State of the art

2.1 FRCM components

Composite are a bright family of materials, obtained by combining at least two constituent elements, that nowadays find application in different fields ranging from consumer goods and common utensils to high tech materials for aircraft bodies and building construction. Generally the constituents that make up the composite can be distinguished in a dispersed phase called the reinforcement and a continuous phase called the matrix. Composite materials can differ for the materials employed but also for the geometry and arrangement of the reinforcement in the matrix. FRCM are composite materials in which the continuous phase consist in a cementitious matrix and the reinforcement is made up of continuous fibers arranged in two or three dimensions. Composite with similar characteristic can be found in the scientific literature under the name of Textile Reinforced Concrete (TRC). Although they are conceptually equivalent usually TRC are associated to new industrial products, while FRCM have been specifically designed for the repair and rehabilitation of concrete and masonry structures. Usually FRCM are considered an alternative to Fiber Reinforced Polymer (FRP), in which the reinforcement fabric is embedded in a polymeric matrix. Although FRP are a well consolidate technique for the reinforcement and rehabilitation of construction, they present some drawbacks mainly due to the use of a polymeric matrix, which include: limited heat and fire resistance, lack of vapor permeability and impossibility of application on humid surfaces. The substitution of the organic matrix with a cementitious one, overcome those problematic and present further advantages such as: a superior compatibility and adhesion with cementitious and masonry support, easier and less health hazardous application techniques, the possibility to remove the intervention if needed.

2.1.1 Fabrics

Although FRCM are considered a relatively new class of composite, the use of composites consisting of fibers reinforcement and cementitious matrices have been employed in modern times since the introduction of asbestos cement at the beginning of the 20th century. Nowadays, the employment of cementitious matrix mixed with short discrete fibers is a well established practice which find different usage in civil

engineering application. Those composite materials are generally call Fiber Reinforced Concrete (FRC) even if, according to the materials employed and the mechanical properties, other terms can be used. Unlike FRC, TRC and FRCM systems make use of continuous filaments, which can be arranged to obtain reinforcement textile or fabric. The great variety of assembling methods that can be employed for the production of textile provide a wide range of fibrous structures, that range from planar to very complex three-dimensional (3D) mesh [1]. A detailed discussion on the common manufacturing techniques for textile reinforcement structures can be found in reference [2]. For the purpose of this thesis the effect of different textile configuration is of no relevance and the discussion will mainly focus on the materials and treatment used for the assembling of yarns. Yarns are made up of hundreds up to thousands single filaments which can be twisted or group together parallelly. Usually for fabric reinforcement the parallel filament bundles are preferred since they present a smaller structural elongation [3]. According to the numbers of filaments, their average diameter and fibers density, yarns can have different fineness indicated as tex which is defined as gram per 1000 meters. In general fiber employed for textile reinforced concrete should exhibit: high fibers' tenacity, high ultimate breaking elongation, an elasticity modulus much higher than that of the concrete matrix, and a good resistance to alkaline environment [3]. Since the use of fibers to strengthen materials has a centuries-old tradition, nowadays various kinds of natural and mane-made fibers are available on the market for the reinforcement of a number of different materials (Fig. 4.1).

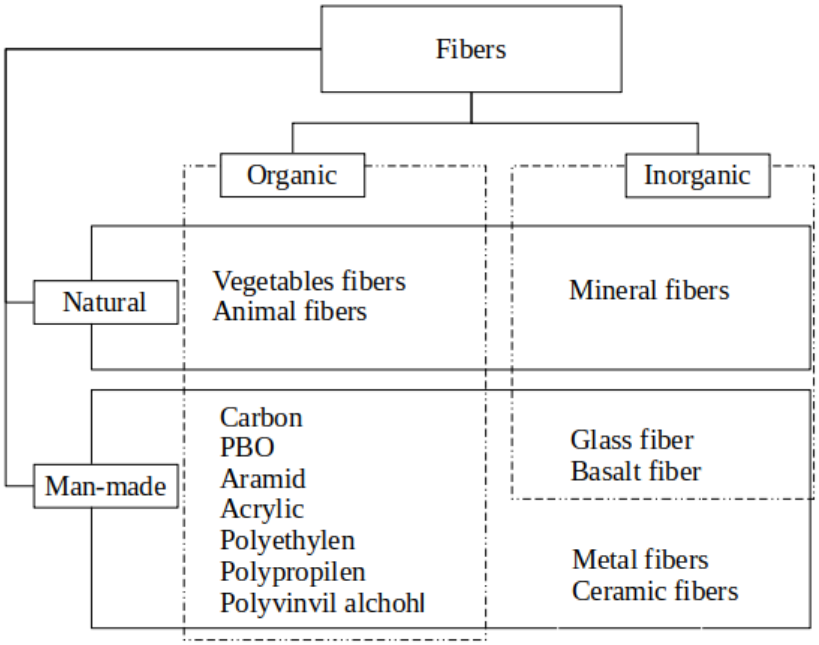

Figure 2.1: Fibers classification.

Regardless of their nature, organic fibers are constituted by macromolecules or polymers with a chain-like structures. Cellulose, hemicellulose, pectin and lignin are the typical example of natural polymers that make up vegetable fibers such jute, sisal and hemp. Although the mechanical properties of some vegetable fibers are much comparable to synthetic fibers, they usually find a minor employment for textile reinforcement application. Indeed, because of the higher mechanical performance and smaller variability of properties, synthetic fibers are usually preferred. Despite the wide choice of synthetic fibers available on the market, mesh employed for FRCM system are mainly made of alkali-resistant glass (AR-glass), basalt, carbon, and polyparaphenylene benzobisoxazole (PBO). Those materials significantly differ in terms of cost, mechanical performance and possible degradation process.

AR-Glass

Thanks to their very good quality to price ratio, glass fibers are among the most widely used fibers for composite materials. Although they can present some difference in the chemical composition according to their application field, they are all mainly composed of amorphous silica, and they are obtained by spinning of molten glass at temperature up to 1350 °C. In its polymeric form SiO_2 present a tetrahedral structure whose spacial repetition constitute the backbone of glass fibers [4] Since glass is an amorphous material the silicon atoms that compose it are organized in an irregular network as represented in Figure 4.2.

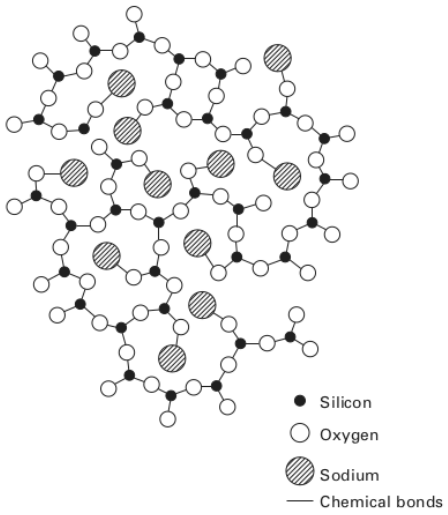

Figure 2.2: Schematic diagram of glass networks (reproduced from Ref.[4])

The non-crystalline arrangement of SiO_2 molecule confers the material a certain ductility. Among with SiO_2, fibers employed for concrete reinforcement required the addition of zirconium oxide and are based on the ZrO_2 -SiO_2 -Na_2O system. Those fibers are called Alkali- resistant glass fibers and they mainly deffer from other glass fibers for the addition of zirconium oxide (ZrO_2) which increase their stability in

alkaline environment [5]. Table 4.1 reports the chemical composition of AR-glass fibers compared with most common E-glass (low electrical conductivity) and high strength S-glass.

Table 2.1: Chemical composition range of commercial glass fibers [5].

Glass	Glass composition [wt%]										
type	SiO_2	B_2O_2	Al_2O_2	CaO	MgO	TiO_2	ZrO_2	Na_2O	K_2O	Fe_2O_2	F
E	52-60	0-6	12-15	21-23	0.4-4	-	0.2-0.5	0-1	0-0.2	0.2-0.5	0.2-0.7
S	60-65.5	-	23-35.5	0-9	6-11	-	0-1	0-0.1	-	0-0.1	-
AR	58.3-60.6	-	0.2	-	-	0-2.8	18.1-21.2	13.0-14.1	0-2.8	-	-

The chemical composition of glass, is responsible, among with the production method, for the final mechanical properties of fibers. Glass fibers from aluminum silicate exhibit the greatest strength, while increase alkali content lead to a reduction of the same. This phenom can be clearly observed comparing the mechanical properties of E-glass AR-glass and S-glass fibers reported in Table 4.3.

Table 2.2: Physical and mechanical properties of E, S and AR-glass fibers [4].

Properties	Types of Fibers		
	E	S	AR
Molding temperature, [°C]	1160-1196	1565	1260-1300
Softening point, [°C]	830-916	1056	770
Density, [g/cm^3]	2.54-2.62	2.48-2.49	2.6-2.7
Strength, [MPa]	3100-3500	4380-4800	3100-3500
Elastic modulus, [GPa]	76-81	88-91	72-74
Elongation to rupture, [%]	4.5-4.9	4.5-4.9	2-2.24

Typical tensile strength of AR-glass fibers usually range from 3100-3500 MPa. The modulus of elasticity of glass fibers range between 72–74 GPa and their density is about 2.7 g/cm^3. They have a good thermal stability, with a softening temperature of about 770 °C. Although S-glass have better mechanical properties than AR-glass, their chemical composition is not adequate for strengthening of concrete, because of the high pH value of this matrix. The low stability of glass fibers in alkali environment is due to the reaction that occurs at the fibers interface between hydroxide ions (OH-) and the SiO_2 according to the following equations:

$$-Si - O - Si - + OH^- \rightarrow -Si - OH + -Si - O^- \tag{2.1}$$

$$-Si - O^- + H2O \rightarrow -Si - OH + OH^- \tag{2.2}$$

Unfortunately the end products of the second reaction gives back the hydroxide ion responsible for the dissolution of the Si – O bond that constitute the glass networks, so that the corrosion process can potentially proceed till the complete destruction of the glass structure. Addition of zirconium oxide is reported to significantly increase

the chemical durability of silicate glasses. The higher stability of glass at high pH value is attribute to very stable hydrated ZrO2 that forms on the glass surface offering a barrier for the diffusion of OH^- ions [6]. As it can be seen from Figure 4.2 the activity of ZrO^{2+}, Zr^{4+} and $HZrO^{5-}$ is very low at pH between 0 and 14, so that addition of zirconium oxide increase the durability of glass in all the pH spectra of aqueous solutions. However, it should be note, that this mechanism do not completely prevent the SiO_2 to react with OH^-, and that reactions 3.4 and 3.5 are only limited by the diffusion of the hydroxide ions, so that in their real work life AR-glass fibers do not present a complete resistance to alkali attack. Other factor that contribute to increase the durability of glass fibers are the application of sizing and coatings, which will be discussed in the following sections.

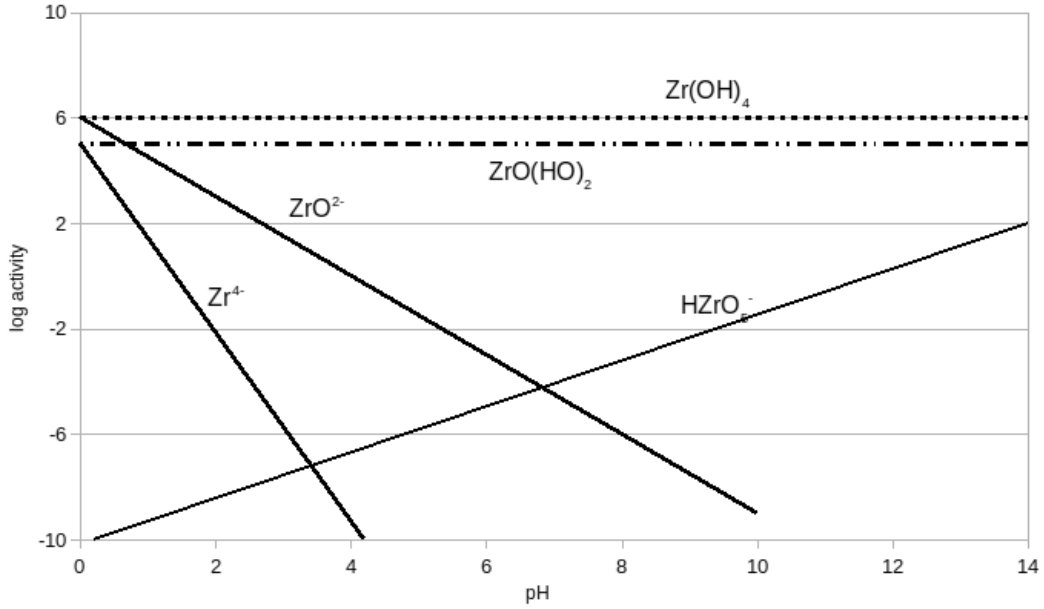

Figure 2.3: Stability of ZrO_2 in aqueous solution at 25°C at different pH values, reproduced from reference [6].

Basalt

Basalt fibers are inorganic synthetic fibers obtained by malting "basalt" rocks, which is a term that indicate a variety of volcanic stones and minerals formed from molten lava after solidification. The chemical composition of basalt fibers is very similar to that of glass fibers with the main component consisting of SiO_2, Al_2O_3, CaO and MgO, even if basalt fiber present a higher content of Fe_2O_3 and FeO which are responsible for their characteristic dark coloration [7]. As natural materials basalt stones are found with a broad range of metal oxide, but only basalt rocks with a minimum SiO_2 content of 46 % can be used for the production of continuous filaments [8]. Indeed, as for glass fibers, the backbone of the fiber consists of amorphous silica organized in an irregular network as depicted in Figure 4.4. Like glass fibers, filament

are obtained in a continuous process in which basalt rocks are crushed, washed and successively melted in a gas-heated furnaces at 1500 °C. The mechanical properties of basalt fibers are usually superior to glass fibers, with a tensile strength ranging between 3000-4840 MPa and a elastic modulus between 93 and 110 GPa [9]. Basalt fibers are reported to have a good thermal/heat resistance with softening temperature of 960 °C, and low humidity absorption. Although as glass fibers they are subjected to corrosion in alkaline environment, they are usually considered more stable in strong alkalies than glass [9].

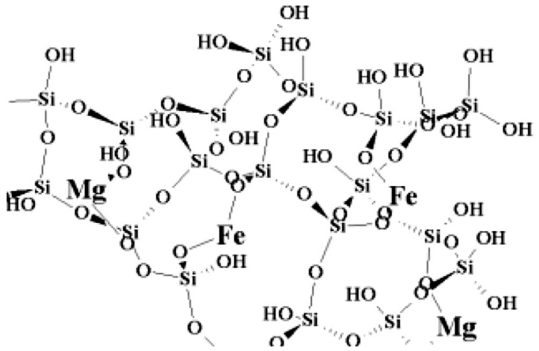

Figure 2.4: Schematic diagram of basalt networks (reproduced from Ref. [9])

Carbon

Carbon fibers refer to organic fibers which have a content of carbon above the 90 %. They are obtained by thermal conversion of carbon fibers spun with an organic precursor like polyacrylonitrile (PAN), pitch, or petroleum. Among them, PAN result to be the most indicated for the production of high strength fibers, so that nowadays PAN process represent the great majority of commercial method used for carbon fibers manufacturing. During this process the linear polymeric chain, that constitute the PAN precursor fibers and contain about the 68 % of carbon, undergoes chemical and structural change converting to a graphite like network. As depicted in Figure4.5 the process basically consists of a preoxidation or stabilization steps (heating in air at temperatures between 200 °C and 230 °C) followed by a carbonization steps (heating in inert atmosphere at temperature between 1000 to 1500 °C) and finally a high temperature thermal treatment, called graphization (at approximately 2000 °C-3000 °C in an inert atmosphere). Those process induce cyclization and armoatization reactions in the polymer chain, associate with release of NH3 and HCN as products of dehydration and denitrogenation.

Carbon fibers present an atomic structure similar to that of graphite since they are also organized in carbon sheets with sp2-hybridization. However, in carbon fibers, the hexagonal layers are rolled, folded and crumpled with each other rather than homogeneously parallel stacked like in graphite, resulting in a non-crystalline structure. This amorphous arrangements prevent the hexagonal sheets to be torn

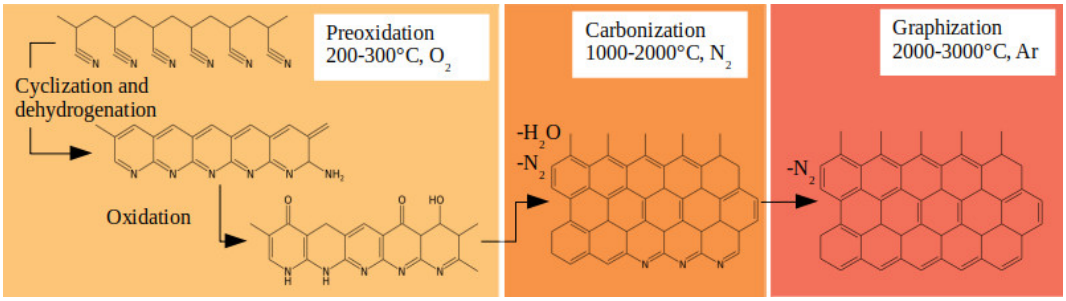

Figure 2.5: Conversion process of PAN fiber to carbon fiber

apart as it appends in graphite, conferring the carbon fibers high tensile strength and stiffness. Figure 4.6 reports the typical turbostratic arrangement of PAN based carbon fibers. Since the carbon layers are preferentially oriented along the fibers' axis, the mechanical, thermal and electrical properties have higher values in this direction rather than the transverse one. Carbon fibers are particularly suitable for the realization of strong lightweight composite, since they present both high tensile strength and modulus and low density. Tensile strength and elastic modulus can significant vary according to the thermal process employed for the fibers' production, and in general high performance grade carbon fibers are classified in high strength type and high modulus type. Typically, carbon fiber employed for FRCM reinforcement have a tensile strength between 3790-4900 MPa and an elastic modulus of 230-255 GPa [10]. Due to the low reactivity of the aliphatic structure, carbon fibers have a very good chemical durability, which make them particularly suitable for the realization of long live materials [11]. However, this chemical stability and in particular the absence of hydrophilic group on the carbon chain, results also in a relatively poor ability of the fibers to build a good interaction with inorganic matrix [11].

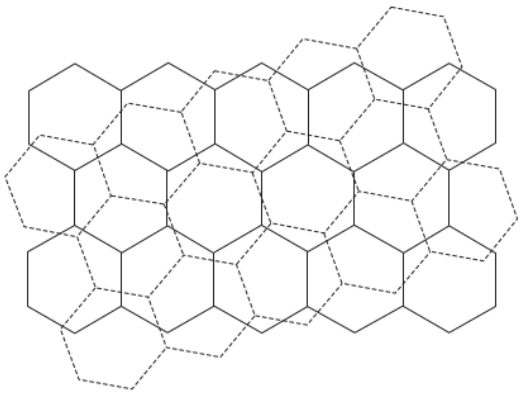

Figure 2.6: Turbostratic arrangement of carbon sheets

PBO

PBO are heterocyclic aromatic polyamide that can be use for the production of fibers with high tensile modulus and tensile strength. Unlike basalt and glass fibers, aromatic polayamide can not be obtained from melt-process since the melting point of the polymer is higher than its decomposition temperature. Those fibers are generally spun from polymer solution thanks to their lyotropic behavior. Lyotropic liquid crystals are polymers which, up to a critical concentration, form an isotropic mesophase, with polymeric chain exhibiting a long-range order in on or two dimension [12]. Molecules that can present this particular chemical structure are characterized by molecular asymmetry and an high chain stiffness. In PBO polymers those properties are provided by the bensobisoxazole aromatic ring and the phenyl group that make up the polymer backbone (Fig. 4.7). The polymer solutions are produced by dissolving the polymer in strong protic acid such as polyphosporich acid, methansulphonic acid, chlorosulphonic acid, 100 % sulforic acid, trifluoroacetic aicd.

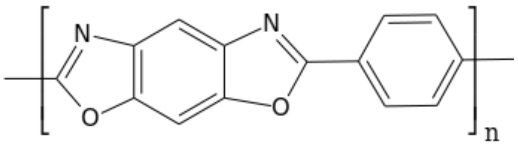

Figure 2.7: Poly (p-phenil-1,4 benzobisaxole)

PBO fiber are obtained from those solutions in a dry jet-wet spinning process. In a typical process, the polymer dissolved in the concentrated acid is extruded by a spinneret through an air gap into a coagulation bath consisting of water and a base to neutralize and wash the fibers from retained acid. Fibers obtained with this process present a high orientated structure which is induced from the shear flow in the capillary hole and the spinning tension in the air gap. The obtained fibers present a characteristics structure in which fibrils consisting of PBO molecules whit high crystallinity content run parallel to the fiber axis. The as-spun fibers are dried and subsequently undergo a heat treatment in which fibers are drawn under tension for a few seconds at temperatures of 500-700 °C in nitrogen atmosphere. This treatment induces an increase and improvement of the polymer crystallization and consequently enhances the mechanical properties of the fibers. Thermal treated and untreated PBO fibers are commercially available under the trade name of Zylon HM and Zylon AS. Zylon AS and Zylon HM present both a tensile strength of 5.8 GPa, similar density (respectively 1.54 gis i/cm^3 and 1.56g/cm^3) and elongation at brake (3.5 % for Zylon AS and 2.5 % for Zylon HM), but significant different tensile modulus equal to 180 GPa for as-spun fiber and to 270 GPa for post-treated fiber.

2.1.2 Cementitious Matrix

According to the guidelines ACI 549.4R-13 [1] he matrix used for FRCM systems is *"a grout system based on Portland cement and a low dosage of dry polymers at less than 5 percent by weight of cement. The organic polymer compounds are sometimes used to ensure proper workability, setting time, and mechanical properties. Nonhydraulic mortars, such as lime-based mortars, may be used for masonry strengthening, particularly in the case of historical structures."* The design of the matrix is a complex task that have to take in consideration different aspects such as the durability of the systems, the chemical compatibility with the textile and the kind of support to be reinforced. For this reason the matrix composition can be quite different according to the specific application. However, there are some general aspects that are typical of FRCM matrix. Those consist mainly in the small grain dimension and the high content of binders. n order to ensure a good penetration of the matrix between the single filaments that made up the reinforcement, FRCM matrix usually have a maximum grain size smaller than 2mm, (while normal concrete have typically a grain size of 32 mm), and are therefore called fine concrete [13]. Pozzolanic additives and plasticizers are also often use in order to improve the flowability of the matrix. Pozzolanic additives usually include flay ash, silica fume and metakoline. Flay ash usually made up the major part of the pozzolanic additive added, while a content higher than 10 % by mass of total binder is not recommended, since the addition of silica fume also influence the consistency of the matrix. The partial substitution of ordinary Portlanc Cement (OPC) with pozzolanic additive its particularly suitable when glass and basalt fibers are employed since the amorphous SiO_2 can react with the $Ca(OH)_2$ present in the pore solution reducing the alkalinity of the matrix. However, concerning the durability of the matrix, it should be considered that matrix contenting amorphous silica can be subjected to alkali reactions. An alternative binder for alkali sensitive reinforcement are phosphate cements, which are acid when fresh and maintain a neutral pH after hardening. However, those matrices find a minor employment, mainly due to their inherent fast setting properties. Polymer modifier are also commonly employed for the formulation of FRCM matrix. Polymer can be added in the form of a dry powder or an aqueous dispersion of particles. The addition of a minor amount of polymer to a cement mix are reported to enhance some properties of the cement mix such as workability, flexural strength, toughness, the bond strength with the reinforcement and durability [14, 15]. Moreover, because of the small dimension of the polymeric particles (about 100 to 200 nm), also the ability of the matrix to penetrate into the spacing between the filaments is improved. Although employment of matrix with high polymeric content (20 % by mass of binder) has been reported for TRC [13], the ACI 549.4R-13 [1] and Italian guideline issued by "Consiglio Superiore dei Lavori Pubblici" [16] ndicate a maximal polymers' dosage of respectively 5 % and 10 % by wight of the inorganic binder, for FRCM systems. Since FRCM systems have been specifically developed for the rehabilitation

of existing structures, in some case, particularly for the rehabilitation of masonry and historical structures, the hydraulic binder can be substituted with nonhydraulic matrix such as lime-based mortars [17, 18, 19, 20].

2.2 Mechanical properties and test methods

In the last decades the mechanical properties of FRCM systems have been widely investigated, resulting in the production of a great variety of analytical and experimental works on both material and structural level [18, 19, 21, 22, 23, 24, 25, 26, 27]. Fabric reinforcement typically present very high tensile strength and stiffness along the fiber direction, whereas inorganic metrics generally exhibit a poor tensile behavior characterized by severe cracking and low tensile strength. When a tensile load is applied on an FRCM system, the tensile stress is mainly absorbed by the fabric, whereas the matrix has the role of protecting the reinforcement and distributing the stress.

2.2.1 Tensile test

The constitutive behavior of the FRCM subjected to tensile loads can be typically derived from uniaxial tensile tests on prismatic specimens. Those test are usually conducted recording the load applied by a tensile testing machine under displacement control on prismatic specimens obtained by applying one or more layers of fabric embedded in the mortar matrix. The stress-strain curved obtained for FRCM under unaxial load are similar to that obtained for TRC and is characterized by three branches that can be distinguished from the stress strain diagram (Fig. 4.8) [28]:

- State I correspond to the uncracked specimens where the composite displays a linear behavior and the overall stiffness is dominated by the matrix properties;

- State II is characterized by the formation and propagation of multiple cracks. The first crack formation, indicates the transition point between Stage I and Stage II. After the formation of the first macro crack the load is transferred through the fabric reinforcement and successively cracking occurs when the stress transferred reached the tensile strength of the matrix. The crack pattern, may widely change depending on the tensile strength of the matrix and its bond between the sleeve filaments. The transfer length at which cracks formed can vary with the fabric geometry and the type of fabric. Generally the response curve in this stage is uneven due to load drop caused by formation of multiple cracks.

- State III is the final phase where no new crack is formed and the composite tensile behavior manly depend on the fabric elastic modulus and tensile strength. The increase of the global displacement produces the widening of existing cracks, and the stress strain curve proceeds parallel to the stress strain curve of the textile used in the composite. State III ends with the final failure of the composite which is caused either by rupture of the fabric which reached its

maximal tensile strength, or by slippage of the reinforcement into the matrix, or a combination of both.

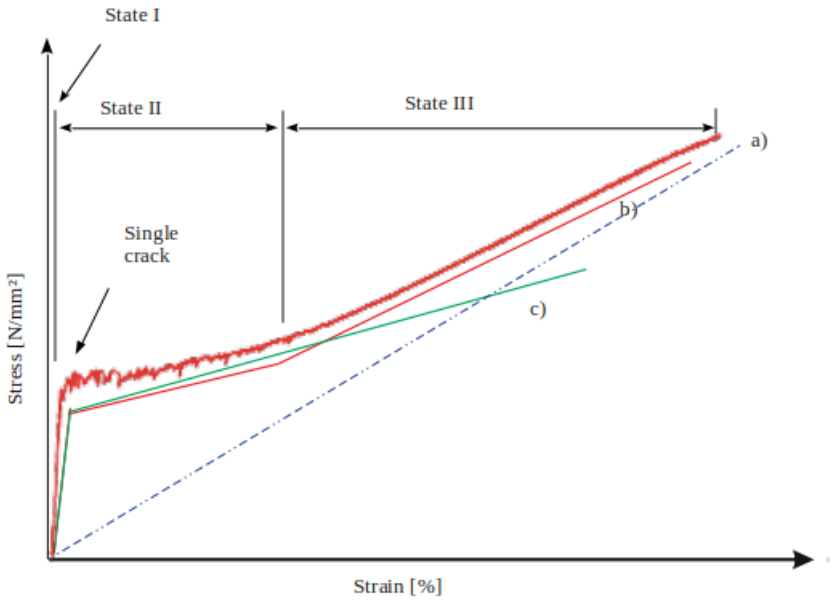

Figure 2.8: Stress-strain curved of textile-reinforced concrete under uniaxial loading. The idealized curves represent the tensile behavior of: (a) the fabric; the composite with (b) clamping grip system; (c) clevis grip system.

Tensile tests performed on FRCM coupons do not always present a three-linear stress-strain curve. The stress strain responses obtained, and the failure mode observed are strongly influenced by the test set-up adopted. The clamping grip system and the clevis-type grip system are technique recommended respectively by the RILEM Technical Committee 232-TDT [29] and the AC434.13 [30]. In the first case a compressive force normal to the plane of the specimen is applied at the sample extremities, while in the second case metal plates are glued on the specimen ends and the load transfer is obtained only by shear stresses (Fig.4.9).

Because of the high compressive stress applied on the specimen ends, the clamping system prevent the slippage of the textile into the matrix so that usually a trilinear stress-strain curved is obtained and the textile reached is maximal stress [26]. On the contrary, for clevis-type gripped specimens usually failure is obtained by slippage of the mesh before the maximal tensile strength of the fabric is reached. Moreover, usually bilinear stress-strain (Fig. 4.8c)curve are obtained, where the second and third phase are indistinguishable one form the other, and the elastic modulus obtained is the contribution of the textile stiffness and pull-out. According to Arboleda et al. the clamping grips are more appropriate when a trilinear stress-strain curves is needed for a complete evaluation of the FRCM mechanical properties [31]. On the contrary, for the investigation of the maximum load-bearing capacity of the system

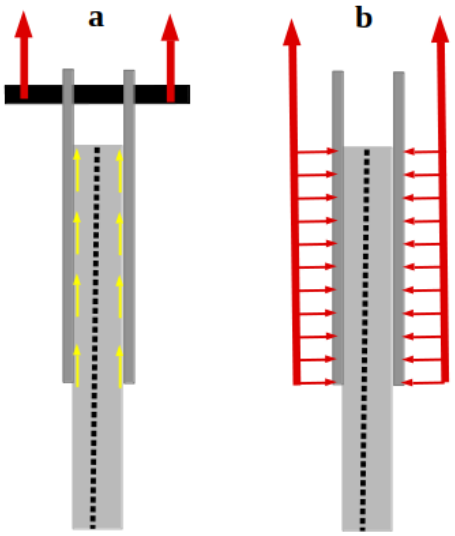

Figure 2.9: Stress applied on the specimens with clevis-type grip (a) and clamping grip (b).

for reinforcing application, the clevis-type grips should be preferred.

2.2.2 Bond with the substrate and inter-laminar shear strength

The unaxial tensile test is a suitable and validate method for the investigation of the load-beargin capacity of the systems, which can also furnished important information on the bond quality at the matrix-fabric interface. However, an accurate qualification of the FRCM systems must also investigate the bond strength of the composite with the substrate and the inter-laminar shear strength between the fiber mesh and the cementitious matrix. The two main tests to determine the bonding properties of FRCM composite on concrete or masonry substrate are the double (or single) push-pull shear test and the pull-off test.

In shear bond tests the FRCM systems is subjected to a shear load at the reinforcement-to-substrate interfaces [26]. The test can be performed either with a single-lap or a double-lap set-up. In a single-lap shear test a reinforcement strip (matrix plus fabric) is applied to a substrate (brick, stone unit, concrete block, etc.) and the test is performed by pulling a portion of the textile left unbonded while the substrate is kept fixed (Fig. 4.10a). In the double-lap scheme the reinforcement textile is bonded to the two sides of the substrate so that the free length of the mesh build a U-shaped strip which is pulled with a saddler or a cylinder (Fig. 4.10b). The test provide the stress-slip response of the composite bonded to the substrate. Depending on the mechanical properties of the substrate, the mortar matrix and the textile, and on the bond developed at the components interface, following failure mode can be observed:

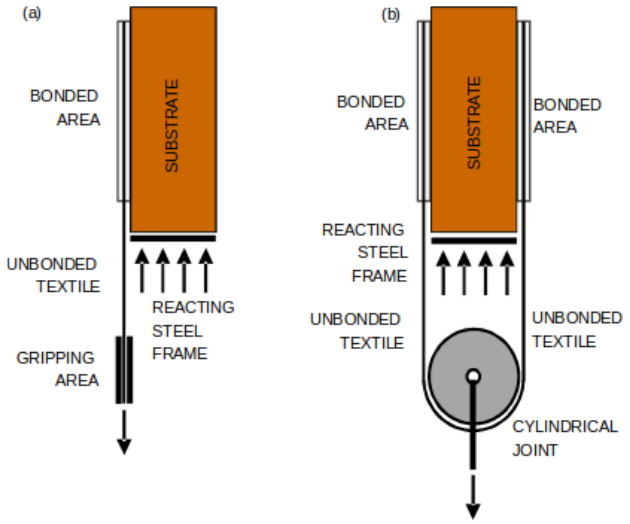

Figure 2.10: Schematic representation of the single-lap (a) and double-lap (b) shear test. From reference [26].

- Debonding with cohesive failure in the substrate (Figure 4.11 A);
- Debonding at the matrix to substrate interface (Figure 4.11 B);
- Debonding at the fabric to matrix interface (Figure 4.11 C);
- Slippage of the fabric within the matrix (Figure 4.11 D);
- Tensile rupture of the fabric out of the bonded area (Figure 4.11 E1);
- Tensile rupture of the fabric within the bonded area (Figure 4.11 E2).

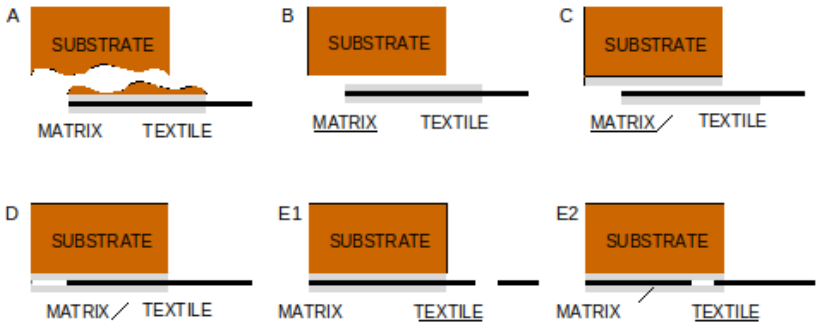

Figure 2.11: Schematic representation of possible failure modes shear bond tests on externally bonded FRCM strengthening systems from ref [26] .

Although FRCM systems are usually reported to have a good compatibility with the support both substrate-matrix and matrix-fabric delamination has been reported. Slippage of the fabric as long as textile failure can also be expected, while cohesive bonding of the substrate are not normally observed. Investigation at the interface

between the different components can be performed also with pull-off test. Differently from shear bond tests in pull-off test the FRCM systems is subjected to a normal load at the reinforcement-to-substrate interfaces. Usually test are performed with simple mechanical hand-operated loading equipment, and the test results are expressed in terms of ultimate load and type of failure. Four possible failure mode can occur:

- Debonding with cohesive failure in the substrate (Figure 3.12 A);
- Debonding at the matrix to substrate interface (Figure 3.12 B);
- Debonding at the fabric to matrix interface (Figure 3.12 C);
- Debonding at the interface between mortar and steel disk (Figure 3.12 D).

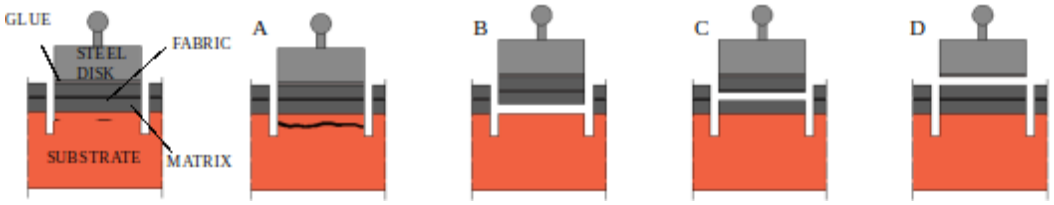

Figure 2.12: Possible failure modes for pull-off test,according to reference [26].

The properties of the composite layers are also responsible for the formation of inter-laminar shear stress and failure. The inter-laminar shear stress can be defined as the out-of-plane stress σ_z τ_{xz} τ_{yz} at the interface between layers in a laminated composite material. This stress tend to shear apart the interface in the corresponding directions and are responsible for delamination failure, which are often observed in laminate composite materials. For the evaluation of the inter-laminar strength the ACI 549.4R-13 refers to the ASTM Standard D2344 "Standard Test Method for Short-Beam Strength of Polymer Matrix Composite Materials and Their Laminates". The test consist in a three-point bending utilized to induce transverse shear in specimens with low support span to specimen thickness (s/h) ratios.

2.2.3 Pull out test

Although they are usually not reported as test method for the qualification of FRCM systems, different studies purpose the employment of pull-out test, in order to evaluate the bond quality between multifilament yarns and inorganic matrix [20, 32, 33, 34, 35, 36]. Basically the test consists in recording the displacement of the fibers in to the matrix and the relative force necessary for the pull-out. Although pull out test has been widely employed as experimental procedure for the evaluation of the fiber-matrix bond quality, the lack of regulations lead to a great variety of test procedure and set-up. Dalalbashi et al. roughly divided the most common test methods used in pull-push and pull-pull tests [20]. n the first case the test is

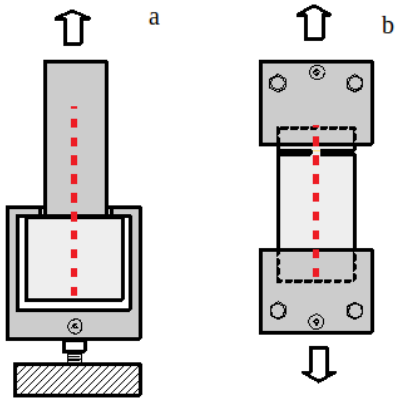

Figure 2.13: Schematic representation of pull out wit a) push-pull and b) pull-pull setup.

performed by pulling the yarn from the top surface of the mortar that is fixed at the same side where the yarn is pulled out (Fig. 4.13a).

Some works report pull-push pull out test in which the yarn has a certain free length, and it is directly gripped to the machine [32, 33], others protect the free length of the yarn with epoxy resin [34] or metal plates [20]. In the pull-pull test set up the yarn is embedded on both sides in the mortar with two different embedded length, and the test is performed by pulling apart the two mortar segments. It follows that the yarn is pulled out from the smaller mortar block. The authors report that the results obtained for the pull-pull methods seems to give a better representation of mechanical behavior of the sample, but pull-push test set up have a smaller data variation and are easier to perform. In the same work the authors also investigate the effect of the embedded length and the fabric configuration. Pull-out test performed on impregnated AR-glass fibers with 50 mm, 75 mm and 100 mm embedded length show that specimens with shorter embedded length fail do to slippage of the yarn, while increasing the embedded length the failure mechanism move to a roving rupture (100 mm) passing through a mixed slippage and rupture failure at 75 mm. In order to investigate the effect of sample configuration the authors performed pull-out tests on a group of roving, and single yarns with and without traversal elements. They found out that were the traversal elements were maintained a light higher maximal load was reached, but the main difference were observed in the post debondded region of the curve. Analytical models developed to describe the pull-out behavior of multifilament roving from cementitious matrix distinguish three stages in the pull-out force-slip curves [37, 38]:

- Stage I is the linear elastic stage, where the fabric is completely bonded with the matrix and the load-slip curve increase linearly till a certain point where the applied force exceeds the adhesion bond strength and debonding starts.
- Stage II is the debondig stage, in which the debonding propagates along the

embedded length. In this stage the stiffness of the load-slip curve decreases, while the applied force increase until it reaches the maximum load. In the post peak region the debondig continues to propagate until the entire embedded length is debonded.

- Stage III is the debonded zone, in which the debonded yarn is pulled out from the matrix and the force measured is mainly due to the friction developed at the yarn-matrix interface.

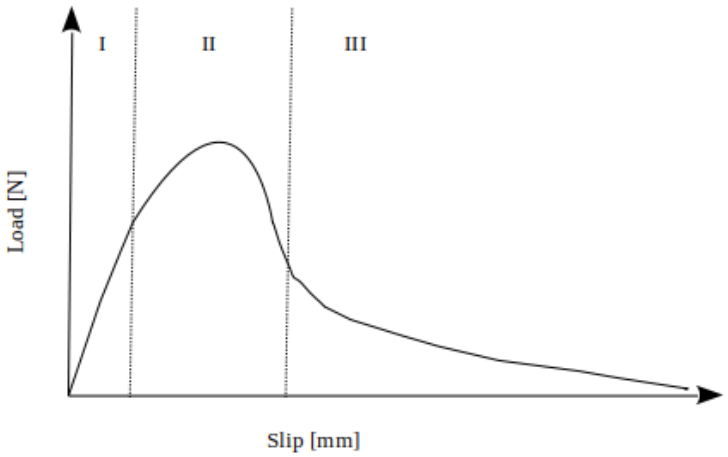

Figure 2.14: Typical pull-out slip-load curve.

The slip-load curve obtained from pull-out test can be used to calculate some parameters such as the adhesional bond strength and the frictional bond strength which characterized the bond at the yarn-matrix interface and can be employed to calibrate the bond-slip law of the system [32, 34, 37]. However, the calculation of those parameters usually necessitate a detailed analysis of the slip-load curve as long with the determination of additional parameters such as the elastic modulus of yarn and matrix, therefore different studies usually do not calculate the shear stress at yarn matrix interface. Since the load versus displacement relation is characteristic for the tested geometric arrangement, those studies do not provide information about a general material property of the tested composite, so that results obtained from different studies can not be directly compare. Nevertheless, comparing sample with the same geometric arrangement, pull-out curve and the maximum load reached, have been used by different studies to evaluate the effect of yarn treatments on the bond quality with the matrix [33, 39, 40, 41].

2.2.4 Single fiber pull-out

In order to determine the shear bonding characteristic at the fiber-matrix interface as long as to develop analytical model capable of simulating the pull-out response

of textile-reinforced composite some studies propose the investigation of their micromechanical and microstructural properties by means of single fiber pull-out test [34, 42, 43, 44]. Single fiber pull out test have been extensively used to determinate the bond strength between fiber and matrices for different kind of fiber reinforced composites, particularly FRP. In a typical experimental procedure a fiber is embedded in a matrix droplet fixed on a substrate, and after curing and consolidation of the matrix, the fiber is pulled out of the matrix and the slip-load curve is obtained by recording the applied force as a function of the fiber displacement. The force displacement curved obtained is usually characterized by fore points [45] as depicted in Figure 4.15:

- A is the debonding point. It is characterized by an abrupt slope-change of the curve which manifest as a "kink" when the applied force reach the critical value Fd (debond force) and the interfacial crack;
- B is the peak point where the applied force reached its maximal value. The Fmax measured at this point results from the contribution of the interfacial adhesion of the intact fiber length, and friction adhesion in the debonding region;
- C correspond with the ful interface debonding. From this moment until complete pull-out the force measured is the result of only frictional interaction between the fiber and the matrix;
- D is the point at which the pull-out is complete, the measured force is zero, and the fiber displacement is equal to the embedded length l_e.

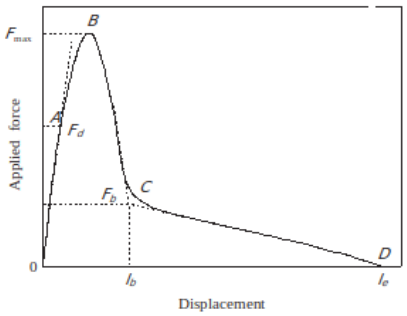

Figure 2.15: Schematic representation of force-displacement curved for pull-out test. Ref.

The interfacial failure for many fiber/matrix systems can be satisfactory described using two main approaches: the fracture mechanical model which is a energy-based approach that consider the critical energy release rate Gic as main interfacial parameter, and the stress based approach (perfect interface model), in which the interfacial debonding is governed by the local shear strength (IFSS) [34, 46, 47].

2.3 Fiber-matrix interface

As for every composite material the final mechanical behavior of FRCM depend, among with the mechanical properties of the constituent materials, also on the bond behavior at the interface between the components that made up the systems. Cement composites are characterized by an interfacial transition zone (ITZ) in the vicinity of the reinforcement, where the micro-structure of the paste matrix considerably differs form that of the bulk matrix, away from the interface [10, 48]. This layer of cement paste, which is in direct contact with the fibers and can extend to several tens of micrometers into the surrounding matrix, present a chemical composition, pore structure and morphological development as curing progresses, that are distinct from the features of the bulk cement matrix. Particularly, it has been observed, that fibers in the mature composite are in intimate contact with a dens layer consisting largely of hexagonal lammelar crystals of calcium hydroxide ($Ca(OH)_2$, CH, potlandite), backed up by a porous layer consisting of hydrated calcium silicate (CSH) and some ettringite. The porous interfacial zone rich in brittle $Ca(OH)_2$ crystals is significantly weaker than the bulk matrix. The development of this ITZ is mainly attributed to formation of water-filled spaces around the fibers in the fresh paste, due to bleeding and entrapment of water and an inefficient packaging of the cement grains around the fibers surface. As a consequence the dense microstructure typical of the bulk matrix does not develop in this zone, and $Ca(OH)_2$ crystals gradually precipitate in the large cavities formed around the fibers. The formation of a $Ca(OH)_2$ rich layer around the fiber surface has been first observed in steel fibre-reinforced concrete and glass fiber reinforced cement where fibers are usually well dispersed into the individual filaments during the production of the composite. A similar process also occurred at the interface with multifilament yarn, with the difference that due to the small size of the spaces between the filaments (≈ 3 μm) compared with the cement grains ($\approx$10 μm), the matrix is not able to penetrate into the yarn. As a consequence, only the outer filaments are direct anchored in the concrete, and they can reach their ultimate stress, while the rest can easily slip within the roving (Fig. 4.16), because only the friction between the filaments can generate a certain bond resistance [49, 34]. This behavior is commonly called telescopic behavior, and it is responsible for a certain pseudo-ductility of the composite. Since only a limited number of filaments are directly involved in the stress distribution, this failure prevent the full exploitation of the fabric tensile strength [34].

Therefore, the fabric-matrix bond strength in dry systems strictly depend on the ability of the matrix to penetrate within the yarns and on the capacity of the matrix itself to wet the single filaments. As already mentioned in the previous chapter superplasticizer and pozzolanic additives are often addtioned to normal Portland cement in the cementitious matrix employed for FRCM and TRC composites. Those additives can on one hand modify the flowability of the matrix improving its penetration between the filaments, and on the other hand they can also change

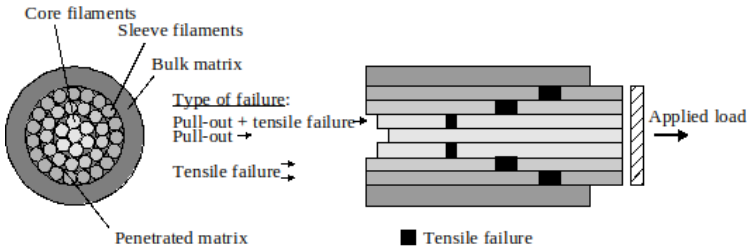

Figure 2.16: Schematic representation of a multifilament yarn embedded in a cement based matrix under a pull-out load according to Björn Banholzer [34]

the microstructure of the ITZ [46, 49, 50, 51]. It is generally expected that the densification of the ITZ may serve to strength the transition zone and enhance the fiber/cement intrefacial bond strength. Pozolanic additives can react with the portlandit deposited in the interface cavities forming a denser and compact CSH layer. Also, the addition of superplasticizer can induce a densification of the ITZ since addition of organic polymer usually consent a reduction of the w/c ratio which determine the initial distribution of cement particles in the layer of water adjacent to the reinforcement. The modification of the ITZ by changing the matrix composition is only on of the different strategies that has been studied to improve the bond in fiber reinforced cement-based composites. Other engineering tools include: fiber deformation and fiber surface modification. Techniques for fiber deformation will not be further discuss in this work, but a brief review can be found in [46]. A popular strategy to modify the characteristic of fibers surface is that of apply an organic coating on the fibers. Impregnation of the reinforcement with an organic coating has been reported by many studies as a promising technique for the improvement of the mechanical performance of FRCM systems [52, 53, 54, 55, 56, 57, 58, 59, 60, 61], and preimpregneted fabrics are also commercially available. The main consequence of coating the filament with an organic coating is that the matrix is prevented to penetrate into the yarns and the bond with the matrix is no longer dependent on the ability of the mortar to wet the single filaments but rather from the interaction between the coating and the matrix. Moreover, when the single filaments are embedded in an organic coating they have a really strong interaction with-another, and the inner bond of preimpregneted yarn becomes larger than the outer bond. Since a higher number of filaments is engaged in the stress transfer, usually higher load value can be reach.This also lead to a change in the failure mode of the composite. Donnini et al. report and increase in the ultimate tensile strength of FRCM coupons by increasing the impregnation level of the fabric, and a change in the failure mode from slippage of the reinforcement in to the matrix to fabric failure for high level of impregnation [53]. Similar results have been obtained by different studies using different type of fabric, coating formulation, and matrix compressive strength [52, 62, 56]. Studies show that the final mechanical properties of FRCM systems with pre-impregnated fabric depends on different parameters. Mäder et al. report

that the maximal pull-out load reached by glass and carbon multifilament roving coated with a styren-butadien polymer was increased by an increased polymeric content [36]. Signorin et al. demonstrate that optimizing the viscosity of an epoxy coating for the impregnation of a glass fabric embedded in a lime-based mortar, higher ultimate tensile strength could be reached due to the better penetration of the polymer into the yarn [56]. Scheffler et al. investigated the effect of different coating formulation on the pull-out behavior of AR-glass multifilament roving embedded in a cementitious matrix, proving that the change in the chemical composition of the coating effect the pull-out behavior of the composite [62]. Although it is generally recognized that the application of organic coatings lead to an increase in the maximal load reached, some studies also report that the slip-load profile of the composite becomes steeper and falls down immediately after reaching the maximal load, so that the pseudo-ductility can not be observed anymore [49]. Moreover, some studies point out that the introduction of polymeric coating at the fiber matrix interface can compromise the resistance of the composite at high temperature due to the relative low softening temperature of polymeric materials. Therefore, alternative treatments have been proposed, which includes for example the employment of inorganic coatings. Since the engineering of the fabrics interface is a promising and wide employed strategies for the improvement of the mechanical performance of the composite, in the next chapter different fiber surface modification techniques will be presented.

2.4 Fiber surface modification techniques

The modification of the fiber/matrix interface has been widely employed has promising technique to improve the overall behavior of composite materials [63, 64, 46, 65]. The engineering of the interface can be conducted by both modification of the cementitious matrix, or the reinforcement. However, for the proposal of this study the first is of minor interest, therefore this chapter will focuse on different methods that have been proposed in the litterature for the modification of textile for cementitious-based composites. Those methods can be broadly divided in techniques which directly modify the fiber surface by means of some chemical-fiscal reaction, and those which make used of additional materials to cover the fiber surface. As already discussed in the previous chapter, the mechanical properties of FRCM composites depend on the interaction of the reinforcement with the cementious matrix, but also on the interaction between the filaments that make up the reinforcement. Moreover, when alkali-sensitive fibers, such as glass and basalt fibers, are employed, also the need to improve the durability of the reinforcement have to be address. So usually the techniques employed to modify textiles used in cement-based composite focus on three aspects:

- improve the stress transfer between the single filament
- improve the interaction of the reinforcement with the matrix
- improve the durability of the fibers

Of course according to the kind of fibers employed some aspects are more relevant than other. For instance glass fibers already have a good adhesion with the cementitious matrix [66], therefore, in this case the first goal of the fibers modification is to any improve the stress transfer between the fibers and their durability rather than improve the adhesion of the external fibers with the matrix. On the contrary carbon fibers present an excellent stability in alkaline environment, but a poor interaction with the cementitous matrix, theretofore studies conducted on these systems mainly focused on the improvement of the fiber-matrix interface rather than on the durability of the reinforcement. Since glass fibers, and carbon fibers make up the great majority of the fibers employed for FRCMs systems the great majority of the techniques discussed in this chapter will focuse on these two materials. Some methods, such application of coatings, have been reported for both glass and carbon reinforcement, while other, such electrochemical modification of carbon fibers, strictly depend on the specific chemical-physical properties of the material.

2.4.1 Sizing and coating

A coating can be generally defined as a continuous or discontinuous layer of some compound, whose chemical nature can vary from thermoplastic or thermoset polymer to thin inorganic particles, which is applied on a substrate for functional and/or

decorative purposes. The ambiguous meaning of the term coating can be sometimes misleading, particularly because no clear definition state which is the minimum and maximum amount of materials that make up a coating. For instance, commercial fabric consisting of loose filament are usually indicated as uncoated, however the fibers that make up the reinforcement are actually covered with a thin layer of polymeric coating, usually indicated as *size* or *sizing*.

Sizing

A sizing is a thin polymeric film, in the range of some tens of nanometers, which typically make up the 0.5–2 % by weight of the finished products [67]. Sizing are known to play a fundamental role in the promotion of the fiber-matrix interaction, as well in the processability and performance of spun fibers [65, 67, 68]. Sizings design for the production of glass fibers usually consist of an organofunctional silane a polymeric film former, that usually make up the 70-90 % of the sizing and a lubricant [65]. The organosilanes, are typically organofunctional alkoxy silane, which are employed as adhesion promoter. Indeed, this class of molecules presents two moieties attached to the silicon atom: a hydrolyzable group, like a methoxy or ethoxy group, that can react with the siliceous backbone of the glass fibers, and an organic moiety that can react with other functional groups such amino, epoxy, vinyl or other typical groups of organic polymers. Usually the organosilane and the film former are chosen in order to be as closely compatible to the matrix as possible. Since glass fibers are mainly employed for the reinforcement of polymeric matrix, the range of the sizing chemical composition reflects the range of the most common matrix employed for FRP materials. Indeed, according to Thomason, despite the great variety of organosilanes available on the market, the great part of all the sizing employed on commercial and laboratory scale consist on γ-aminopropyltriethoxysilane (APTES), γ-glycidoxypropyltrimethoxysilane (GPTMS), γ-methacryloxypropyltrimethoxysilane (MPTMS) and vinyltriethoxysilane (VTES) [65]. Despite consisting in a few tens of nanometer coating, sizing have been reported to play a fundamental role in determining the mechanical properties of the fibers and the composite. Sizing are known to improve the tensile strength of the fibers thanks to their ability to mitigate surface defects, inducing healing of surface flaws and preventing the possibility of creating new defects [69, 70]. Tailoring of the sizing composition is a common practice to obtained FRP with superior mechanical properties [67, 70]. Although the number of studies conducted on the role of the sizing formulation in cement-based composite is very limited, compared to the wide scientific production available for FRP, some studies suggest that optimization of the sizing formulation can lead to an enhanced durability of glass fibers in alkaline environment [36, 51, 71, 72] , as well as an improved interaction with the inorganic matrix [43, 66]. The sizing formulation plays an important role also in the prospective of further fiber modification by impregnation with organic coatings [62].

Organic Coatings

Organic coating have been widely employed to improve the load-bearing capacities of FRCM and TRC systems [36, 52, 53, 54, 55, 57, 58, 59, 62, 40]. In general the increase in the mechanical properties observed by impregnating the reinforcement with a polymeric coating is attributed to the ability of the coatings to penetrate into the yarn, increasing the stress transfer between the single filaments. As a consequence, a larger load-bearing cross-section can be activated in the roving, leading to an improvement in the efficiency of the mechanical properties of the reinforcement. As it can be observed in Figure 4.17 when the reinforcement is impregnated with an organic coating the cementitious matrix is prevented to penetrate into the yarns. As a consequence the bond with the matrix is no longer dependent on the ability of the mortar to wet the single filaments but rather from that of the coating to engage the filaments in the stress transfer and to interact with the cementitious matrix.

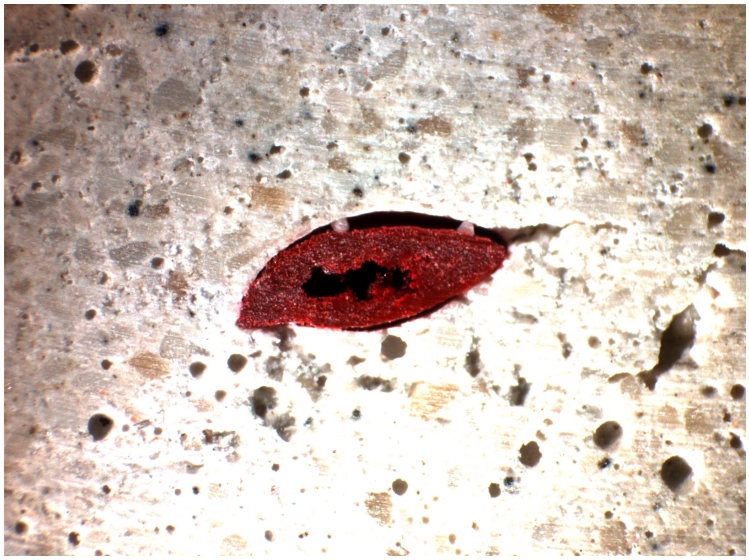

Figure 2.17: Cross section of a preimpregnated glass yarn embedded in a cementitious matrix.

The properties of the composite become than strongly dependent on the physical-mechanical properties of the coating itself. According to Schleser et al. polymers with a high elastic modulus such epoxy resin are more efficient in improving the tensile strength of the composite [55]. However, although a stiffer reinforcement can improve the tensile strength of the composite, flexible textiles, such a styrene-butadiene coated ones, performed better under flexural load [73]. Moreover, fabric with a low flexibility are less suitable for the reinforcement of existing structures with complex geometry. Other important parameters that have been reported to influence the final mechanical properties of the composite obtained with polymeric coated reinforcements are: the impregnation grade of the fabric [53, 56], the roughness of the coatings and its degree of hydrophilicity at the surface. Epoxy resins have been

successfully employed in different studies to improve the load bearing capacity of FRCM systems [32, 52, 53, 58, 74]. Significant increase in the composite tensile strength have been reported for both glass fibers [52, 58, 74] and carbon fibers [53]. Although some polymeric coatings have been reported to increase the interaction of the reinforcement with the cementitious matrix [36, 62, 75] the increased load-beargin capacity of epoxy impregnated fabric are mainly attributed to the ability of the coating to distribute the load between the yarn's filaments. In some case it has been observed that epoxy impregnated fabric can act as a separating layer [57], resulting in delamination failure, which has been reported in some studies [28, 74]. Styrene-butadiene coatings have been also be employed for the modification of the fiber-matrix interface in textile reinforced cementitious composites [36, 62, 40, 75, 76]. Mäder et al., investigated the effect of different styren-butadien coating formulation on the mechanical properties of concrete reinforce with ARG multi-filament yarns [36]. Single fibers pull-out test performed on the fibers with and without coating show that selected styren-butadien coatings provide a higher adhesion strength with the matrix compared to the untreated fibers. Moreover, regardless of the coating formulation applied an increase in the yarns tensile test was also observed. However, the authors also observed that a superior interaction between matrix and coating and an increase in the load bearing capacities of the reinforcement are not sufficient conditions to improve the mechanical properties of the composites. Indeed, the same styrene-butadiene coating applied on two different commercial AR-glass yarns was not always effective in increasing the overall mechanical properties of the composite. Similar results have been reported by Sheffler et al. in [62]. In this study the authors demonstrated that the compatibility between sizing and coating play a fundamental role in the final properties of the composite. Beside increasing the load bearing capacity of the composite, polymeric coating have been extensively employed to enhance the chemical stability of glass fibers in alkaline environment and realize composites with improved durability [77, 36, 75, 76, 60]. The ability of the coating to protect the glass filaments depends on the stability of the coating in alkaline environment and the ability of the coating to act as a barrier against the penetration of water molecules and ions [77, 36, 76].

Inorganic coatings

Inorganic coatings have been proposed as alternative to organic coating mainly in order to overcome the limited resistance of polymeric coating to high temperatures [78, 39]. Different impregnation techniques and coating formulations have been proposed [33, 39, 73, 79, 80, 81, 82, 78, 83]. Weichold at al. prepared a cement-in-polymer dispersion using a ultra-fine grained cement with a particle size of < 7 μm and a water-soluble polymer [83]. When the textile is embedded in the fresh cement paste the polymer dissolves and the non-hydrated cement contained in the inorganic coating can react with the portland cement. In this way also the inner

yarns filaments are embedded in the matrix and a very homogeneous cement-matrix interface is obtained. As a consequence the load bearing capacity of the composite is increase and instead of experimenting a sudden drop of the pull-out load, after debonding, a further increase in the pull-out load is observed. Another technique proposed by Homoro et al. i consists in passing the textile covered with the powder between two electrodes where a strong alternative electrostatic field in order to promote the penetration of the dry inorganic coating in the yarns [80]. Before casting the yarns are sprayed with water. The authors report an improved matrix penetration between the filaments which corresponds to superior tensile properties of the composite. Different studies propose the impregnation of the reinforcement with inorganic coating based on silica particles [33, 39, 79, 81, 82]. For this purpose silica particles of different dimension can be used. Signorini er al prepared a nano-silica coating using the sol-gel method, where tetraethyl orthosilicate (TEOS) was employed as SiO_2 and a micro silica coating obtained by stirring silica fumes with particle size of 0.15 μm for one hour in distilled water [81]. The coatings were than applied on a ARG fabric by bathing the fiber in the colloidal solution and the micro-silica suspension. In both case diffuse mortar patches attached to the fabric could be detected on the SEM images of the composite after tensile test. The same was not observed for the untreated reinforcement which confirm the ability of the silica particles to promote a good adhesion with the matrix. The improved fabric-matrix interaction results also in the increase of the composite tensile strength which was found to be 60.3 % and 96.7 % higher with respect to dry systems for the fabric with, respctively, nano-silica and micro-silica. Also Cohen and Peled report an increase in the maximum tensile stress of the composite by coating the reinforcement with 200 nm silica fume particles [79]. However, in the same studies the authors report that coating with smaller silica dimension (50 nm) has no beneficial effect on the composite mechanical properties. The results were attributed to a partial wash out of the small particles when the reinforcement is immersed in the fresh cementitious paste. Similar results have been reported by Nadiv et al. and are attributed to the brittle segmentation of the nano-silica on the fibers surface [39]. A potassium silicate dispersion have been proposed by Quadflieg et al. for the impregnation of AR-glass fabric [73]. A roll-to-roll coating machine was employed to apply the inorganic coating on a AR-glass fabric. According to the authors a better penetration of the matrix within the reinforcement was obtained and the reacts of the inorganic coating with the cementitious matrix, and improved the adhesion at the fibers-to-matrix interface. This resulted in an increase in both the composite tensile strength and flexural strength using the silica coated fabric instead of the unmodifed one. Beside improving the chemical compatibility of carbon and glass-fibers with the cementious matrix inorganic coating containing amorphous silica have also been reported to enhance the durability of the composites [79, 84]. This is attributed to the ability of the amorphous silica to react with the portlandite crystals that accumulate at the fiber-matrix interface, transforming the brittle CH layer in a more porous and

homogeneous stratum of CSH.

Hybrid coatings

The interaction between organic hydrophobic polymer with the inorganic hydrophilic matrix is not always optimal. For this reason some studies have proposed to increase the interaction between polymeric coating and cementious matrix by adding inorganic particles in the polymer formulation [62, 40, 85]. Zamir et al. reports that hybrid micro-silica epoxy coating confer the composite superior performances in comparison to the fabric modified with only epoxy resin or micro-silica coating [85]. Particularly they report that the best results in terms of composite bending and tensile strength are obtained by first impregnating the fabric in the epoxy resin and then apply silica particles on the partially hardened polymeric coating. Improved interaction between polymeric coating and cementitious matrix has also been reported for the addition of nanoclay particle in styren-butadiene coatings [62, 40]. The improved fiber-matrix bond has been attributed to the ability of clay-aluminates to serve as nucleation points for the development of hydration products, forming a denser fiber-matrix interface. However, according to Hempel et al. addition of nanocalys particle in the coating formulation reduced the ability of the coating to preserve the composite properties overtime [40]. Nevertheless, nanostructured styren-butadien coatings, obtained by intercalating nanoclay particles in the polymeric matrix, have been proved to increase the ability of the coating to protect the fiber from chemical degradation in alkaline solution [86]. This is attributed to the superior ability of polymer layered silicate to act as barrier against water molecules and ions. However, an effective enhancement of the polymer barrier properties ca be obtained only for nanostructured polymer where the polymeric matrix is intercalted between the layered silicates [87]. On the contrary when the nanoclay agglomerate in the coating an opposite effect of reduced resistance to alkali -attack can be obtained [75].

2.4.2 Oxidation of carbon fibers

The oxidation of carbon fibers to increase their surface energy is commonly used method to improve the interfacial bond between fibers and matrix [11]. Oxidation can be conducted by wet processes using chemical [88, 89] or electrochemical procedures [90, 91], or by gas-phase oxidation for example in the case of plasma treatments [88, 92]. Although the literature available on this topic mainly concern carbon fibres used as reinforcement for polymeric matrix some studies have been conducted also on cement based composites. Xuli et al. conduced single fibre pull-out test on carbon fibres treated with acetic acid, nitric acid, sodium hydroxide, hydrogen peroxide solutions and O_3 embedded in a cement-based paste. They observed that the bond strength between carbon fiber and cement increased particularly after oxidative treatment such O_3 and stirring in nitric acid solution [93]. Lavagna et al. investigated the effect of different oxidation protocols based on oxidation solution

on the mechanical properties of cement-based matrix reinforced with short carbon fibres [94]. They reported that all the treated fibres give composites with superior flexural strength. Particularly they found the highest improvement of the composite mechanical properties by sonicating the carbon fibres in a piranha solution (1:1 H_2SO_4 : H_2O_2) for 30 minutes at 30 °C. Although they do not report the chemical composition of the fiber after oxidative treatments, on the base of other work thy conclude that the improvement of the composite mechcanical properites is due to the formation of an optimal amount of hydroxyl and carboxylic groups on the fiber surface. Oxidative treatment of carbon fibers have also been proposed in order to prefunctionalize the fibers surface before coating the filaments with a inorganic coating [95, 96]. Schneider et al. treated carbon fibers with different plasma process (O_2, O_2/Ar and oxygen/CF_4) before applied a mineral based coating on the yarns. They report that the best results in terms of fiber-coating-matrixi interaction were obtained by treating the carbon fibers with oxygen plasma for 100s with a gas flow of 10 mL/min, however a remarkable increase in the composite pull-out load was also observed for the O_2/Ar treated fibers. This is attributed to the increased affinity of the functionalized carbon fibers for the water-based slurry used for the coating process. Similar results have been reported in [96], where oxygen plasma was used varying the treatments time, the plasma flow rate, the applied pressure and pulse duration. Best results where obtained for short time treatment at high oxygen flow rates, low pressure, and long pulse duration. Eletrochemical oxidation methods have also been proposed for the accretion of inorganic coating on carbon fibers surface [97]. In this case the carbon yarn serve as anode in an electrochemical cell immersed in a cementitious pore solution. According to the authors the oxygen-bearing functional groups formed on the carbon fibers surface due to anodic oxidation, promote the formation of calcite layer on the fiber surface. The increased fiber roughness and chemical affinity with the cementitious matrix provided by the calcite coating resulted in an enhanced pull-out behavior of the composite. However, the tensile strength of the carbon fiber was found to be strongly influenced by the voltage and treatment time. Optimal results were obtained for treatment at 3V for 15 min.

2.5 Durability

The ability of building materials to maintain their mechanical performance and withstand the exposure to aggressive environment during their life of service, is a safety and economic concern, as well an decisive factor for the design of sustainable construction. This information is needed in all the stages of a building cycle, from the first phases concerning programming and preliminary design of the construction to the following interventions for the removal and rehabilitation of its damaged parts. Ideally, the change in the material characteristics over time should be known or estimated form real-time measurement of case of study. However, for new materials such as FRCM, usually no anecdotal information or documented long-term performance are available, so that durability assessment are usually conducted by modeling the long-term behavior on the base of short therm test conducted on laboratory scale. Tests designed to evaluate the durability of FRCM composite systems under environmental exposure should consider the environment resistance of each component (the cementitious matrix and the fabric reinforcement) and the change occurring over time at their interfaces (fiber-matrix interface, matrix-substrate interface). Moreover, the procedures should be design in order to reproduce, as faithfully as possible, the real degradation process that the material is expected to undergo during its life service. Due to the lack of information about FRCM-specific durability issues, first studies conducted on the topic were based on the literature regarding the durability of FRC [51, 98] and FRP [23, 24, 99]. Because TRC are made up of the same basic ingredients of FRC the RILEM technical committee purpose to model their deterioration mechanism and detrimental environment after those for FRC studies [98]. Other studies suggest that since FRCM systems were developed as alternative to FRP they should withstand the same service conditions [23]. Although some standard procedures have recently be proposed to evaluate the durability of FRCM systems [100, 30], most of the research available on the topic adopted different test procedures and aging protocols.

In this chapter test method propose form guidelines and experimental protocols described in the scientific literature will be reviewed, paying particular attention to three main issues:

- which test method are more appropriate to evaluate the change in the mechanical performance of the systems;
- which are the environmental exposure more determinant for its degradation;
- which experimental protocols are more appropriate to simulate the aging of the material under environmental exposure.

2.5.1 Test methods

Durability test for building materials are generally conducted by comparing some mechanical properties of the material before and after exposure to accelerated aging. In the definition of the test method it is therefore of crucial importance to define which properties are expected to be more effected by the environmental exposure as well as which are considered essential for the proper exploitation of the materials' performance. For instance some FRC composite display an increase in strength and reduction in toughness over time [10], so that evaluation of the durability based on compressive test would reveal an improvement of the performance, while on the contrary tensile test would suggest a decrease in the mechanical properties. Benture et al. studied the aging of cementitious matrix reinforced with continuous and chopped glass fibers and reported that in both case the toughness or ductility of the composite (estimated from the area under the load-deflection curve) was much more sensitive to aging than the Module Of Rupture [98]. According to Mechtcherine, the strain capacity is a decisive property for TRC composite that can not be considered as truly durable if its strain capacities decrease at a substantial rate over time [101].Nevertheless, as already discussed in section theoretical and analytical studies have shown that, among with tensile properties, also the bond between the FRCM and the substrate plays a major role in determining the overall properties of the system. Test methods adopted by studies conducted on the durability of FRCM and TRC includes uniaxial tensile, three point bending, pull out, and direct shear tests [102]. However, those methods investigate different properties and component that can not be directly compared. Unaxial tensile test are particularly appropriate to describe the tensile behavior of FRCM composite, however they furnished no information about the change at the matrix-substare interface. Nevertheless, analyses of the stress-strain curved obtained, can furnish different information on the effect of environmental exposure on the composite behavior and its component. One of the most important parameter obtained from tensile test, that has been use for the evaluation of FRCM durability is the ultimate strain of the composite [23, 103, 104, 105, 106, 107]. However, the stress strain curved can also furnish some information about the effect on the single components. In [104, 105, 108] he effect of conditioning protocol on the matrix has been evaluated by comparing the first crack tensile strength and the module of the uncracked curve obtained before and after the relative conditioning procedure. The same parameters calculated in the last phase of the curve give information about the reinforcement and its interaction with the cementitious mortar. The effect of aging protocols on the different components has also been investigated by coupling different kind of mechanical test. Three [23, 31, 109] and four [110] point bending test and compression test [109] were used to evaluate the effect of the artificial exposure on the cementitious matrix. Single fiber tensile test, single yarn tensile test [109] and fabric tensile test were employed to study the durability of the reinforcement. Change at the matrix-substrate interface

has be investigated by single-lap shear test [109][111] and pull of test [23]. Pull out test were employed to study the environmental effect at the fiber-matrix interface [51, 105].Moreover, mechanical results were often coupled with scanning electron microscopy (SEM)[51, 99, 104, 109, 110] n order to investigate the degradation mechanism at the fiber interface, as well as the densification of hydration products at the interface wit the matrix. For the qualification of FRCM systems the Italian guide CSLP [100] prescribes the evaluation of environmental exposure by means of unaxial tensile test on both the fabric and FRCM composite coupons. Also in the AC 434-13 [30] tensile test performed on the composite are employed for durability test, along with interlaminar shear test.

2.5.2 Environmental exposure

Since they are externally bonded, during their service life FRCM can be affected by different environmental exposure such as wet-dry and freeze-thaw cycle, heat and saline exposure. Because of the variety of materials that can be employed for the realization of FRCM reinforcement as well as the different type of processes that can affect their performance, it is difficult to devise a universal test to evaluate the durability of FRCM systems. A first approach is that of considering which chemical and physical process are more determinant for the durability of FRCM components. Since the fabric reinforcement are embedded in a cementitious matrix, assessment of the processes which can lead to durability issues can be partially obtained on the based of degradation mechanism known for conventional concrete. Alkali aggregate reaction, sulphate attack and freeze-thaw cycles are chemical-physical conditions that are known to promote the formation of expansive compounds usually responsible for crumbling or spalling of cementitious materials [112]. Alkali aggregate reactions occurred when alkali hydroxide, such NaOH and KOH react with thermodynamically unstable silica which can be present in some aggregate and in glass fibers. Caused of the damage is the alkali-silica gel formed, which absorb water into the matrix inducing expansion and cracking of the concrete [112, 113]. Sulphate, which can be found in soil as a consequence of fertilizers use or are naturally present in seawater, can cause a sequence of chemical reactions that promote the decalcification of the matrix as long as crumpling and spalling of the mortar because of expansion phenomena [112]. The decalcification of the matrix is due to sulpahte ions reacting with portlandite (Eq.3.6) and calcium silicate hydrate (Eq.3.7).

$$Ca(OH)_2 + SO_4^{2-} + 2H_2O \rightarrow CaSO_4 \cdot 2H_2O + 2OH^- \tag{2.3}$$

$$Ca \cdot 2SiO_2 \cdot 3H_2O + SO_4^{2-} + H_2O \rightarrow CaSO_4 \cdot 2H_2O + 2SiO_2 \cdot H_2O \tag{2.4}$$

Crumpling and spalling of the mortar are reported to accrued because of the

formation of Ettringite according to equation 3.8.

$$3CaO \cdot Al_2O_3 + 3CaSO_4 \cdot 2H_2O + 26H_2O \rightarrow 3CaO \cdot Al_2O_3 \cdot 3CaSO_4 \cdot 32H_2O \quad (2.5)$$

Also degradation process due to freeze-thaw cycles are due to expansion process, which in this case are caused by the increased of volume (about 9 %) of water inside the concrete or mortar pores. Since damages occurred when the dilating pressure exerted by water in the capillary pores exceeds the tensile strength of the matrix, usually its resistance to freeze-thaw cycles depend on the tensile strength of the matrix and its microstructure [112, 114].A similar dependence has been observed also for salts attack where the decay of the mechanical properties seams more significant in matrix with high porosity and low strenght [114]. Also the impact of alkali hydroxide exposure depend on the characteristics and composition of the cementitious matrix. Aggregates that have been found to give Alkali-Silica reaction (ASR) are: opal, tridymite, cristobalite, volcanic glass, chart, cryptocrystalline (or microcrystalline) quartz and strained quartz [115]. Matrix where such aggregate or other source of amorphous silica are not present are not expected to be damaged by alkali oxide or hydroxide. Among with freeze-thaw cycle, alkaine and saline exposure the AC 434-13 [30] recommends investigating the resistance of FRCM to fuels and the Italian CSLP [100]also that to thermal stress. For the evaluation of chemical-physical process that can effect the properties of fabric in FRCM systems, durability studies on FRC are a good starting point. Those studies show that the chemical degradation of fibers embedded in cementitious matrix can result on one hand, from the attack of the fiber by external agents that penetrate through the porous matrix , and on the other hand, from the corrosion caused by the hydroxyle ions present in the high alkaline pore water of the matrix [10]. Since FRCM fabrics can be made with different natural and synthetic fibers their durability in the matrix and under environmental exposure will depend on their chemical composition and their reactivity with chemical agents. As already described in section 2.1.1 the siliceous backbone of glass and basalt fibers deteriorate in presence of OH^- and those fibers are therefore sensitive to environment with high pH value. However, the degradation of glass in aqueous media can occur also at lower pH value. It is widely recognized that the corrosion process involves two stages [116, 117]: the leaching of the alkaline ions (Na^+ and K^+) from the glass surface (eq. 3.9) and the break down of the oxygen bridge bonds which causes an irreversible disruption of the glass network (eq. 3.10).

$$\equiv Si - O - M^+_{(s)} + H_2O_{(l)} \rightarrow \equiv Si - OH^-_{(s)} + M + OH^-_{(l)} \quad (2.6)$$

$$\equiv Si - O - Si \equiv_{(s)} + OH^-_{(l)} \rightarrow \equiv Si - O^-_{(s)} + \equiv Si - OH^-_{(l)} \quad (2.7)$$

2.5.3 Artificial aging

Change of the mechanical properties of composite during their lifespan are due to time-dependent processes which can occurred over months or years. It follows that one of the main issue in designing test to estimate the durability of materials is that of reproduce their long-term behavior in a short time span. This results in the need to accelerate the processes that induce change in the mechanical performance of the composite overtime. Since several of those processes are chemical reactions a rather widespread approach to model long-term behavior of material is that of use the Arrhenius equation [10, 98, 118]. According to Arrhenius equation the natural logaritm of the rate constant k of a chemical reaction is proportional to the inverse of the absolute temperature (1/T). It follows that rates of chemical reaction, whit few exceptions, increase with temperature according to the following equations:

$$k = Ae^{\frac{-E_a}{RT}} \tag{2.8}$$

or

$$lnk = lnA - \frac{E_a}{R}\frac{1}{T} \tag{2.9}$$

where
k is the rate constant
T is the absolute temperature in kelvins,
A is the constant factor characteristic of the chemical reaction,
E_a is the activation energy and
R is the universal gas constant.

An Arrhenius type relationship was used by Proctor and co-workers to correlate the accelerated aging of glass reinforced concert made up of ordinary Portland concrete and AR-glass fibers, whit in-service weathering [119, 120]. In this work the authors developed an empirically derived durability model, in which 1 day immersion in water a 50 °C was calculated to be equivalent to circa 100 days of weathering in UK climatic conditions. The validity of this model is based on the evidence that the same activation energy was applicable for different temperature range, which indicates that the same reaction mechanism was responsible for the strength loss in long and short term test. However, this is not always the case. Indeed, raise of the experimental temperature also affect the Gibbs free activation energy $\Delta G^{\prime}$ of chemical reactions, so that test conduced at high temperature may promote reactions that do not occur at natural service temperature. Although the method developed by Proctor furnished a good predictive model for Glass fibers Reinforced Concret (GFRC) with ordinary Portland concrete, Purnell et al. demonstrated that it does not apply to other FRC systems [121]. Nevertheless, immersion of FRC and in hot water is a popular and widespread accelerating method that has been employed also for aging test with TRC and FRCM system [98, 103, 109, 122]. Alternatively,

accelerate aging can be performed by placing the specimens in fog chamber at high relative humidity and temperature [100, 23, 30, 51]. The advantage of this method compared with immersion in water is that it prevent undesired leaching of the cementitious matrix, and it is therefore more appropriate to mimic change at the fiber-matrix interface due to continued hydration processes. On the contrary, the simulation of seasonal changes, humidity fluctuations and moisture penetration over natural environmental exposure, can be better performed by exposing the composite to wet-dry cycle. Difference in the result obtained for sample immersed in aging solution or expose to wet-dry cycle have been reported to be particular significant for saline environment [109, 123]. Although wet-dry cycle has been employed in some FRCM durability studies [17, 109, 111], it should be specified that at present there are no standard procedure to perform wet-dry cycles on FRCM systems [102]. Test conduced on the durability of FRCM systems under saline exposure also deffer for the chemical composition of the saline solution employed. Arboleda used ocean water and does not report the chemical composition [23], Donnini used a solution with 3,5 wt% NaCl in tap water [109], Franzoni exposed the composite to a saline solution made with 2 wt% NaCl and 8 wt% $Na_2SO_4 \cdot 10H_2O$ (which correspond to the 3.53 wt% of Na_2SO_4) [17, 111]. Also standard procedure propose different composition for saline solution. The EN 12370:2020 suggest a solution made with 14 wt% $Na_2SO_4 \cdot 10H_2O$ (4.41 wt% Na_2SO_4), the RILEM test method MS-A.1 proposes a solution with 10 wt% of both NaCl and Na_2SO_4 anhydrous [124], the AC 434-13 [30] and the Italian CSLPP [100] suggest preparing a solution according to the ASTM D1141 [125] in which the two main salts dissolved in the solution are NaCl and Na2SO4, respectively 2.4 5wt% and 0.41 wt%, plus several minor salts such as $MgCl_2 \cdot 6H_2O$, $CaCl_2$ and $SrCl_2 \cdot 6H_2O$. A great variability in the composition of the solution employed for the conditioning protocol can also be found in studies conducted on the durability of FRCM in alkaline environment. Stander procedure for the investigation of FRP composite in alkaline environment has been proposed to investigate the effect of cementitious matrix on laminate and FRP bars [126]. In general all standard procedures recommend the immersion in solution of pH higher than 9.5. Since $Ca(OH)_2$ has a solubility in water of 1.7 g/l at 20 °C, the highest pH value that water solution with only $Ca(OH)_2$ can reach (at 20 °C) is 12.66. On contrary NaOH has much higher solubility in water than $Ca(OH)_2$ so that aqueous solution of pH 14 can be obtained. In general studies conducted seams to be more concern with the pH of the solution than its composition, and alkaline environment have been reproduced with both NaOH solution $Ca(OH)_2$ solution or a combination of both with also KOH. An extensive study on the corrosion mechanism of sized and unsized glass fibers immersed in NaOH and cement solution have be conducted by Scheffler at al. [77, 72]. According to the authors the peeling of the fiber external layer is typical for the storage in NaOH solution, can be observed at different pH value and aging temperate, and is characterized by different stage as described in Figure 4.18. According to the authors, immersion in NaOH solution lead to the

formation of peeling shells, which were not observe on fibers immersed in a cement solution, which on the contrary displayed some holes of different sizes and depths on their surface. Since the same corrosion pattern was observed for glass and basalt fiber, the authors concluded that the different reaction mechanism are typical for the two different alkaline solutions. Figures described respectively the corrosion mechanism observed for fiber storaged in NaOH and cement solutions. In an initial state the corrosion mechanism caused by the NaOH solution leads to a clear separation of fibers defects in two flaw populations, where the failure stress of filaments having large defects is reduced, while that of filaments having small defect remain more or less unchanged. A two-parameter Weibull distribution obtained for the failure stress of the glass fibers in this stage is characterized by a bimodale function with two distribution. The Distribution I present high shape and scale parameters that remain more or less constant, while the Distribution II presents much lower shape parameter and the scale parameter decrease over time. With the proceeding of the alkaline attack a thin but continuous corrosion shell is formed, water molecules penetrate into the glass network leading to increasing volume and swelling of the shell and the amount of size defect increases. As a consequence the shape parameter of the distribution decreases. At some point, the corrosion shell formed on the filaments surface starts to peel of from some areas of the fiber surface so that the original diameter of the filaments becomes smaller. However, the glass surface underneath the corrosion shell remains intact so that in a final state D, where the corrosion shell is completely peeled off, an enhancement of the failure stress is observed, since this is no longer affected by the corrosion shell. The corrosion process will than eventually start again from state A.

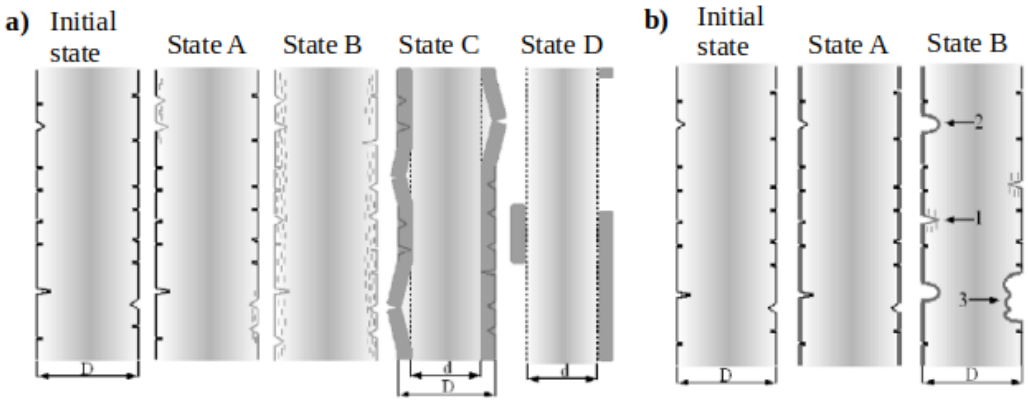

Figure 2.18: Corrosion mechanism of glass fibers in a) NaOH solution and b) cement solution according to Scheffler et al.

On the contrary glass fibers stored in cement solution display a completely different corrosion pattern, characterized by the formation of holes of different sizes and depths rather thane by the peeling of the filaments external shell. The different corrosion mechanism also account for a different change of the fibers' failure stress over time.

Indeed, a constant decrease of the scale and shape parameters is observed which indicates a change in the filament surfaces due to corrosion. However, in a first stage the filament are covered with a hardly soluble Ca-Si-layer therefore nor change in the Weibull parameters neither mixed failure stress distribution are observed in a first period. At some point occurrence of mixed failures stress is observed, resulting in a bimodal two parameter Weibull distribution. Figure 4.18b schematizes the different damages promoted by the cement solution:

1. chemical attack,
2. expansion of the existing defect forming the typical hole observed on the fibers surface,
3. formation of large cavities on the surface when neighbor holes marge.

Chapter 3

Materials and Methods

3.1 Materials

3.1.1 Textile Reinforcements

In this work the following reinforcements were used:

- a commercial carbon fabric compatible with Epoxy resin obtained form the company Microtex Composite srl.
- a Styren Butadien pre-impregnated AR-glass fabrics obtained from the company Biemme s.r.l (BM ARG);
- AR-glass rovings spun at the Leibniz-Institut für Polymerforschung (IPF) of Dresden (IPF ARG).

Carbon and glass fibers' reinforcement were chosen on one hand because are between the most commonly employed fibers for FRCM systems, and the other hand because they present different chemical properties: carbon fibers are stable in alkaline environment, while glass fiber are known to undergo degradation in presence of OH^- ions; carbon fibers have a very low interaction with the cementitous matrix other than glass fibers.

Commercial Carbon Fabric

Tabel 4.1 reports the mechanical properties of the as delivered carbon yarns. Test were conducting according to ISO 10618. The cross-sectional area of a single yarn was calculated from the resistant area per meter reported by the producer. Figure 4.1 report the geometrical specification of the fabric.

Table 3.1: Mechanical and geometrical properties of carbon yarns. Coefficient of variation in brackets.

Maximum tensile strength $\sigma_{max,yarn}$ **[MPa]**	**Elastic modulus** $\mathbf{E}_{yarn}$ **[GPa]**	**Ultimate strain** $\varepsilon_{u,yarn}$ [%)]	**Cross sectional area** $\mathbf{A}_{yarn}$ **[mm^2]**
1732.07	145.46	1.39	1.04
(6.88 %)	*(0.53 %)*	*(0.82 %)*	-

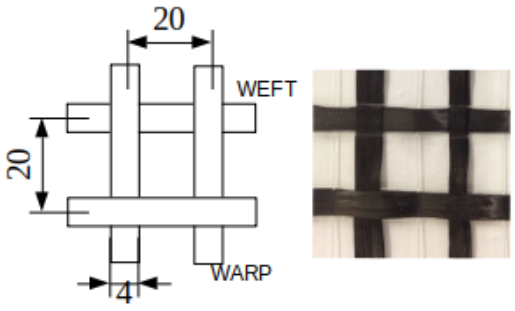

Figure 3.1: Carbon fabric, value in mm.

For the modification of the reinforcement, yarn were cut from the fabric in the warp direction a subjected to different treatments, which are summarized in Table 4.3

Table 3.3: Treatments employed for the modification of the carbon yarns.

Name	Treatment	Material Used
Dry	-	As delivered fabric
C-E	Application of commercial bi-component epoxy resin by means of a metallic spatula. Curing of the resin at 60 °C overnight.	Elan-tech® EC 98N/W 52 Viscosity 2000-3000 mPas Tensile strength 0.7-09 MN/mm^2 Elongation at break 60-80 %
C-NS	Immersion of the yarns in a nanosilca dispersion under stirring for 15 minutes and let dry at room temperature. The nanosilica dispersion was obtained by sol-gel method as described in [82]	Tetraethyl orthosilicate (TEOS) was obtained by Evonik. Analytical grade Ethanol from Sigma-Aldrich and 65 % Nitric Acid from Merck were employed
C-Ox	Sonication of the yarn in a HNO3/H2SO4 oxidative solution for 15 minutes, followed by washing with distilled water until a decrease of the washing water pH to approximately 6. The oxidative solution was prepared according to [127], with 1:3 HNO3 /H2SO4 volume ratio. Yarn were let dry at room temperature.	65 % Nitric Acid (HNO3) from Merck 95 % Sulfuric Acid (H_2SO_4) from Sigma-Aldrich

Commerical AR-glass Fabric

The geometrical and mechanical properties of the BM ARG fabric are reported in Figure 4.2 and Table 4.4. Tensile strength of the glass yarns were determinate according to ISO 10406-1, the cross-sectional area and the coating weight are reported according to the technical data sheet provide by the producer.

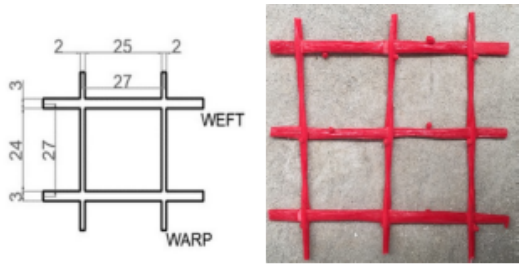

Figure 3.2: BM ARG fabric.

Table 3.4: Mechanical and geometrical properties of BM ARG yarns

Maximum tensile strength $\sigma_{max,yarn}$ **[MPa]**	**Elastic modulus** $\mathbf{E}_{yarn}$ **[GPa]**	**Ultimate strain** $\varepsilon_{u,yarn}$ **[%)]**	**Cross sectional area** $\mathbf{A}_{yarn}$ **[mm^2]**	**Coating [wt%]**
1236	75	0.789	35	
(10.30 %)	*(8.72 %*	*(12.32 %)*	-	*5 %*

Since the chemical composition of the glass fibers is not declared by the producer, EDX analysis were performed on glass fibers samples after removal of the SB coating in refluxed toluene. Table 4.5 reports the Atomic percentage (At %) of Si, Zr Na and Ca as average of three acquisitions, the coefficient of variation is reported in brackets.

Table 3.5: Chemical composition of the BM ARG according to EDX analysis

Elements	**Si (SiO_2)**	**Zr (ZrO_2)**	**Na (Na_2O)**	**Ca (CaO)**
At%	72.9	12.5	7.6	6.9
		(0.80 %)	*(3.40 %)*	*(6.90 %)*
	-	17.1	10.4	9.5
		Zr/Si	*Na/Si*	*Ca/Si*

IPF AR-glass Fibers

In order to evaluate the effectiveness of experimental coatings on the durability of glass fibers and their interaction with the cementitious matrix, AR-glass fibers were spun at the Leibniz-Institut für Polymerforschung Dresden (IPF) by using a

continuous pilot plant spinning equipment. The spinning equipment make use of prefabricated alkali-resistant glass balls whose composition is reported in Table 4.6. The glass balls are melted in a platinum-rhodium alloy bushing at the temperature of 1350 °C. The molten glass passes in to 204 nozzles at the bottom of the bushing, forming the desired glass filaments. Varying the haul-off speed the strands' fineness can be adjusted from 10 µm to 19 µm. After cooling a sizing is applied by a roll. Figure 4.3 reports a schematic description of the spinning plan, further details can be found in reference [128].

Table 3.6: Chemical composition of the IPF ARG.

Elements	**O_2**	**Al_2O_3**	**B_2O_3**	**ZrO_2**	**Na_2O**	**CaO**	**TiO_2**	**MgO**	**K_2O**	**Fe_2O_3**
Wt%	59.56	0.52	0.04	18.44	12.75	6.07	0.24	0.03	1.55	0.17

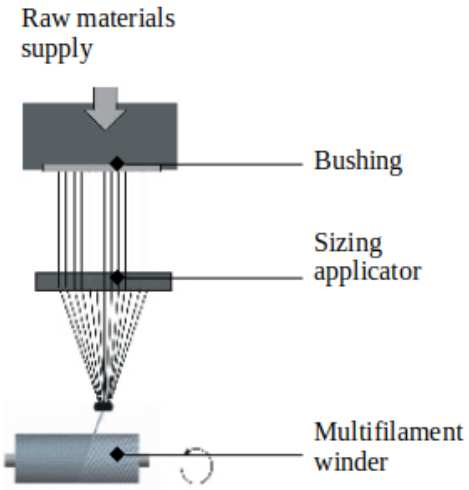

Figure 3.3: Schematic representation of the spinning plant at the IPF. Image properties of the Leibniz-Institut für Polymerforschung, Dresden.

Fibers with a diameter of 14 μm were spun with distilled water and successively deep coated in different sizing and coatings dispersions. Those fibers were employed for the micro-mechanical tests. Strands of fiber with 17 μm diameters were spun with a sizing suitable for styrene butadiene coating. The strands where than assembled in to multi-filament rovings and used for the macro-mechanical test with and without application of farther coatings. Table 4.7 reports the main characteristics of filament and roving.

3.1.2 Sizing and Coatings

Singel Fiber Dip-coating

The employment of a sizing during the spinning process of glass fibers is crucial on one hand to the handle-ability of the filaments but on the other hand also to

Table 3.7: Mechanical and geometrical properties of IPF fibers and rovings.

	Maximum tensile strength $\sigma_{max,yarn}$ **[MPa]**	**Elastic modulus** $\mathbf{E}_{yarn}$ **[GPa]**	**Ultimate strain** $\varepsilon_{u,yarn}$ **[%)]**	**Cross sectional area** $\mathbf{A}_{yarn}$ **[mm^2]**	**Number of filaments**	**Finesse [tex]**	**Density [g/cm^3]**
Filament	1534 *(28.3%)*	76 *(1.3%)*	2.35 *(30.1%)*	-	-	0.588	2.78 -
Roving	487 *(6.1%)*	73 *(1.6%)*	0.67 *(8.2%)*	0.463	2040	1200	2.78 -

promote the adhesion of further coatings on the fiber surfaces. For this reason, before applying a polymeric coating on the fiber surface, the uncoated 14 µm AR-glass fibers had to be treated with a silane based sizing. However, previous works have shown that single fibers isolated from sized strands present regions where the sizing is accumulated between filaments leading to a non-homogeneous distribution of the sizing and of the successive layer of coatings on the fibers surface (Fig. 4.4). A significantly more homogenous sizing and coating distribution can be obtained by dip-coating the single filaments in the desired solution or dispersion. For this propose single fibers were isolated from the unsized 14µm Ar-glass strands and singularly dip coated. For the micro-mechanical pull-out test, for which few millimeters of coated fibers were sufficient, the coating process was conducted by fixing one end of the fibers to a small plate and dipping the free length in the sizing solution or/and coating dispersion under controlled velocity, as shown in Figure 4.5.

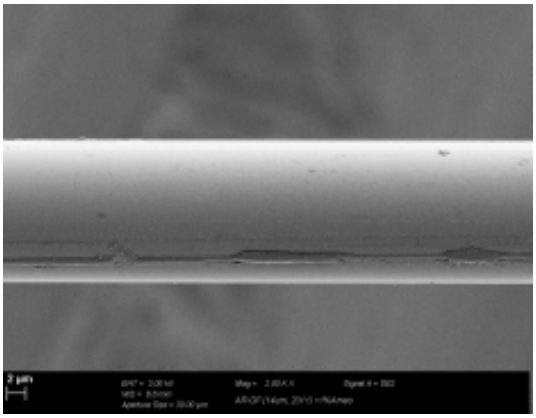

Figure 3.4: Fiber isolated from a filament bundle immersed in a 1 % AMEO solution.

For this propose a Dataphysics testing device was adapted using the following settings for both sizing and coating procedure: immersion depth 15 mm, motor speed: 0,25 m/s, stop at turning point: 60s. For the single fibers tensile test, where a minimum fiber lengths of 50 mm was required, the fibers were dip-coated by tensing

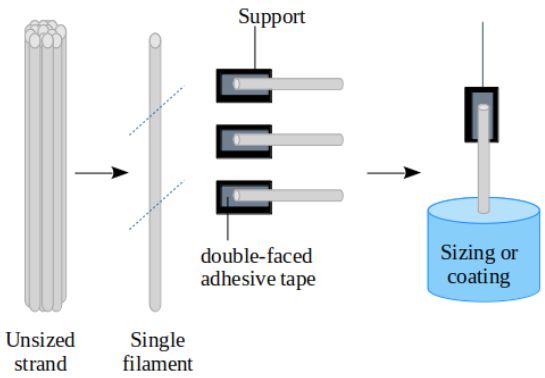

Figure 3.5: Schematic representation of the single fiber dip coating process used for the fiber employed in the single fiber pull out test.

the singles filaments in a metallic frame (Fig. 3.6a) which was than immersed in the sizing solution or coating dispersion (Fig. 3.6b).

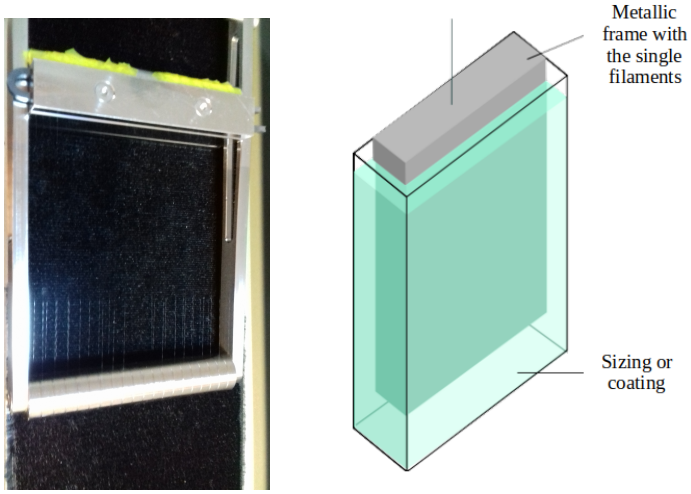

(a) Single filaments fixed in the metallic frame used for the dip coating process.

(b) Schematic representation of the dip coating process used for fibers employed in single fiber tensile test.

Figure 3.6: Filaments dip-coating.

Table 4.8 reports the sizing and coatings formulation employed for the modification of the 14 µm AR-glass fibers.

The sizing for single fiber dip-coating was realized by stirring a silane coupling agent in distilled water for 1h.

An aliphatic organosilane coupling agent, N-propyltrmiethoxysilane (PTMO, Evonik) and an (3-Aminopropyl)triethoxysilane (AMEO) were employed. The coating dispersion were realized using a carboxylated and self-crosslinking Styrene-Butadiene

Table 3.8: Sizings and coatings formulation used for the modification of the fibers employed in the QSFPO tests.

Sample name	**Sizing (1^{st} treatment step)**	**Coating (2^{nd} treatment step)**
PTMO	1 % N-propyltrimethoxysilane (PTMO) in distilled water	none
SB	1 % 3-Aminopropyltriethoxysilane (AMEO) in distilled water	Self-crosslinking Styrene-Butadiene copolymer (SB)
CSB	1 % AMEO in distilled water	SB + crosslinking agent (C, 7 wt% in rispect to the SB solid content)
SB_MMT	1 % AMEO in distilled water	SB + 5 % montmorillonite (MMT)
CSB_MMT	1 % AMEO in distilled water	CSB + 5 % MMT

(SB) latex (Lefasol VL 90/1, Lafatex Chemie GmbH). The as delivered SB latex (with a solid content of 50 %), was diluted in order to obtaine a dispersion with a polymeric content of 20 % in weight. Coating SB5 were realized by dispersing in the SB latex a sodium montmorillonite powder, with a typical dry particle size <25 μm and basal spacing of 1,17 nm, produced from Southern Clay Products Inc., under the trade name of Cloisite®Na^+. In order to obtain an optimal dispersion of the nanoclay particle in the polymeric matrix the following protocols was used:

1. First 2.5 g of nano-clay particles were slowly added to 50 ml distilled water in a 100ml round flask under vigorous stirring. The mixture was stirred for about 5 minutes and then was placed in an ultrasound bath at 40 °C for 1 hour. Later it was refluxed for 3 hours at 80 °C. The obtained dispersion was then filtered with a 14-19 μm filter in order to remove not well-dispersed particles. The particle size distribution of the dispersed nano-clay was analyzed using a Malvern Zetasizer Nano ZS Particle and ZetaPotential Analyzer. Samples were highly diluted (c<0.1 wt %). The distribution obtained was found equal to that reported in the technical sheet for Cloisite®Na^+.

2. The MMT water dispersion was than mixed with the SB dispersion and distilled water. In order to obtain the desired proportion of polymer and MMT particles the solid content of the MMT water dispersion (MMTD) was determined according to DIN EN ISO 3251, along with the exact solid content of the as delivered SB latex.

The final coating was obtained by stirring for 15 minutes the SB latex (SB), the MMT water dispersion (MMTD) and distilled water. The mixing proportion was

calculated according to the following equation:

$$SB[g] = \frac{scSBx \times SBMMT_x[g]}{scSBC[\%]} \times 100 \qquad with \quad scBx = \frac{a}{1+x} \tag{3.1}$$

$$MTTD[g] = \frac{scSBx \times SBMMT_x[g] \times 0.05}{scMMTD[\%]} \times 100 \tag{3.2}$$

$$H_2O = SBMMT_x[g] - SB[g] - MTTD[g] \tag{3.3}$$

where
$scSB_x$ is the solid fraction of the SB polymer in the SB_MMT coating;
a is the solid content of the dispersion employed which was 20 wt% (a=0.2) for the single fiber dip-coating;
$SBMMT_x$ is the desired amount of polymeric dispersion used for the modification of the fibers express in gram;
scSBC and scMMTD are respectively the solid content in percentage of the as delivered SB latex and the nanoclay aqueous dispersion determined according to DIN EN ISO 3251;
and x is the amount of nanoclay express as fraction, which is equal to 0.05.
The parameter scSBx was obtained considering a final solid content of the polymeric dispersion (SBMMTx) of 10 %. Coating CSB and CSB5 were obtained by adding a methylolmelamine crosslinking agent (Lefasol VP 4-5 LF, Lafatex Chemie GmbH) under stirring to the SB and the SB5 dispersion respectively. The amount of the cross-linking agent employed was the 7.5 % of the Lefasol VL 90/1 according to what suggested by the producer.

Rovings Coating

The sizing used for the 17 μm multifilaments strands consist of the N-propyltrmiethoxysilane coupling agent a non-ionic surface active agent (Genapol DU 50, Clariant) and a small percentage of the carboxylated and self-crosslinking Styrene-Butadiene latex Lefasol VL 90/1 used as film former. After spinning and assembling process four different coatings were applied on the obtained rovings by means of a pilot coating plant at the IPF (Figure 3.7).

The roving was pass with a speed of 0.10 $mmin^{-1}$ through a pipette containing the polymeric dispersion whose composition and solid content is summarized in Table 4.9. The polymeric latex was constantly pumped in the pipette as shown in Figure 4.8 . Successively the rovings were dried by passing through a IR-drying sector and a convection oven set at 140 °C.
After coating the rovings were directly catted in 50 cm stabs and placed in oven at 140°C for 3 h to ensure the complete filmation of the polymer. The effective quantity

(a) Assembled roving passing through the coating and entering the IR-drying sector.

(b) Roving exiting the IR-drying sector.

Figure 3.7: Coating plant at IPF.

of coating applied on the rovings (Table 3.7) was determined by pyrolysis (600 °C, 60 min), according to DIN EN ISO 3251.

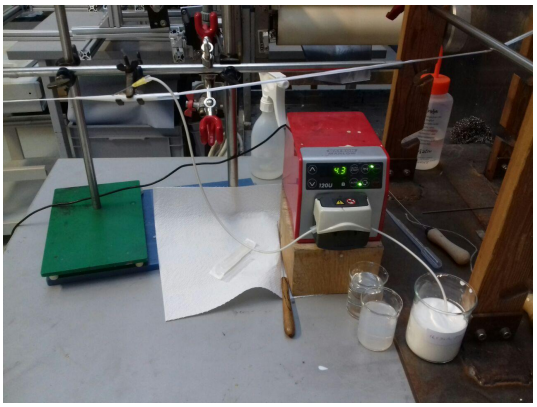

Figure 3.8: IPF PTMO roving passing through the pipette with the coating.

Coatings SB20 and SB80 were obtained following the same procedure described for the coating SB5, varying the proportion of polymer and MMT dispersion. The final amount of MMT in the coatings SB20 and SB80 is the 20 % and 80 % of the polymer content. Therefore, the parameter x, used for the calculation of the polymer and MMT dispersion ratio, is equal to 0.2 for SB20 and 0.8 for SB80. The parameter scSBx was obtained considering a final solid content of the polymeric dispersion (SBMMTx) of 10 % (a=0.1).

Table 3.9: Composition and percentage weight of the applied coatings.

Sample name	**Coating composition**	**Dispersion solid content [wt%]**	**Sizing/Coating weight [wt%]**
PTMO	-	-	0.46
IPF SB	Carboxylated self-crosslinking styrene-butadiene compolymer (SB)	9.94	5.59
IPF SB5	SB with 5 % MMT	10.11	4.24
IPF SB20	SB with 20 % MMT	10.17	4.19
IPF SB80	SB with 80 % MMT	9.22	3.53

3.1.3 Cementitious Matrix

The matrix employed in this work consists in a mix of cement, hydrated lime, calcium carbonate and dry polymers (Tab. 4.10), according to the typical composition of commercial available premixed mortars employed for rehabilitation intervention on masonry structures. Table 4.11 reports the compressive and flexural strength of the two matrix evaluated on prismatic specimens, with dimensions of 40x40x160 mm^3, cured 28 days at 20 °C, 70 % relative humidity (RH), according to UNI EN 1015-11:2019.

Table 3.10: Matrix Composition.

Material	**CEM II/B-LL 42.5 R**	**CEM II/B-LL 32.5 R**	**$Ca(CO_2)_3$ 600**	**$Ca(CO_2)_3$ 400**	**Aerial Lime**	**Dry polymer**	**Water**
kg/m^3	165.1	82.7	206.3	715	110.1	20.8	260
% p/p	*12.7*	*6.4*	*15.9*	*55*	*8.5*	*1.6*	w/b=0.7

b: cement + aerial lime

Table 3.11: Mechanical properties of the cement-based mortar at 28 days curing.

Compressive strength σ_c[MPa]	**Flexural strengthσ_f [MPa]**
17.95	5.66
(4.35%)	*(5.61%)*

3.2 Methods

The analytical methods employed in this work can be roughly divided in mechanical test and chemical-physical analysis. The mechanical tests conducted are: compressive and bending tests, tensile test and pull-out test. These tests have been carried out on the materials components and the composite as characterization methods and to evaluate the effect of chemical treatments on the mechanical properties and durability of the material. For IPF-AR-Glass fibers tensile test and pull-out test have been carried out on a macro and micro scale. The chemical-physical analysis adopted include: Furier Transformed Infrared-spectroscopy (FTIR)-analysis, Scanning Electron Microscopy (SEM) and SEM-EDX-analysis, Atomic Force Microscopy (AFM)-analysis, Electronic Microscopy, Thermogravimetric Analysis and Differential Scanning Calorimetry (TGA and DSC), Xray-diffraction (XRD) and Ion Chromatography (IC) analysis. They have be used to investigate the chemical composition and properties of the sample in the different phases of the experimentation, for example in order to characterize: the obtained materials, the effectiveness of chemical treatments, the properties of experimental coatings and the effect of environmental exposure on the chemical composition of the sample.

3.2.1 Macro-mechanical Tests

Single Yarn Tensile Test

Tensile test on multifilament yarn is a standard practice for the determination of yarn tensile strength, elongation at break and modulus. It should be kept in mind that even considering an ideal bundle, consisting of continuous filament, evenly loaded, and exactly parallel to the load axis during testing, the tensile strength measured will be less than the mean strength of single fibers. This results from the distribution of the single filaments tensile strength that compose the yarn [129]. When the filaments with a tensile strength lower than the mean fail, the other fibers will be subjected to a higher load, resulting in a reduced overall stress required for the failure to occur. Moreover, in real sample, single filaments are not uniformly elongate between the machine gripping, enhancing the phenomena of overload of single filaments. Finally, when single filament fail in a yarn during the test, interfilament friction might cause a premature fracture of adjacent fibers. For those reason single fiber tensile strength usually furnished more accurate date for the characterization of the material. However, single yarn tensile test is particularly suitable to evaluate the effect of coating on the tensile test of the reinforcement. As already discussed in section the application of sizing and coating on multifilament yarn can have a grate impact on the tensile behavior of the reinforcement since they can improve the stress transfer between the single filaments, resulting in higher tensile strength. In this case the yarn can be considered as a composite itself, which characteristic can be determinate according to the ISO 10406-1:2015 [130]. The same test procedure was

employed for both dry and coated multifilament yarns.

For the realization of the samples 300 mm long single yarns were cut from the wrap direction of the Carbon and BM-AR-glass fabric and reinforced at the two extremities of the yarn with fiber reinforced polymer tabs (Fig.4.9). A macroextensometer with gauge length of 50 mm was positioned at the yarn center and used to calculate the tensile strain and elastic modulus. The test were performed in displacement-control with a velocity of 0.5 mm/min for glass fibers and 1 mm/min for carbon fibers.

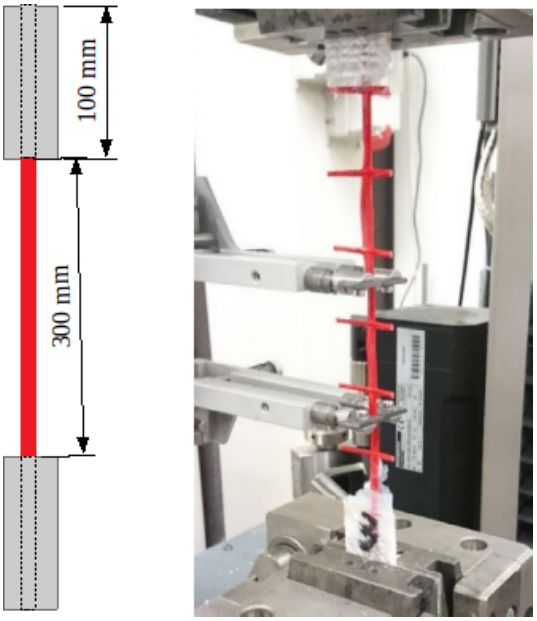

Figure 3.9: Tensile test specimen.

The mechanical properties of the yarns can be characterized by means of three parameters: the maximum tensile strength σ_{max}, the Young's modulus E and the ultimate strain ε_u. The tensile strength σ_{max} expressed in pascal is calculated at the maximum tensile force F_{max} expressed in newtons divided by the cross-sectional area A expressed in square millimeters (Eq. 3.4). The Young's modulus E is calculated from the difference between the tensile force obtained at the 20 % and 50 % of the load capacity divided the difference for the correspondent strain values (Eq. 3.5). The ultimate strain is defined as the strain corresponding to the ultimate tensile capacity.

$$\sigma_{max} = \frac{F_{max}}{A} \tag{3.4}$$

$$E = \frac{F_{50} - F_{20}}{(\varepsilon_{50} - \varepsilon_{20})} \tag{3.5}$$

Matrix Compressive and Flexural Strength

Sample were realized using a metal molds in accordance with UNI EN 1015-11 (Fig. 4.10. Specimens were cured under different protocols according to the purpose of the test and will be specified in further sections. For the characterization of the mortar

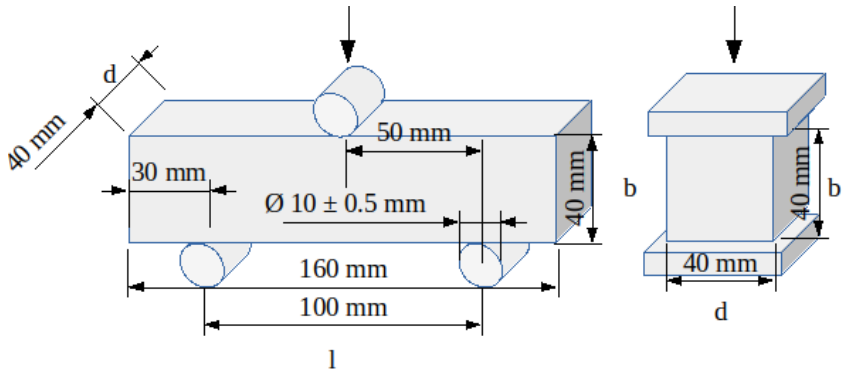

Figure 3.10: Geometrical parameters of mortar samples.

two main parameters were evaluated, the compressive and the flexural strength, performed according to UNI EN 1015-11. The test consists in a three point flexural test conducted on prismatic sample with dimension 160x40x40 mm^3, followed by a compressive test performed on the two halves of the sample obtained. Test were performed with a universal testing machine StiroLab ES.50 with a loading cell of 50 kN. The load was applied with a constant rate of 50 N/s for the flexural test and of 350 N/s for the compressive test. Compressive and flexural strength are calculated according to respectively Equation 3.6 and 3.7

$$\sigma_f = 1.5\frac{Fl}{bd^2} \tag{3.6}$$

$$\sigma_c = 1.5\frac{F}{bd} \tag{3.7}$$

where F is the maximum force measured and b,d and l are the specimen dimension as reported in Figure 4.10.

Pull-out

Pull out specimens were realized by embedding a multi-filament roving or a single yarn without transverse element cut from the warp direction of the fabric in a cubic mortar with the dimensions of 50x50x50 mm^3. The specimens were realized by placing the yarn between to layers of mortar (Fig. 4.11). The casting form was realized so as to obtain a smooth surface on the up face of the mortar cube. The free length of the carbon yarn was coated with a rigid epoxy resin to facilitate the gripping during the test and avoid undesired yarn rupture out of the embedded

section. For IPF glass roving the free length was glued between to metal plates (Fig. 3.12), in order to prevent the damage to the fibers and the deformation of the specimen out of the matrix. Test were performed by blocking the mortar cube in a metallic frame and pulling the yarn from the top side of the specimen as shown in Figure 3.12. A tensile testing machine with a load cell of 5 kN was used. The test was conducted under displacement control at 1 mm/min (0.016 mm/s).

Figure 3.11: Casting form used for the realization of the pull-out samples.

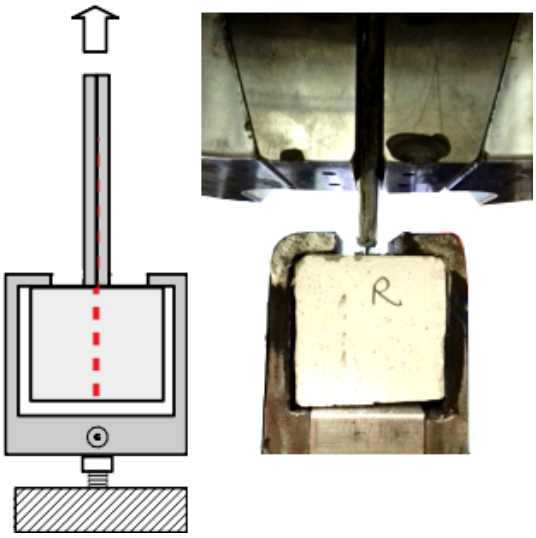

Figure 3.12: Pull-out setup.

For the characterization of the pull-out behavior the following parameters were considered: the maximum force F_{max}, the corresponding displacement s_e, the maximum shear stress τ_e, and the pull-out work W. The shear stress was calculated according to the following equation:

$$\tau_e = \frac{F_{max}}{hp} \tag{3.8}$$

where
h is the embedded length

p is the perimeter of the yarn cross-section.

The perimeter was determined measuring the cross-section of the yarn in the specimens after pull-out, using a macroscope Laica DFC320. For carbon yarn the different chemical treatment and coatings employed, were not found to particularly influence the geometrical properties of the yarns. Therefore, for all the specimens the perimeter was considered equal to 12 mm. This vale was determined as the average of values obtained measuring the cross-section of specimens with different carbon yarns. On the contrary coated IPF roving exhibit a marked reduction of the external perimeter compared to IPF PTMO (Fig. 4.13). Therefore, two different parameters for the sized and the coated rovings were used. The perimeter was calculated as an average value obtained from at least 4 samples for uncoated and coated yarns and correspond to 8.1 mm for the uncoated rovings and 3.9 mm for the coated ones.

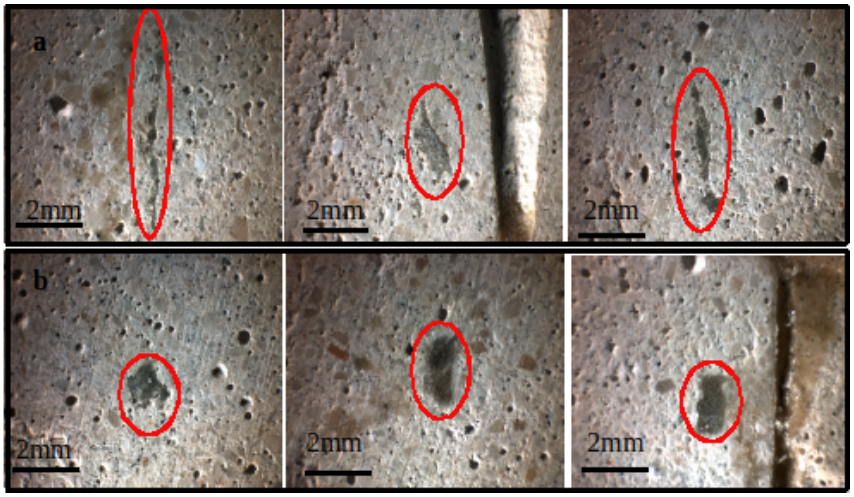

Figure 3.13: Macroscope images of the pull-out sample cross-section for uncoated yarn a) and coated yarn b).

The pull-out Work was calculated as the area under the pull-out curve, till a maximum displacement of 3 mm for glass fibers and 4 mm for carbon fibers.

Tensile Test

As discussed in Chapter 2.2.1 the grip systems employed to fix the composite coupons at the testing machine influenced the stress-strain curved obtained from tensile test analyses. The clamping grip is reported to prevent the fabric to slip inside the cementitous mortar, and since the pull-out of the fabric is of relevance for the purpose of this work a clevis-grip was preferred. Sample where realized according to the AC434.13. For what is concern the contact length of the metal tabs this is not specifed by the AC434.13, that only recommend a minimum length of 75 mm. Previous studies conducted by Donnini et al. reports that a length of 150 mm was the most suitable for the characterization of the FRCM specimens, therefore this

specimen geometry was adopted [53].
Sample consist of prismatic coupons with dimension 400x70x12 mm^3 realized by successively application of a first layer of mortar of about 50 mm, the reinforcement fabric, and a final mortar layer (Fig. 4.14). The reinforcement was cut in order to have three yarns inside each coupon. Specimens were tested using a universal testing machine with a total capacity of 50 kN. Tensile test were conducted under controlled displacement of 0.5 mm/min, the axial force was recorded by means of an integrated loading cell. The axial deformation was measured by means of a macro extensometer with a 100 mm gauge length positioned on the free length of the coupon. Sample were griped at the testing machine using a clevis type grips according to the Annex A –AC434.13. The steel tabs employed were glued to the coupons by using an epoxy adhesive.

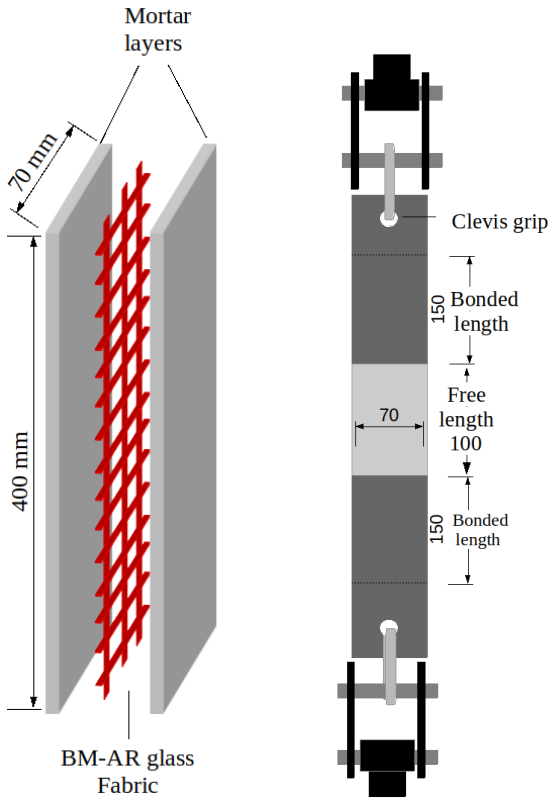

Figure 3.14: Schema of the FRCM coupon used for tensile test.

The ultimate tensile stress was obtained by dividing the maximum force by the cross-section of the fabric in the load direction 3.9. The modulus of elasticity in the cracked phase (E_u) has been calculated as the slope of the stress-strain curve in the region between 0.60 and 0.90 $\sigma_{u,f}$.

$$\sigma_{u,f} = \frac{F_{max}}{A_3} \tag{3.9}$$

with A_3 being the cross-section of the fabric calculated as the cross section of the single yarn multiplied for the number of the yarns embedded in the matrix.

$$E = \frac{\sigma_{60} - \sigma_{90}}{(\varepsilon_{60} - \varepsilon_{90})} \tag{3.10}$$

3.2.2 Micro-mechanical Tests

Single Fiber Tensile Test

As already discuss in the previous sections the single filaments composing a yarn, present a variability in tensile strength, which is the result of surface defects that arise during the manufacture of the products. Fibers behave as brittle, elastic solids whose failure occur at the largest flaw in the sample and the tensile strength of the materials is given from the strength of the fibers on its weakest region. It follows that the tensile strength of single fibers is a statistical value that can not be fully characterize by a single parameter. A more accurate description of the fibers tensile behavior can be obtained using a two parameter Weibull distribution, where the scale value σ_0, represents the stress at which 63,2 % of the sample break, and the Weibull modulus m, also call the shape parameter, gives a measure of the data distribution. The model consider the fibers as the sum of N units each characterized by a tensile strength σ_n and a probability of failure $P_{(\sigma n)}$ [131]. The probability of failure is than described by the equation:

$$P_{(\sigma)} = 1 - exp[\frac{-L}{L_0}(\frac{\sigma}{\sigma_0})^m] \tag{3.11}$$

where L is the length of the fibers tested (the gauge length), σ is the strength at failure, and L_0 and σ_0 are scaling constant. The equation is usually used in is logarithmic form: The probability of failure is than described by the equation:

$$ln[ln(1 - P_{(\sigma)})] - ln(\frac{L}{L_0}) = mln(\sigma) - mln(\sigma_0) \tag{3.12}$$

that for constant value of L can be rewritten as:

$$ln[ln(1 - P_{(\sigma)})] = mln(\sigma) + k \tag{3.13}$$

where k is a constant.

This equation consents a graphical determination of the Weibull modulus as the slope of the data obtained plotting $ln[ln(1 - P_{(\sigma)})]$ against ln(σ). The probability of fracture P will be determinate from a set of samples fracture, ranking the data from weakest to strongest and applying the following equation:

$$P_i(\sigma) = i - \frac{0.5}{N} \tag{3.14}$$

where i is the rank for the ith value and N is the number of fibers tested. The interpolation of the data, which in this work was conducted with the method of the last squares, gives a straight line whose angular coefficient is the Weibull modulus and the interception with the y-axis is the scale parameter σ_0. It follows that high value of m will give line with a steep slope, while change in the scale parameter σ_0 shift the line to the right or to the left respectively for higher or smaller value (Fig. 4.15).

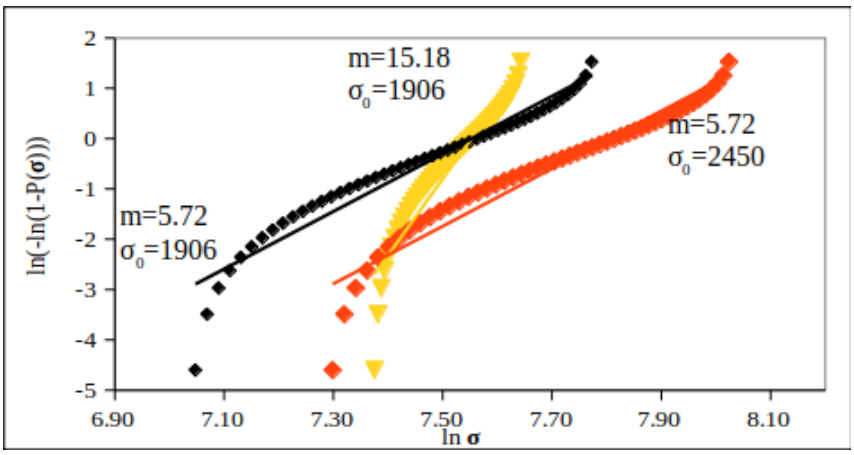

Figure 3.15: Wiebull distributions with different shape and scale parameters.

Single fiber tensile test was conducted with a Favigraph$^+$ testing device (Texchno, Mönchengladbach, Germany) equipped with a 1 N load cell and integrated with a vibroscope for the determination of fibers fineness according to ASTM D 1577. The single filaments were carefully separated from the multifilament strand with the help of apposite needle and tweezers, and elongate in the machine clamps. The filaments' fineness is than measured from the resonance frequency of the fibers detected by the integrated vibroscope. The resonance of the fibers is induced by a sinusoidal sound wave produced by the testing machine, while the fibers is subjected to a pretension load of 1 cN/tex. The filaments fineness (T) will than be automatically calculated according to the following equation:

$$T = \frac{F}{f^2 l^2} \tag{3.15}$$

with F being the pretensions load, f the detected frequency and l the gauge length. For an accurate statistic evaluation results are based on 50 measurements for each sample.

Single Fiber Pull-out

Single fiber pull out tests were conducted using a specialized pull-out apparatus at the IPF, with force accuracy of 1mN and a displacement accuracy of 0,07 μm [132, 133]. Test were conducted in quasi static condition with a loading rate of 0,01 μm/s at

ambient conditions. Sample were prepared using a specific equipment designed and constructed at Leibniz-Institut für Polymerforschung, Dresden [132, 133, 134] under controlled atmosphere and temperature (23°C, 50 %). Samples were realized by embedding the fibers for a length of 1000 µm in droplets of fresh mixed matrix, placed on cylindrical samples holder with an inner diameter of about 2.6 mm. Those were obtained by mixing the premixed matrix with tap water in a speed mixer with a 1.14 water : binder ratio. The higher water dosages employed, compared to that used for the realization of matrix prisms and yarn pull out specimens, was necessary to obtain an adequate shape of the matrix droplets. 19-20 specimens were tested for each fiber/matrix combination. The specimens were cured for 28 days at a constant temperature of 23 °C and 90 % relative humidity. The effect of the coatings on the fibre-matrix interface and pull-out behavior was evaluated comparing the interfacial shear strength (IFSS) and the pull-out work obtained for the different coatings investigated. The IFSS was calculated from the maximum force Fmax according to the following equation

$$IFFS = \frac{F_{max}}{\pi \cdot d_f \cdot l_e} \tag{3.16}$$

were d_f is the fiber diameter and l_e is the embedded length, which were measured after test by optical microscopy.

3.2.3 Chemical-Physical Analysis

Fourier-Transform Infrared Spectroscopy

IR analyses were conducted on the BM reinforcement in order characterize the chemical composition of the coating. For this propose a Spectrum GX1Perkin Elmer spectrometer, coupled with a microscope Autoimage equipped with a U_ATR (SensIR Technologies), was used. IR analyses were performed also to investigate the chemical composition and the cross-link mechanism of the SB coating employed for the modification of the IPF fibers. For this propose a Vertex 80v (Bruker) spectrometer equipped with a Golden Gate Diamant ATR element (SPECAC) and an MCT detector was used.

X-Ray Diffraction

X-Ray diffraction analyses were conducted on the matrix after aging in the saline solution in order to investigate the possible formation of gypsum or etringite. X-ray diffractrograms were also used for the characterization of the SB polymer with dispersed nano-clay particels. A physical admixture of nano clay and polymer does not necessarily form a nanocomposite. A fundamental prerequisite to obtaine a polymer-layered silicate nanocomposite is that the nano-clay particles incorporated into the matrix are either intercalated or exfoliated in the polymeric matrix. XRD is commonly employed for this scope [87]. Indeed, when polymeric chains intercalate

between the nano-clay platelets the distance between the layer increase, and the diffraction angle measured with XRD decreases according to the Bragg's law,

$$sin\theta = \frac{n\lambda}{2d}, \tag{3.17}$$

where λ is the wavelength of the incident wave, θ is the angle of incidence d is the interplaner distance between the lattices planes (the silicate layers) and a positive integer. In case of exfolation of the silicates' particle the diffraction lattice is lost so that no more diffraction peaks are visible in the XRD diffractograms. XRD analyses were conducted with a Bruker D8 Advance difractometer, with incident wave length radiation of 1.54060 Å. Data acquisition was performed between 2° and 30° using a scanning speed of 2 s/step.

Thermogravimetric Analysis

Addition of small amount of nanoclay in polymers usually lead to an enhanced thermal stability of the polymer which can be measured by TGA analysis [87]. This phenomenon is usually observed in exfoliated nanocomposites and it is explained by a decreased permeability of volatile decomposition products because of the formation of a char. Thermal degradation was determined on approximately 10 mg samples in a TGA Q500 balance in nitrogen atmosphere with a 10 °C/min heating ramp. Thermo-oxidation was determined in the same way in air atmosphere.

Differential Scanning Calorimetry

Although experimental results are sometimes contradictory, an increase of T_a values is usually considered an evidence of polymer intercalation due to the confinement of polymeric chains into the nanoclay layers [87, 135]. For this reason DSC analysis were conducted as supporting method for the characterization of the nanoclay-SB coatings. DSC was performed on a DSC Q2000 in the 95°–200° at the programmed heating rate of 10°C/min. Both TGA and DSC analyses were conducted at the IPF.

Scanning Electron Microscopy

SEM analyses were conducted on the IPF glass fibers to obtained topographical information of the fibers surface after modification of the coatings, and aging in alkaline and saline solutions. These analyses were conducted at IPF with a Ultra plus (Carl Zeiss NTS) microscope in high vacuum and an accelerating voltage of 3 kV. SEM images of the IPF rovings and pull-out specimens after test were acquired with a FESEM ZEISS SUPRA 40 in high vacuum and accelerating voltage of 25 kV.

Energy Dispersive X-ray

SEM-EDX analyses were employed to investigate the surfaces of carbon fibers after oxidative treatment and immersion in the nano-silica dispersion. For this propose a

FESEM ZEISS SUPRA 40 with a EDX-Detector Bruker Quantax 200-Z10 was used. SEM-EDX evidences were also coupled with the results obtained from the XRD difractogram in order to characterize the polymer with incorporated nano-clay. For this purpose a SEM Ultra Plus (Zeiss, Oberkochen, Germany) with a EDX-Detector X-Flash 5060F (Bruker, Berlin, Germany) available at the IPF was used.

Atomic force microscopy

Atomic force microscopy (AFM) was used to investigate the morphological structure of the IPF fibers surface after modification with different coatings. Analysis were conducted using a Dimension Icon (Bruker Corporation, USA) equipped with a Tap300-G BudgetSensors (Innovative Solutions Bulgaria Ltd., Bulgaria) cantilever made of monolithic silicon with a rotated pyramid shaped tip and a tip radius less than 10 nm. Roughness parameter in terms of arithmetic average roughness ($R-a$) and maximum roughness (R_{max}) were obtained recording topography images with dimension 3 μm $\times$ 3 μm and 512 px $\times$ 512 px in tapping mode. Results were reported as the average of at least 3 images for each fiber type.

Ion Chromatography

Ion Chromatography analysis (IC) were conducted to investigate the permeation of ions in the cementitous matrix after conditioning in NaOH and saline solution. A total of 500 mg of fine-grained samples collected from the core of prismatic specimens was added to a 500 mL volumetric flask and made up to volume with distilled water. The flasks were immersed in an ultrasonic bath at 40 °C for 20 min. The pH of the dispersion obtained was measured with a pH meter Denver Basic and found equal to 11.7 for all three samples. The solution was then filtered with a 0.2 μm pore size membrane filter and analyzed with an Ion Chromatograph Dionex ICS-900 and DX-100. The mass percentage was than calculated considering the all soluble ions in the matrix to be extracted.

Formation of Hydration Products

Addition of nanoparticle in polymeric coating for modification of fibers employed in concrete reinforcements is reported to favorite the formation of hydration products at the fibers-matrix interface [40]. However, the detection of hydrated products on the surface of fibers extracted from the cementitous matrix is not possible, since during the pull-out the coating on the fiber surface is removed. Therefore, an alternative method was developed which consisted of immerse the coated fibers in an aqueous concrete solution In order to evaluate the promotion of crystal formation at the fibers surface, fibers coated with SB polymer and SB-nanoclay polymer were immersed in an aqueous concrete solution. The solution was obtained by adding 40 g of a cement matrix (BMK-D5-1) in 200 ml distilled water in a volumetric flask. The flask was

ultra-sonicated for 1 hour, after that the solution was filtrated with a 10 to 15 μm filter. Both single fibers and rovings where immersed in the solution and let stay overnight. Then, they were removed from the solution, washed 1 hour in distilled water and successively observed by SEM to analyse the effect of nano-clays on the formation of hydration products. Microscopy images of the fibers were than acquired with a Digital-Mikroskop Keyence VHX2000.

Matrix pH

It is well known that the pH value of cementitous matrices decrease over time due to the carbonation, that occurred when CO_2 dissolves in the concrete pore fluid and reacts with $Ca(OH)_2$. In order to investigate how the aging protocols effect the carbonation of the matrix tests according to EN 13295 were performed. The test consists in spraying a phenolphthalein solution on the surface of the concrete sample. Phenolphtalein solution are commonly used as pH indicator. At pH lower than 8.3 phenolphtalein exists in its lacton form an is colorless, while at pH between 8.3 and 10.00 it deprotonats assuming a typical pink coloration. Typical pH value of uncarbonated concrete are greater than 9, therefore the depth of carbonation can be measured by measuring the portion of the sample that remains colorless when it comes in contact with the phenolphthalein solution. The phenolophthalein solution was obtained by dissolving 0.5 g of phenolphthalein powder in 50 ml Ethanol and make up the volume to 100 ml by adding distilled water. The obtained solution was sprayed on the cross-section of the matrix after aging protocol and one year after aging protocol.

3.2.4 Aging Protocols

The environmental exposure investigated in this study consist of accelerate aging tests in alkaline saline and freeze-thaw cycles in accordance to the AC 434-13 and the Italian CSLPP. Table 4.13 reports an overview of the protocols adopted and the test performed.

Mortar prisms and FRCM coupons were cured for 28 days at laboratory conditions (20 °C, 70 % RH) and then subjected to different aging protocols. By doing so, the total curing time of all specimens was about 70 days (111 for IPF specimens). Exposure to alkaline or saline environments was conducted by completely immersing the specimens in the solutions, for the pull-out specimens the free length of the yarn was kept out of the solution.

Table 3.12: Aging protocols.

Denomination	**Time of exposure**	**Temperature**	**RH**	**Solution**	**Specimens tested**
Reference (Rif)	-	20 °C	70 %	-	3 Matrix prisms, 5 Pull-out specimens, 4 Tensile test coupons (SB-BM), 5 Tensile test yarn.
Water (W)	1000 hrs	40 °C	100 %	Tap water	3 Matrix prisms, 5 Tensile test yarn.
Saline (S)	1000 hrs	40 °C	100 %	2.45 % NaCl + 0.41 % Na_2SO_4	3 Matrix prisms, 5 Pull-out specimens (carbon fibers), 4 Tensile test coupons, . 5 Tensile test yarn (carbon, ARG-BM), 50 Single fiber tensile test
Saline (S)	2000 hrs	40 °C	100 %	2.45 % NaCl + 0.41 % Na_2SO_4	5 Pull-out specimens, 5 Tensile test yarn . (IPF roving)
Alkaline NaOH (NaOH)	1000 hrs	40 °C	100 %	4 % NaOH	3 Matrix prisms, 5 Pull-out specimens, 4 Tensile test coupons (ARG-BM), 5 Tensile test yarns (carbon, ARG-BM), 50 Single fiber tensile test.
Alkaline 3 Ions (3)	1000 hrs	40 °C	100 %	1.7 % $Ca(OH)_2$ 0.9 % NaOH 1.82 % KOH	5 Tensile test yarn (ARG-BM), 50 single fibers tensile test
Alkaline 3 Ions (3)	2000 hrs	40 °C	100 %	1.7 % $Ca(OH)_2$ 0.9 % NaOH 1.82 % KOH	5 Tensile test yarn, 50 Pull-put specimens (IPF roving)
Freeze-Thaw (FT)	960 hrs (40 cycles)	-18 °C/ +40 °C	40 %/ 100 %	-	3 Matrix prisms 5 Pull-out specimens (carbon, ARG-BM) 4 Tensile test coupons (ARG-BM)

Chapter 4

Results

4.1 Cementitious Matrix

In this chapter the results obtained for the tests conducted on the cementitious matrix will be present. First the compressive and flexural strength of the specimens subjected to different aging protocols will be compared. Secondly some insight in the chemical physical change of the matrix under saline and alkaline exposure will be illustrated presenting the XRD and Ionchromatography results. Finally, some consideration on the carbonation process of the matrix in different aging condition will be presented. The results presented in this chapter will be essential to explain the aging behavior of the composites that will be illustrated in the following chapters.

4.1.1 Accelerate Aging

Compressive and Flexural Strenght

Tabel 4.1 reports the average compressive strength $\sigma_{c,m}$ and flexural strength σ_f , together with the corresponding coefficient of variation, CoV (%).

A significant difference in the mechanical properties of samples cured under laboratory conditions (20 $\circ$ C, 70 % RH) can be found after 28 days (Mortar_Rif_28) and 70 days curing (Mortar_rif_70). The increase in the compressive (+26 %) and flexural strength (+73 %) of the matrix after the supplementary 42 days proves that the curing process was not completed in the first 28 days. Similar results have been reported by Garijo et al. for hydraulic lime mortars [136]. Because the matrix employed in this work contains both cement and aerial lime, the hardening process of the matrix is expected to be governed on one hand by the hydration of tricalcium silicate (C_3S) and dicalclium silicate (C_2S), and on the other hand by the carbonation of $Ca(OH)_2$. According to Lanas, the increment in strength of hydraulic based mortars is mainly due to the hydration of C_3S in the first 28 days of curing [137]. Over this time period the carbonation of the matrix has not taken place yet. Moreover, the hydration of C_2S is known to be much slower than that of C_3S [138]. Therefore, the increase in the mechanical properties of Mortar_rif_70 can be attributed on both the hydration of C_2S and the carbonation of $Ca(OH)_2$. After immersion in alkaline and saline solutions both the mortar compressive and the

Table 4.1: Mechanical properties of the FRCM matrix.

Specimen	**Compressive strength σ_c [MPa]**	**Increase/ Decrease**	**Flexural strength σ_f [MPa]**	**Increase/ Decrease**
Mortar_Rif_28	17.95 (4.35%)	-	5.66 (5.61%)	-
Mortar_Rif_70	22.55 *(11.72%)*	-	9.81 (6.41%)	-
Mortar_W	23.10 (4.20%)	+2.96 %	10.09 (6.41%)	+ 2.44
Mortar_S	24.99 (3.83%)	+ 8.2%	12.08 (8.58%)	+ 19.7%
Mortar_NaOH	25.37 (3.27%)	+ 9.8%	11.98 (9.63%)	+ 18.7%
Mortar_$Ca(OH)_2$	24.24 (5.74%)	+7.49%	10.21 (14.32%)	+4.18 %
Mortar_FT	21.83 (3.93%)	- 5.5 %	8.88 (7.04%)	- 12.0%

flexural strength are slightly higher than those of the same samples cured at standard condition. The higher mechanical properties observed are probably the result of an additional curing of the matrix promoted by the higher humidity and temperature (100 %RH, 40 °C). This is confirmed by the light improve in the compressive and flexural strength compared to Mortar_rif_70 observed also for the samples immersed in tap water. However, for samples immersed in the saline and alkaline solutions the improvement of the mechanical properties is even higher than for sample Mortar_W. This is probably due to the ions dispersed in the saline and alkaline solutions, that prevent the leaching of the matrix. On the contrary, samples subjected to freeze-thaw cycles showed a slightly lower compressive and flexural strength with respect to reference specimens. However, no evident sign of deterioration was observed by a first visual investigation of the specimens. As discussed in section 2.5 the process of cementitious materials subjected to freeze-thaw cycles, is usually related to the tensile strength of the matrix and its microstructure [112]. Lanas et al. found that hydraulic matrix are less damaged by freeze-thaw cycle than matrix based on aerial lime, and attribute the higher resistance of the first to its higher compressive strength and lower porosity [114]. On the base of the results obtained the mortar employed in this work doesn't seem to be particularly affected by freeze-thaw cycles. The lower mechanical performances observed are probably the consequence of the compromised curing process due to the low temperature and relative humidity (-18 °C, 40 % RH), rather than the results of a deterioration of the matrix. However, micropore investigation could help to correlate the microstructural nature of the matrix and its durability to

freeze-thaw cycles.

X-Ray Diffraction

As reported in section 2.5 usually degradation of cementitious mortars exposed to saline envioronments occurs due to sulphate attack, which causes the decalcification of the matrix when sulpahte ions react with portlandite (Eq. 2.3) and calcium silicate hydrate (Eq. 2.4), and crumpling and spalling of the mortar due to the formation of Ettringite (Eq. 2.5). Figure 4.1 shows that neither gypsum nor ettringite formed in the mortar immersed in saline solution, thus confirming that the mortar employed was not affected by this exposure condition, which is in accordance with the results obtained for the mechanical test.

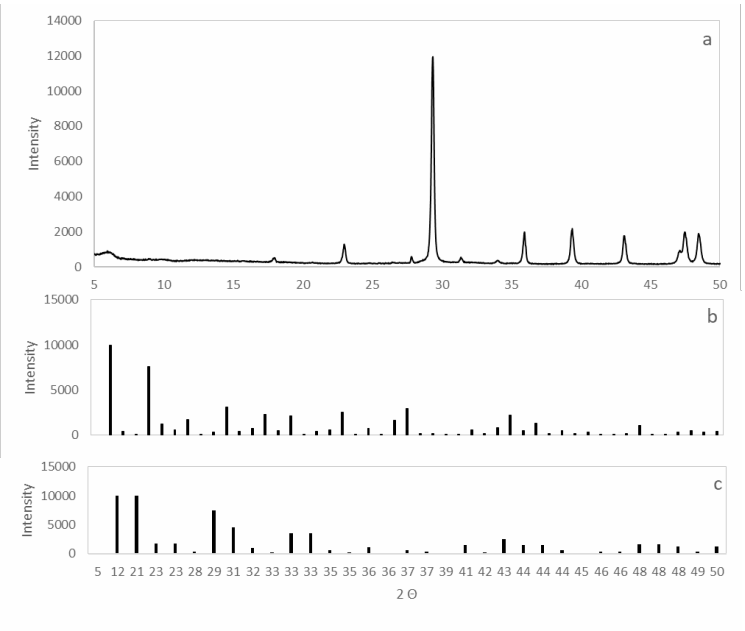

Figure 4.1: X-Ray diffractogram of Mortar_S simple a) compared with Ettringite diffractogram, b) and Gypsum diffractogram c) from database.

4.1.2 Ion chromatography

Tabel 4.3 reports the IC results from the Mortar samples.

Table 4.3: Ions detected in sample Mortar_70, _S and NaOH

	Sodium Na^+ [%]	**Calcium** Ca^{2+} [%]	**Chloride** Cl^-[%]	**Sulphate** $SO4^{2-}$ [%]
Mortar_70	0.04	4.44	0.01	0.10
Mortar_S	0.12	4.51	0.24	0.10
Mortar_NaOH	0.03	4.02	0.01	0.11

The percentage of chlorine and sodium ions in Mortar_S is much higher than that detected in the other samples, thus demonstrating the ions ability to penetrate inside the matrix. However, the same is not true for sulphate ions, probably because of the much lower concentration of Na_2SO_4 in the aging solution. It was also observed that sodium concentration in Mortar_NaOH specimens was lower than those of Mortar_S samples, even though the molar concentration of Na^+ was higher in the NaOH solution than in the saline solution. Because the studies conducted on the permeability of ions in concrete matrix usually aim to evaluate the exposure to saline solution, no studies on the migration of sodium from NaOH solution in concrete matrix are available. Moreover, while different data are available on the diffusivity of chlorine ions in concrete, experimental studies are usually less concern with the mobility of sodium in inorganic matrix. However, according to theoretical studies conducted on the diffusion of mixture of ions in concrete, the ionic species present in the solution may affect the mass flow of anions and cations [139] [140]. Moreover, experimental studies that document the effect of counter-ions and pH of the exposure solution on chloride binding in concrete matrix are also available [107]. Based on these studies, it seems reasonable to believe that the different penetration of Na^+ ions in Mortar_S and Mortar_NaOH samples was due to the high concentration of OH^- in the alkaline solutions. However, further studies are certainly needed to better investigate this phenomenon.

pH Values

As reported in section 2.5 alkali hydroxides, such NaOH and KOH, are known to be potentially harmful for the matrix, because they can promote Alkali-Silica Reaction (ASR) in presence of thermodynamically unstable silica [112, 113]. However, the matrix employed in this work do not contained aggregates that have been found to give ASR such as: opal, tridymite, cristobalite, volcanic glass, chart, cryptocrystalline (or microcrystalline) quartz and strained quartz [113]. Indeed, the compressive and flexural test results confirm that the matrix was not affected by the immersion in alkaline solutions. However, although high pH values are not usually considered to be potentially harmful for cementitious matrices, they are known to affect the properties of glass fibers, and polymeric coatings. Figure 4.2 shows that the matrix cured in laboratory condition presents a higher carbonation depth (about 0.77 mm) compared to sampled subjected to accelerate aging in saline and NaOH solution. Matrices subjected to saline and alkaline exposure both show a lower carbonation depth. This is probably due to the lower concentration of CO_2 dissolved in the aging solutions particularly at high pH value. Another reason for the higher pH of the matrix after immersion in saline and alkaline solutions can be its higher hydration rate compared to Mortar_rif_70, since $Ca(OH)_2$ is produced by the hydration reactions of C_3S and C_2S. Despite the different pH value of the Saline and NaOH solutions after 1000 aging the matrices display similar carbonation rate.

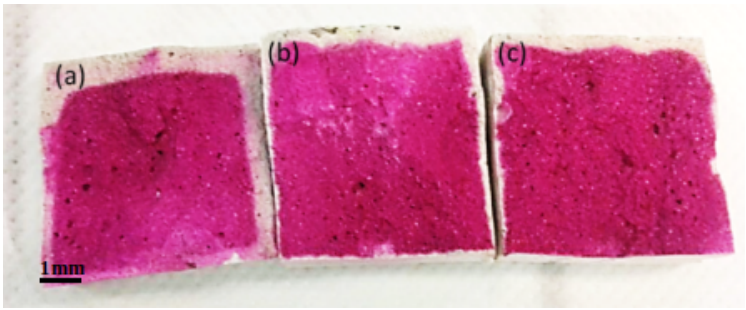

Figure 4.2: Carbonation depth of the matrix after a) 70 days curing in laboratory condition, b) accelerate aging in NaOH solution c) and saline solution.

On contrary Figure 4.3 shows that after further aging in saline and alkaline solution the carbonated area of the saline specimens has become brighter, and the pH of the matrix cured at laboratory is drastically decreased. This proves that immersion of the samples in the alkaline solution artificially keep the pH of the matrix at high level, while in a natural aging process the pH of the matrix would decrease over time.

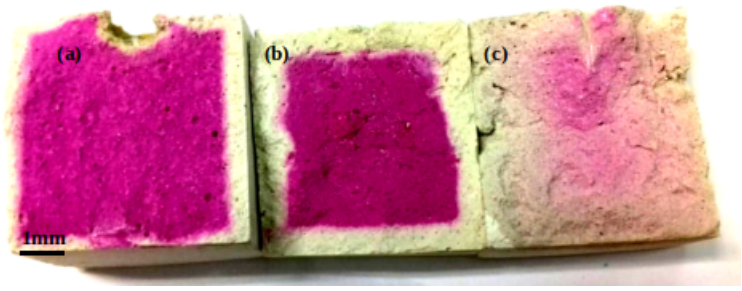

Figure 4.3: Carbonation depth of the matrix after 111 days curing in a) 70 in laboratory condition, b) accelerate aging in NaOH solution c) and saline solution.

4.1.3 Remarks

According to the results obtained the following remarks about the aging process of the matrix under different environmental exposure can be made:

- The curing process of the matrix is not completed in the first 28 days and the matrix experiment a significant increase in the compressive strength and flexural strength is observed at 70 days regardless of the curing protocols.
- No aging protocols particularly affected the mechanical properties of the matrix, which results slightly higher after immersion in alkaline and saline solutions, and slightly lower for samples exposed to freeze-thaw cycles.
- In general the mechanical properties of the mortar are meanly influenced by the temperature and relative humidity of the curing environments, with higher

RH % values and temperature resulting in higher compressive and flexural strength.

- Penetration of Na^+ and Cl^- ions in Mortar_S samples could be observed, although it has no consequence on the mechanical properties of the samples.
- The immersion of the samples in aqueous solution slows down the carbonation of the matrix, which display higher pH values over time compared to the reference, particularly after aging in alkaline solutions.

4.2 Preimpregnated ARG Fabric

This chapter reports the results obtained for the durability test conducted on the FRCM system based on a commercial available preimpregnated fabric in combination with the cementitious matrix which mechanical properties have been presented in the previous chapter. First the IR spectrum of the commercial coating will be presented in order to verify its chemical composition. Secondly, the results obtained from the aging test conducted on the fabric will be presented. Successively, these results will be compared with that obtained for the composite.

4.2.1 Coating Characterization

Figure 4.4 reports the IR spectrum obtained for the preimpregnated BM ARG fabric.

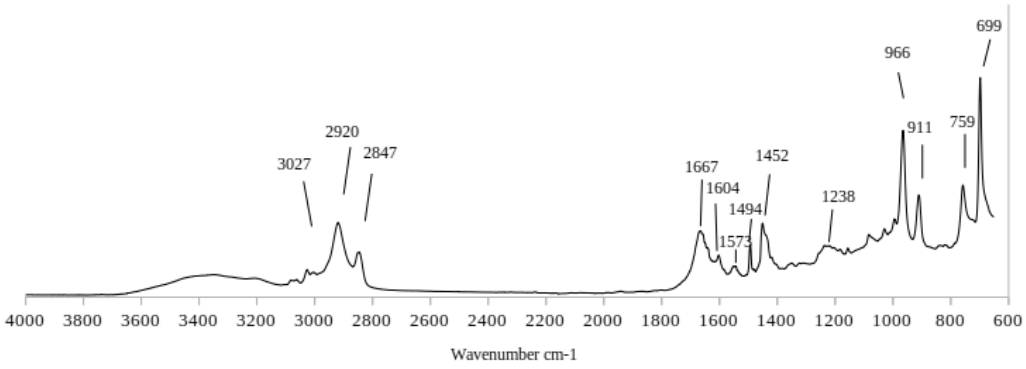

Figure 4.4: Spectrum of the coating on the as received BM-ARG fabric.

The IR spectrum of the SB coating is characterized by a strong band at 700 cm^{-1} and a smaller pick at 759 cm^{-1} which can both be attributed to the out of plan bending of the C-H on the phenil ring. The bands at 911 and 966 cm^{-1} arises form the C-H of the alkenes in the trans from. The absorption at 1452 is due to the C-H bending in alkenes groups. Between 1604 and 1667 cm^{-1} the absorption related to the C=C stretching mode of the alkenes and aromatic groups can be observed. The absorption at 2847 and 2920 cm^{-1} can be attributed to the C-H stretching of the alkyl chain of the polymer, while the pick 3027 cm^{-1} is in the region for the C-H stretching of aromatic and alkenes groups.

4.2.2 Accelerate Aging

Fabric

Figure 4.5 report the images of the SB fabric before and after aging protocols. It can be observed that on the surface of specimen S_40 have formed some salt crystal, those immersed in the alkaline solution present a darker coloration, while any remarkable change can be observed on sample FT.

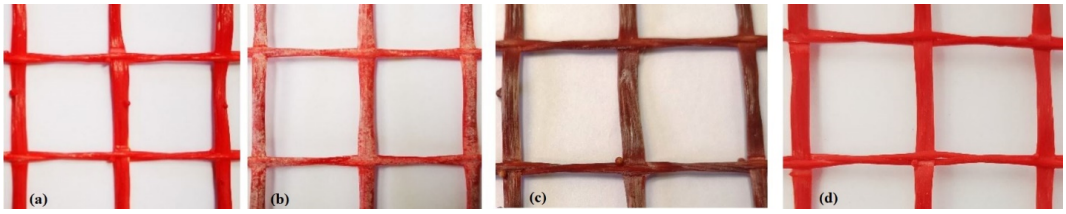

Figure 4.5: BM Fabric a) before aging and subjected to different aging protocols: b) saline, c) NaOH d) and Freez-thaw cycles.

Figure 4.6 reports the stress strain curves obtained for the BM yarns after different environmental exposures. The results obtained in terms of yarns tensile test ($\sigma_{max,yarn}$), elastic modulus (E_{yarn}), and ultimate tensile strain ($\varepsilon_{u,yarn}$) and the corresponding coefficient of variation (CoV) can be found in Table 4.4. For all the specimens a linear elastic deformation is observed, up to the failure of the specimens in its central part. All the specimens immersed in an aqueous solution show a decrease of the ultimate tensile strength σ_{max}. The more sever n the contrary tensile strength is observed for specimens subjected to the NaOH protocol (-25 %), however a similar loss in performance was observed also for sample BM_W (-20 %), while yarns immersed in the saline solution experiment a minor decrease of the tensile strength (-8 %). The ultimate tensile strain $\varepsilon_{u,yarn}$ was also reduced, while the elastic modulus E_{yarn} remained almost unchanged. Glass yarns exposed to freeze-thaw cycles (FT) showed a reduction of the ultimate tensile strength of about 8 %. AR-glass fibers are known to partially degrade in alkaline environment despite the presence of Zr which slows down the corrosion process. However, the results obtained for the yarn immersed in tap water at 40 °C, suggest that the degradation of the glass filament is probably not the only factor responsible for the loss in tensile strength of the yarn. As already discussed in the previous chapters, organic coatings are reported to increase the tensile strength of the reinforcement since they enable a better stress distribution between the single filaments. As can be observed in Figure 4.7b and c, after immersion in aqueous solution at 40 °C for 1000h hours a significant swelling of the yarns cross-section can be observed. This can be attributed to the low stability of the SB coating to the aging temperature. A partial dissolution of the organic coating would also facilitate the penetration of alkaline solutions within the yarn cross-section reducing the ability of the coating to protect the fibers from the alkaline attack. Experimental results showed that, although the yarns were constituted by AR glass filaments, the alkaline environment was found to be the most aggressive. For unknown reasons the yarns immersed in the saline solution were less damaged. Similar results have been reported from Nobili who observed a reduction of tensile strength of about 11 % for impregnated AR glass yarn immersed in a solution of 3.5 % NaCl [111]. However, the durability of glass-fibers in saline solution has been purely investigated and further studies are certainly needed.

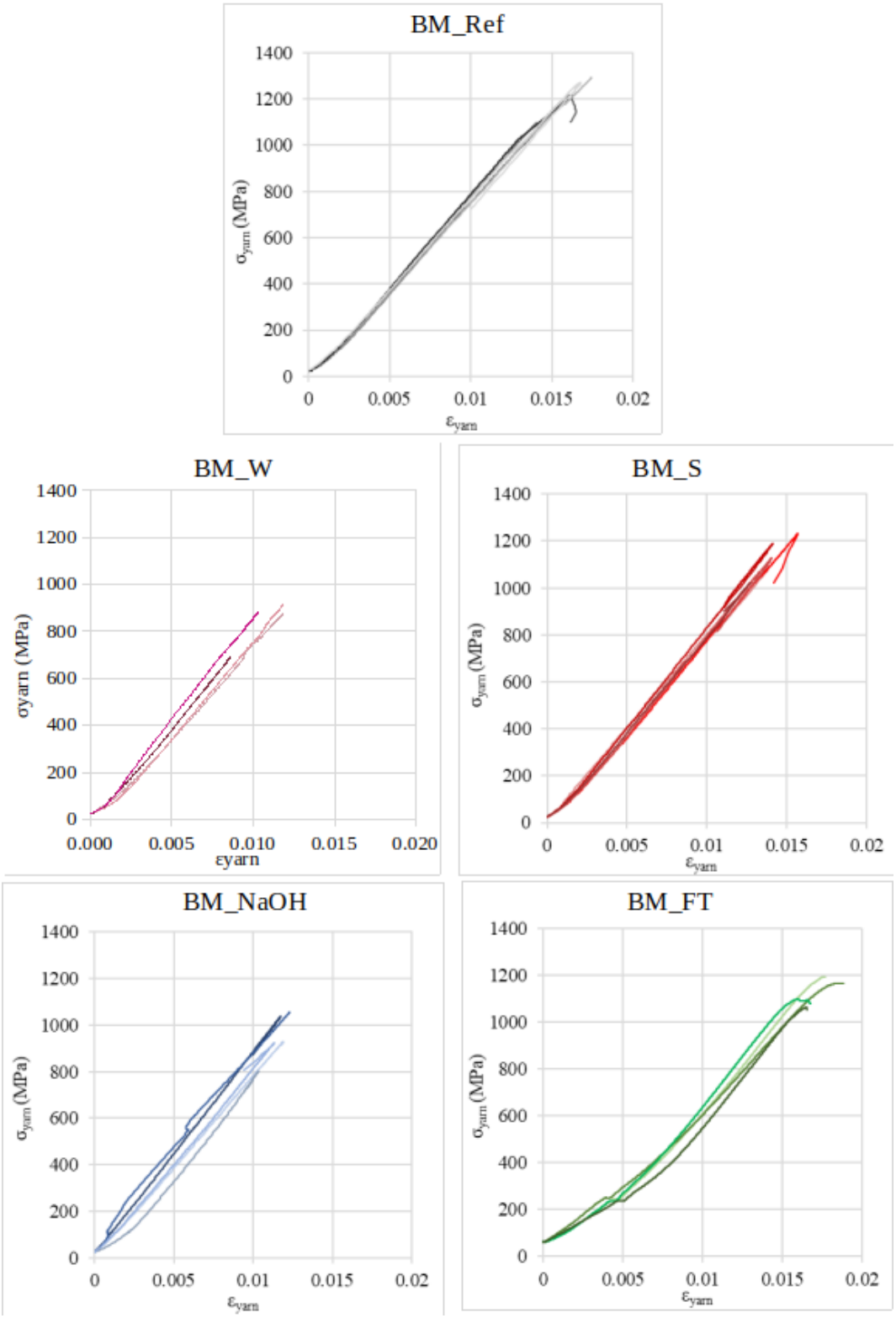

Figure 4.6: Stress-strain curves obtained from the tensile tests conducted on the ARG-BM yarns.

Table 4.4: Mechanical properties of the glass yarns before and after environmental exposure (CoV in round brackets).

Specimen	**Maximum tensile strength** $\sigma_{max,yarn}$ **[MPa]**	**Tensile strength increase/ decrease [%]**	**Elastic modulus** $\mathbf{E}_{yarn}$ **[GPa]**	**Ultimate strain** $\varepsilon_{u,yarn}$ **[%]**
BM_Ref	1236 *(10.3%)*	-	67.58 *(5.04%)*	1.7 *(12.32%)*
BM_S	1133 *(7.2%)*	-8.35	67.87 *(13.44%)*	1.4 *(9.73%)*
BM_NaOH	924 *(10.4%)*	-25.22	69.37 *(10.16%)*	1.1 *(5.75%)*
BM_W	*896* *(2.35%)*	*-20.92*	*75.32* *(33.47%)*	1.02 *(16.24%)*
BM_FT	1131 *(5.26%)*	-8.50	66.21	1.7

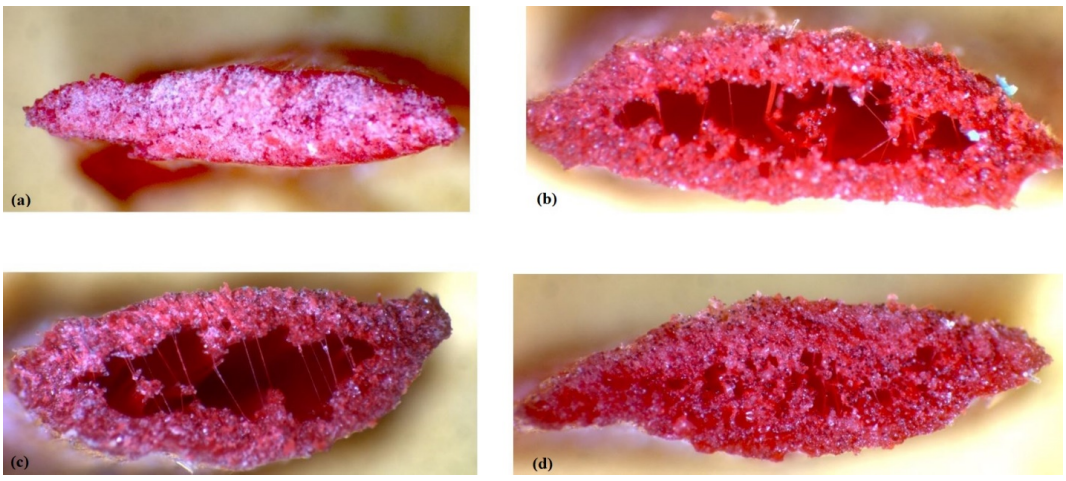

Figure 4.7: Corss-section of the yarns a) BM_Rif, b) BM_S, c) BM_NaOH and d) BM_FT.

Composite

Stress-strain curves for all tested FRCM coupons are shown in Figure 4.8. The typical tensile behavior of FRCM coupons tested by using a clevis grip anchoring system is observed for all the specimens [30, 31]. At low strain value a drop of the tensile stress is observed, when first crack forms, which is probably due to the low amount of fabric reinforcement area which is not able to absorb the energy released [141]. In the second stage of the graph a strain hardening behavior is observed up to the failure of the reinforcement, which occurs in all specimens regardless of the aging protocols (Fig. 4.9). Table 4.5 reports the experimental results obtained for the tensile test of the FRCM coupons in terms of maximum force (F_{max}max), ultimate tensile stress ($\sigma_{u,f}$), ultimate tensile strain ($\varepsilon_{u,f}$) and the corresponding coefficient of variation (CoV). The slight differences observed among the average values of mechanical properties must be considered within the variability of the results. Therefore, the reduction of the tensile strength observed in glass yarns does not reflect on the mechanical properties of FRCM composites expose to the same aging protocols. This is in accordance with the hypothesis that the loss in performance of the yarn is mainly due to the dissolution of the coating rather than to the corrosion of the glass filaments. Moreover, it should be noted that also in the specimens which have not been subjected to any aging protocols the reinforcement fail before reaching its maximum tensile strength. Therefore, if the composite can not fully exploit the mechanical properties of the reinforcement, a small reduction in the tensile strength of the yarns has no significant effect on the mechanical of the composite.

Table 4.5: Results of tensile tests on FRCM coupons (CoV in round brackets).

Specimen	**F_{max}[N]**	$\sigma_{u,f}$ **[MPa]**	$\sigma_{u,f}$ **Increase/ decrease [%]**	$\varepsilon_{u,f}$ **[mm/mm]**	**$E_{u,f}$ [MPa]**
Ref	2213 *(6.8%)*	935 *(6.8%)*	-	0.033 *(10.1%)*	38.2 *(10.2%)*
Saline	2333 *(5.2%)*	986 *(5.2%)*	+ 5.5	0.031 *(19.3%)*	33.0 *(10.4%)*
NaOH	2234 *(12.6%)*	944 *(12.6%)*	+1.0	0.029 *(18.1%)*	36.6 *(16.9%)*
Freeze-Thaw	2142 *(8.4%)*	905 *(8.4%)*	-3.2	0.031	33.1

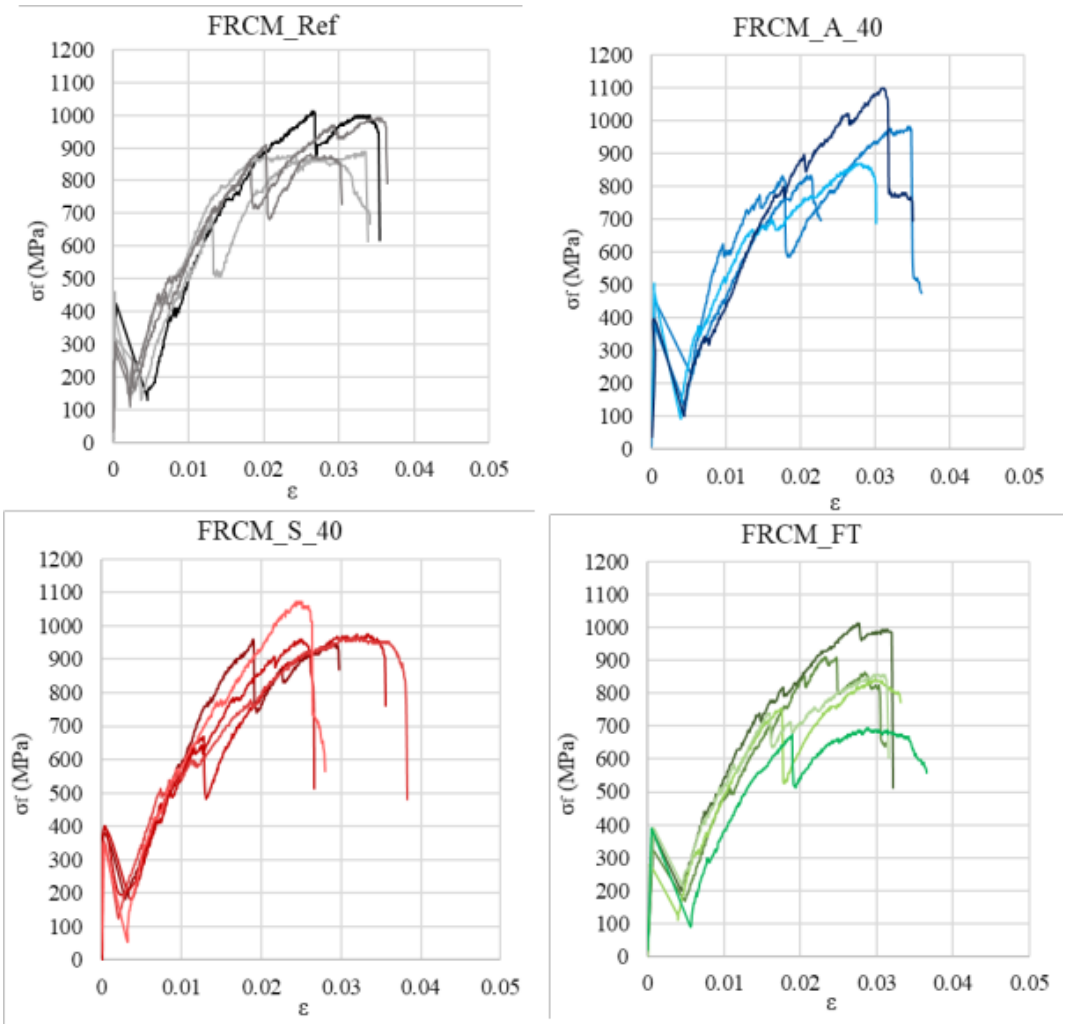

Figure 4.8: Tensile tests on FRCM coupons: stress-strain curves.

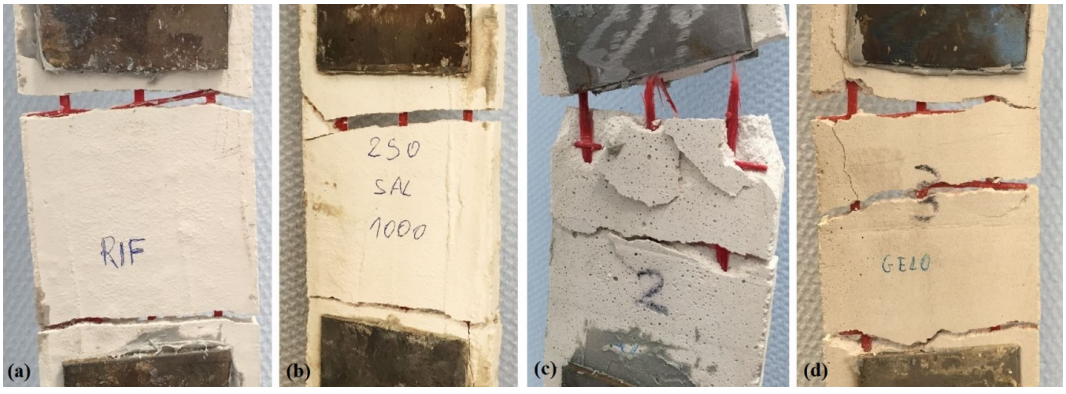

Figure 4.9: Tensile tests on FRCM coupons: failure mode observed a) FRCM_Ref, b) FRCM_S_40, c) FRCM_A_40, d) FRCM_FT.

4.2.3 Remarks

The results obtained can be synthesized as follows:

- BM ARG yarns are considerably affected when immersed in aqueous solution at 40 °C. Particularly a reduction of tensile strength of about 25 % was observed when immersed in the NaOH solution and of 20 % when immersed in tap water. For some unknown reason the aging in the saline solution was less aggressive and the decrease of the tensile strength was only of the 8 %. A similar loss in performance was observed also for the yarns subjected to freeze-thaw cycles.
- Macroscope observations of the yarns' cross-section showed that the immersion of AR glass yarns in saline and alkaline solutions at 40 °C causes the formation of voids and swelling at the center of the yarn.
- FRCM coupons always failed due to tensile breakage of the internal glass yarns, regardless of the type of environmental conditioning. The reinforcement always failed before the maximum tensile strength of the composite has been reached.
- FRCM composite specimens showed a greater resistance to environmental exposures, compared to the glass yarns, an no significant change in the mechanical properties is observed after aging.
- Further studies are necessary in order to gain a deeper understanding of degradation mechanism of the reinforcement and the composites over time.

4.3 Carbon Yarns

This chapter presents the results obtained for the durability test conducted on carbon yarns modified with different techniques reported in the literature. First EDX results will be illustrated in order to obtain an insight on the chemical-physical change of the carbon fiber surface after treatment with the silica nanocoating and the oxidative solution. Secondly the effect of the treatment on the mechanical properties of the reinforcement will be commented based on the yarn tensile test results. Successively, the effect of the coatings on the mechanical properties of the composite will be elucidated on the base of the pull-out tests. In the last part of the chapter the durability tests conducted on the reinforcement and the pull-out specimens will be presented.

4.3.1 Yarns Characterization

EDX-Analysis

Table 4.6 reports the atomic percentages of carbon, silicium and oxygen detected by EDX analyses on the surfaces of the yarns C-Dry, C-NS and C-Ox. As expected for all the samples the main element detected is carbon, moreover all samples present some oxygen and silicium in their spectrum. The presence of oxygen and silicium atoms on the untreated fibres can be attributed to the commercial sizing applied during the manufacturing process of the fabric. The chemical composition of C-Ox present no significant difference with that of the as delivered yarn. Particularly the same quantitative of oxygen observed in C-Dry and C-Ox indicate that no oxidation of the carbon fibres has taken place. On the contrary the clear increase in the percentage of oxigen and silicium atoms observed for sample C-NS compared to the untreated yarn, confirm the presence of nano-silica particles between the yarn's filaments. However, Figure 4.10 shows that the nono-silica coating is not uniformly distributed between the filaments, and forms a discontinuous layer on the fibers surface. For C-Ox no significant difference can be detected on the surface morphology of the fibers before and after treatment with the oxidative solution (Fig. 4.11)

Table 4.6: EDX Results.

Sample	**C [At %]**	**Si [At %]**	O **[At %]**
C-Dry	93.47	0.23	6.31
C-NS	83.9	1.47	14.63
C-Ox	94.11	0.12	5.76

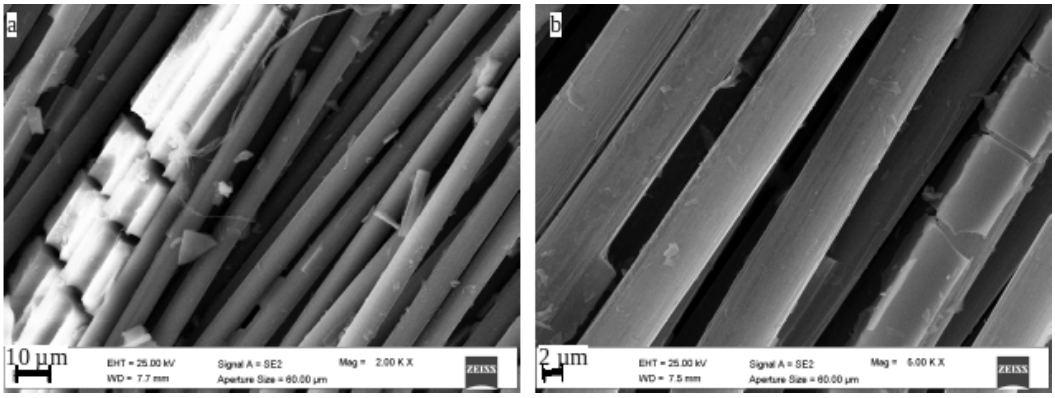

Figure 4.10: SEM images of C-NS. Magnification 2.00 Kx (a), and 5.00 Kx (b).

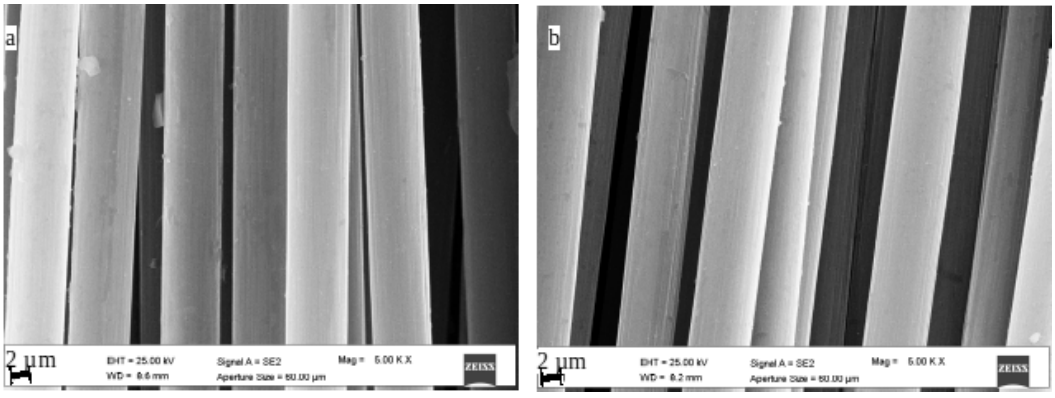

Figure 4.11: SEM images of a) C-Dry, and b) C-Ox. Magnification 5.00 Kx.

Yarn Tensile Test

Figure 4.12a and 4.12b report respectively the maximum tensile strength and the elastic modulus of the carbon yarn C-Dry, C-E, C-NS and C-Ox. The corresponding stress-strain curves can be found in Figure 4.13 It can be observed that the elastic modulus is not effected from the coatings or chemical process employed, while some difference can be observed in the tensile strength. The highest values are obtained for the yarns impregnated with the epoxy resin that reach a maximum tensile test of 2328 MPa. These correspond to an increase of the load bearing capacity of the 34.4 % compare to the untreated yarn. Also, the impregnation with nano-silica dispersion lead to a slight increase (9.7 %) of the tensile strength from 1732 MPa to 1901 MPa, while apparently the oxidative treatment has barely influenced the mechanical properties of the fibers. The ability of coating to improve the mechanical properties of multi-filament reinforcements have been reported in different studies, and it is attributed to an increase in the stress transfer between the single filaments [55, 36, 73, 141]. The efficiency of the coatings to improve the load-bearing of the reinforcement depend on its ability to simultaneously engaged the single filament that make up the yarns. This is in accordance with the results obtained for C-E and C-NS. Figure 4.14c shows the majority of the C-NS samples fail before all the fibers have reached their maximum tensile strength, suggesting that the nano-silica coating is not able to efficiently activate all the yarn's filaments. This is in accordance with the SEM images acquired for C-NS (Fig. 4.10), which clearly show that the filaments are not embedded in the coating, but rather covered with a thin layer of nano-silica. On the contrary three of five C-E experiment a complete break of all the yarns' filaments (Fig.4.14b). The superior ability of the epoxy resin to uniformly distribute the stress between the single filaments can be observed also comparing the stress-strain curved of the carbon yarns reported in Figure 4.13 C-Dry, C-SN and C-Ox display a progressive failure of the yarn filaments, while C-E experiments an abrupt break of all the yarn's filaments.

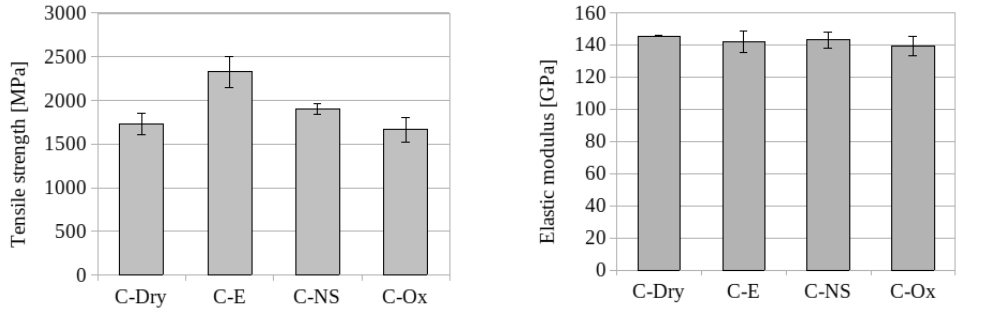

(a) Maximum tensile strength of carbon yarns C-Dry, C-E, C-Ns and C-Ox.

(b) Elastic modulus of carbon yarns C-Dry, C-E, C-NS and C-Ox.

Figure 4.12: Carbon yarns tensile strength and E modulus.

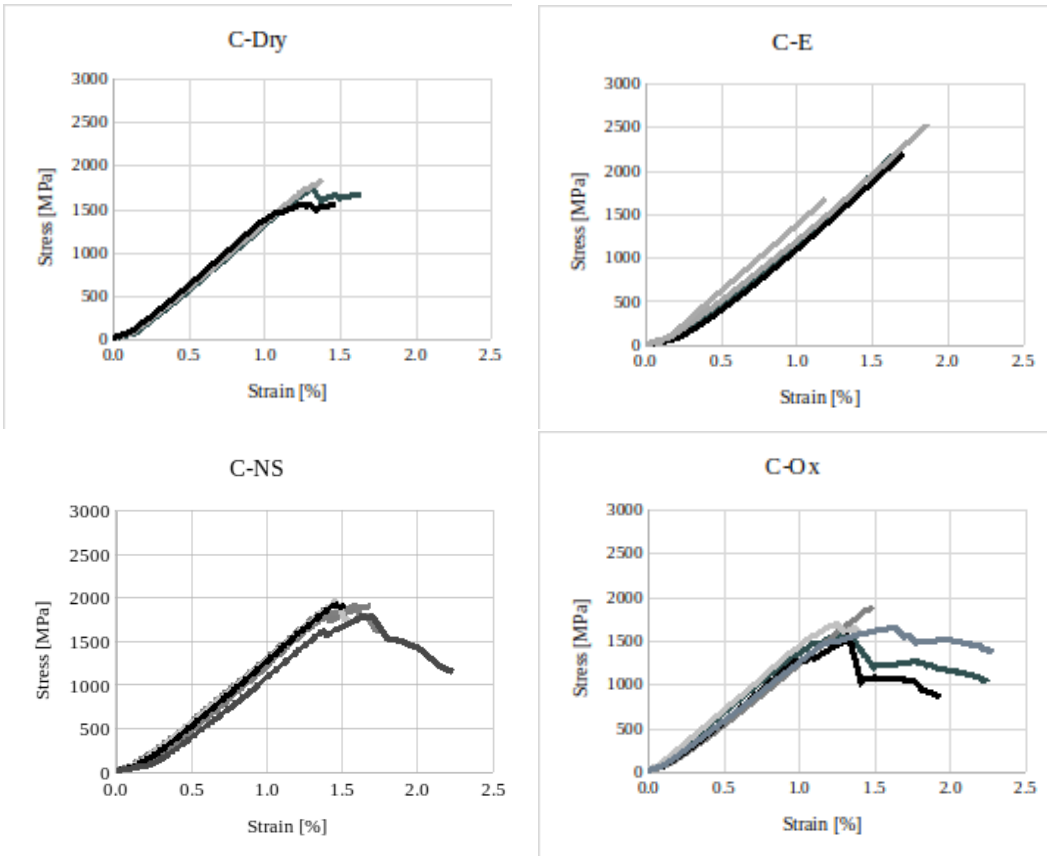

Figure 4.13: Stress-strain curves of the carbon yarns.

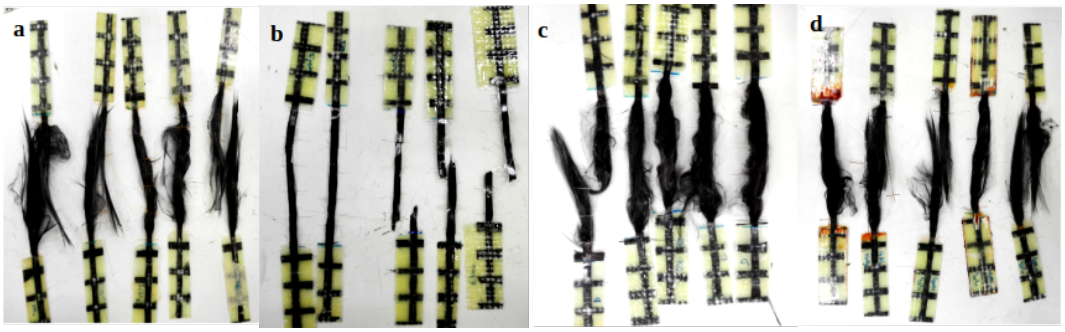

Figure 4.14: Failure mode of carbon yarns C-Dry (a), C-E (b), C-NS (c) and C-Ox (d).

4.3.2 Yarn-matrix interface

Pull-out

Figure 4.15 shows the load-displacement curves obtained for the unmodified and modified carbon yarns. C-Dry C-NS and C-Ox display a similar pull-out behavior characterized by a first linear increase of the load, followed by a pronounced load decrease after reaching the maximum load F_{max}. On the contrary the C-E yarn,

experiment a first load drop at very low displacement level, followed by an increase of the force which than reaches value much higher than that obtained for the first peak. The F_{max} of C-E sample occurred at very high displacement level, and it is not followed by an abrupt load decrease. Indeed rather than reaching a maximum peak C-E curves mainly displace a plateau with force oscillating at about the F_{max} value and occasionally the formation of farther pecks at very high displacement level (Fig. 4.16). This behavior can be explained observing the surface of the C-E yarn after pull-out. Figure 4.17 shows that the epoxy coating has been partially removed from the fibers surface and has accumulated on some point of the yarn. This accounts for a important increase of the friction developed at the yarn-matrix interface and as a consequence for very high pull-out work.

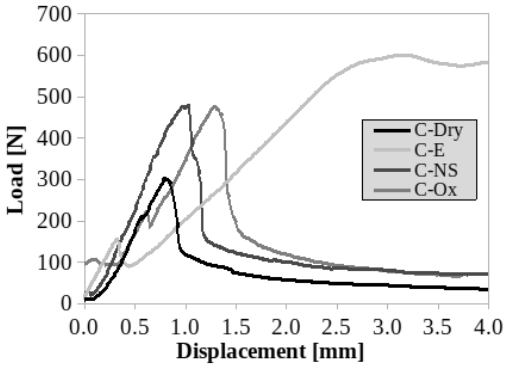

Figure 4.15: Typical load-displacement curve obtained for the pull out of yarn C-Dry, C-E, C-NS and C-Ox

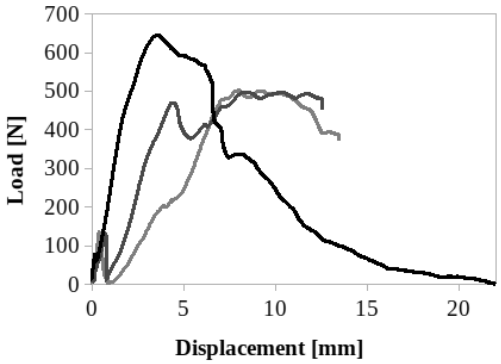

Figure 4.16: Load-displacement curves of C-E yarns at high displacement values.

For practical reason the majorities of the C-E pull-out test were stopped before the pull-out load fell back to zero. Therefore, the complete pull-out work of C-E could not be calculated, and the value obtained for a displacement of 4 mm (W_4) were used instead. The W_4 of the specimens are reported along with the maximum load and shear stress in Table 4.7. For C-E both the shear stress at the maximum

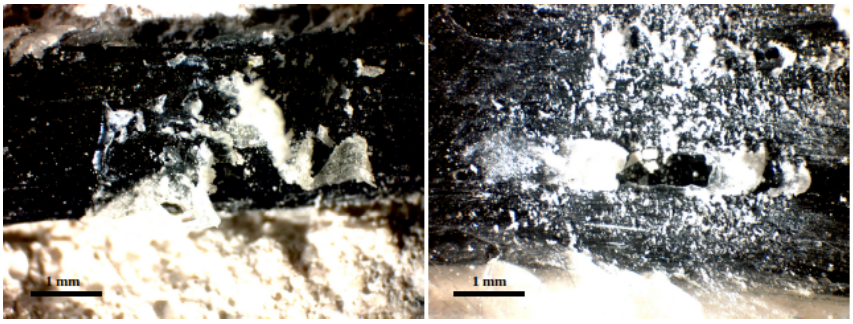

Figure 4.17: C-E yarns after pull-out.

force (τ_{max}), and that corresponding to the first load peak (τ_1) were calculated.

Table 4.7: Pull-out parameters obtained for the pull-out of carbon yarns with and without surface modifications.

Sample	$\mathbf{S}_e$ **[mm]**	$\mathbf{F}_{max}$ **[N]**	τ_{max} **[MPa]**	τ_1 **[MPa]**	$\mathbf{W}_4$	**Failure mode**
C-Dry	0.58 ± 0.17	257 ± 70	0.45 ± 0.12	-	334 ± 102	P
C-E	5.41 ± 0.19	534 ± 84	0.94 ± 0.15	0.27 ± 0.04	969 ± 379	P
C-NS	1.10 ± 0.77	435 ± 140	0.77 ± 0.25	-	517 ± 42	P
C-Ox	0.88 ± 0.23	451 ±107	0.80 ± 0.19	-	577 ± 145	P/T

P: Pull-out, T: telescopic effect

C-Dry fails at very low load values, which are due on one hand to the low interaction of carbon fibers with the cementitous matrix and on the other hand to the low compressive strength of the matrix employed. Usually uncoated yarn are reported to fail because of the breakage of the external filaments and consequent slippage of the internal filaments. This pull-out behavior is known as telescopic effect, but was not observed for the uncoated yarns. Figure 4.18 shows that the yarn filaments are intact after pull-out, and in Figure 4.19 can be observed that few filaments are attached to the matrix. This confirms the very low interaction of carbon fibers with the cementitious matrix. The modification of carbon yarns with oxidative solution and nanosilica dispersion leads to similar increase in the maximum load and the pull-out work. Since neither the nanosilica coating nor the oxidation treatment influence the graph shape in the post debonding region it can be assumed that those treatments did not influence the frictional shear stress of the composite. On the contrary the maximum shear stress obtained for C-NS and C-Ox was respectively 69 % and 75 % higher than the C-Dry. Therefore, the higher load values obtained in both case are the consequence of a higher bond with the cementitous matrix. For C-NS this can be attributed to the silica particle which are reported to react with the $Ca(OH)_2$ in cementitious matrix materials forming a calcium silicate hydrate (CSH) layer in the proximity of the fibers [142] .

For what it concerns the C-Ox samples, studies conducted on cement-based

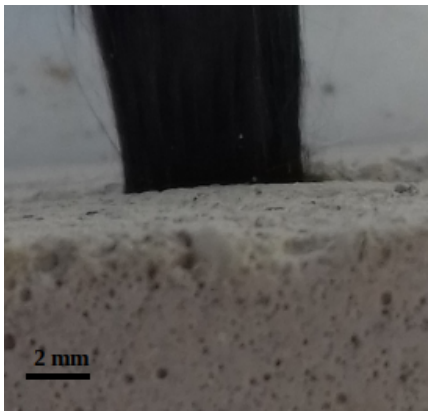

Figure 4.18: Detail of C-Dry yarn embedded in the matrix after pull-out.

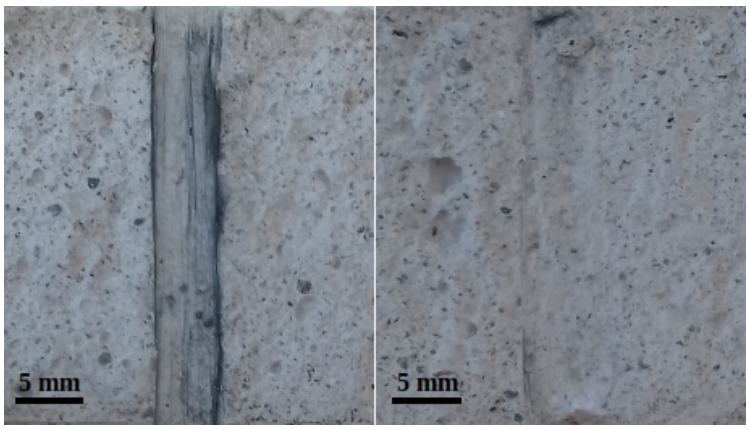

Figure 4.19: Fibre-matrix interface of C-Dry samples.

composite reinforced with carbon fibers treated with concentrated acid, attribute the improved interaction between the matrix and the fibers to the formation of hydroxyl and carboxyl groups on the fibers surface [94]. However, EDX analyses conducted on the C-Ox yarns exclude formation of new oxygen bearing groups on the carbon fibers surfaces. A possible explanation for the improved interaction observed for C-Ox samples is that the chemical treatment was not sufficient to promote the oxidation of the carbon back-bone but has attack the fibers surfaces causing an improvement of its roughness. However, this could not be confirmed from SEM images (Fig. 4.11). As already discussed in the previous section the presence of oxygen atoms on the untreated carbon yarns can be attributed to some kind of organic sizing used for the production of the reinforcement. Therefore another possible explanation is that no oxidation took place, but the acid has promoted some rearrangement of the oxygen bearing groups in the sizing leading to an increase of the fibres hydrophilicity. For example acid are known to catalyze the ring opening of epoxy groups. However, since the exact chemical composition of the sizing is unknown it is no possible to state which reaction are more probable to occurre. Moreover, because no clear FTIR spectrum of the fibres before and after chemical treatment could be acquired this hypothesis can not be confirmed.

For what it concerns the C-E, the load drop observed at small displacement values, can be attributed to the debonding of the yarn, followed by an increase in the pull-out load due to the high friction developed at the fibre-matrix interface. The investigation of the fiber-matrix interface after pull-out suggests that the epoxy coating does not have a high adhesion with the cementious matrix. Figure 4.20 shows that despite the epoxy coating has detached form the yarn, no trace of polymeric material can be found in the cementitous matrix at the interface with the yarn. Similar results have been reported by Dilthey et al. [57] who conducted EDX analysis at the interface between the cementitious matrix and an epoxy impregnated ARG mesh and observed a clear-cut interface between concrete and reinforcement. Nevertheless, epoxy impregnated yarn lead to the highest load values. This is due on one hand to the higher friction developed at the yarn-matrix interface, on the other hand to the improved stress transfer between the single filaments. Indeed, in C-E specimens the epoxy resin prevent the filament to come in direct contact with the matrix so that no break of the sleeve fibers was observed, and the yarn was pulled out as a monolithic bar.

Although all the modified carbon yarns present improved mechanical properties compared with C-Dry samples, the load reached is far above the load-bearing capacities measured for the yarn. Figure 4.21 compares the yarn tensile strength with the pull-out strength. The pull-out strength ($\sigma_{pull-out}$) was calculated as the maximum pull-out load (F_{max}) divided the yarn cross section (A_c):

$$\sigma_{pull-out} = \frac{F_{max}}{A_c} \tag{4.1}$$

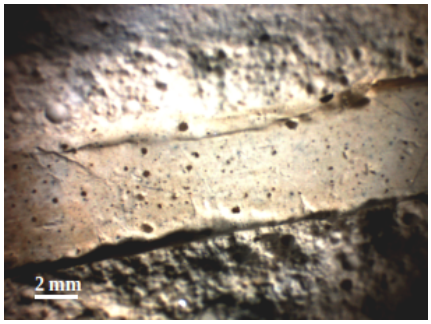

Figure 4.20: Cementitous matrix in contact with yarn. Image obtained by breaking apart the pull-out specimen after pull-out.

It can be observed that C-E and C-NS reached only the 22 % of the yarn bearing capacities, and C-Ox the 26 %. This confirms that during the pull-out the yarn tensile strength could not be used to fully capacity.

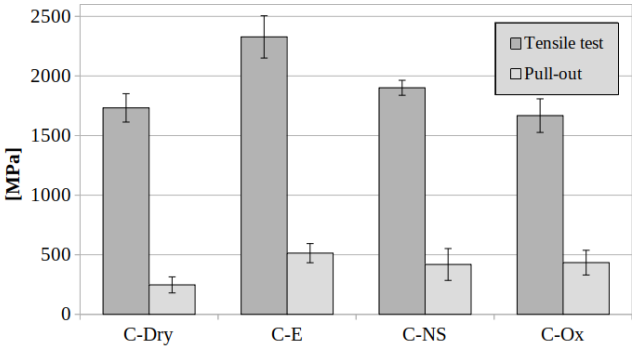

Figure 4.21: Maximum tensile strength compared with the maximum pull-out strength.

4.3.3 Accelerate Aging

Yarns

Figure 4.22 shows that the maximum tensile strength of the carbon yarns was in general barely effected by the exposure to saline and alkaline environment regardless of the coating and treatment applied. The most significant reduction of the yarns tensile strength is observed for C-NS. After immersion in the alkaline solution the maximum tensile strength of the C-NS yarn decrease from 1901 MPa to 1651 MPa (-13 %). Similar results are obtained after immersion in the saline solution, with a 12 % decrease of the load-bearing capacity corresponding to a tensile strength of 1672 MPa. Those values are in the range of that obtained for the yarns C-Dry. Therefore, it is probable that the reduction of the mechanical properties obtained for the C-NS samples after exposure is due to the dissolution of the Nanosilica coating rather than a damage of the carbon fibers.

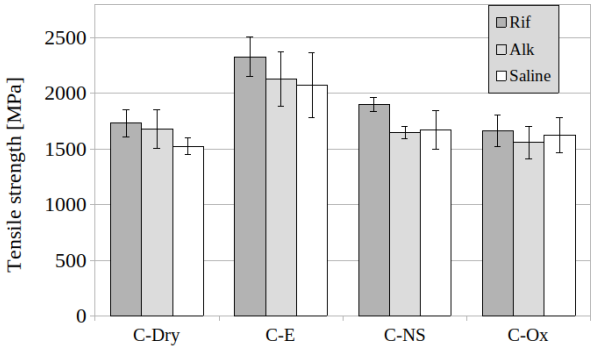

Figure 4.22: Tensile strength of carbon yarn after 1000 hours accelerate aging.

Pull-out

Figure 4.23 shows the load-displacement curves obtained for the pull-out of the unmodified and modified carbon yarns after aging in different environments. With the exception of C-E the pull-out curved of the aged sample display a similar pull-out behavior than the same specimens aged at standard condition. On the contrary, it can be observed in Figure 4.23a and c respectively that C-E-NaOH and C-E-FT show and abrupt failure at high load and displacement value. This was due to the breakage of the matrix in two halves, and complete detachment of the yarn from the matrix (Fig.4.24). This kind of failure was observed in three of five sample for the specimens immersed in alkaline solution and two of five for that aged in the saline solution and subjected to freeze-thaw cycles. This confirms the low chemical adhesion of the cured epoxy resin the cementitious matrix, and the tendency of the preimpegnated yarn to act as a separating layer and promote delamination failures, as has been observed in other studies [28][52].

Table 4.8 reports the F_{max} and the W_4 obtained for the pull-out of carbon yarns after different aging protocols. It can be observed that regardless of the environmental exposure, the unmodified yarns always display the lowest pull-out load and pull-out work. However, significant differences can be observed comparing the increase or decrease of the F_{max} and W_4 values after aging for sample C-E, C-Ox and C-NS. After 1000h immersion in the NaOH solution all the specimens display an increase in the maximum load. Particularly the F_{max} of C-Dry C-E and C-NS is respectively 53.6 %, 73.3 % and 41 % higher compared to the same samples cured at laboratory condition. On the contrary after freeze-thaw cycles the maximum pull-out load decrease for C-Ox (-25 %) and C-NS (-18 %), while it doesn't experiment considerable change for C-Dry and C-E.

Results obtained for the matrix compressive strength and yarn tensile strength after aging suggest that neither the matrix nor the yarn are directly damaged from exposure to saline environment. Therefore, it seems reasonable to suppose that the fibre-matrix interface plays a predominant role in the change of composite properties over time. As already discussed in the previous chapter, the curing mechanism of the matrix in

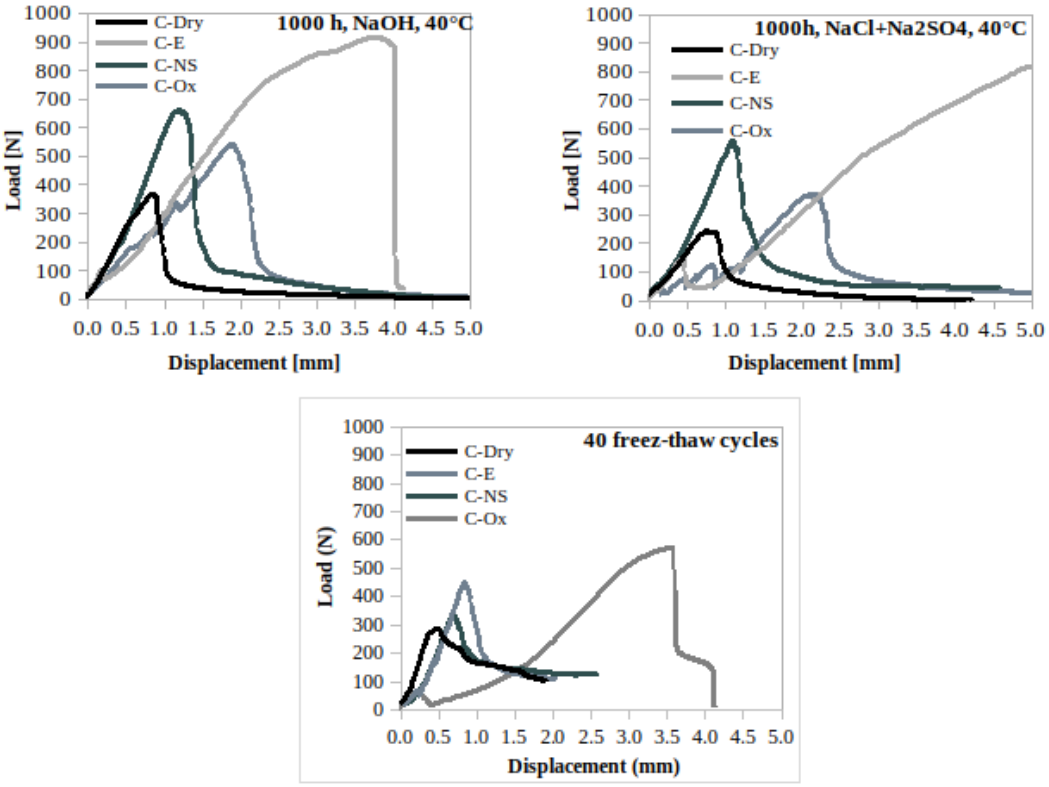

Figure 4.23: Pull-out curve of the samples subjected to different aging protocols.

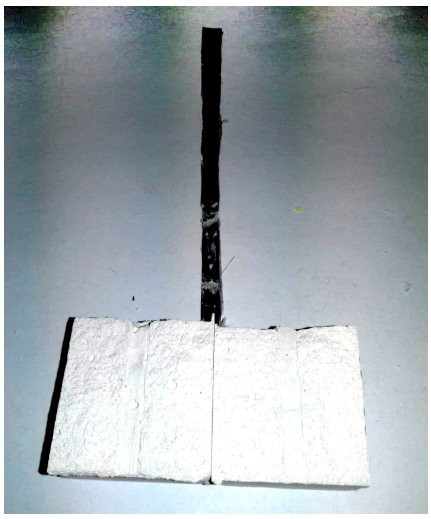

Figure 4.24: Breakage of the matrix during the pull-out test.

Table 4.8: Pull-out parameters obtained for the pull-out of carbon yarns with and without surface modifications after different aging protocols.

Sample	**F_{max} [N]**	**F_{max} variation [%]**	**W_a**	**W_4 variation [%]**	**Failure mode**
C-Dry-NaOH	394 ± 136	53.57	423 ± 117	26.73	T/P
C-E-NaOH	925 ± 29	73.32	2108 ± 398	117.62	P/M
C-NS-NaOH	613 ± 155	40.85	698 ± 216	10.28	T
C-Ox-NaOH	494 ± 137	9.65	657 ± 112	13.95	T/P
C-Dry-S	226 ± 114	-12.06	257 ± 122	-22.99	T
C-E-S	939 ± 383	75.89	1311 ± 877	35.34	P/M
C-NS-S	520 ± 64	19.53	632 ± 139	22.60	T
C-Ox-S	357 ± 82	-20.82	488 ± 156	-15.32	T
C-Dry-FT	244 ± 98	-5.06	-	-	P
C-E-FT	579 ± 84	8.44	1118 ± 325	15.46	P/M
C-NS-FT	338 ± 18	-17.65	-	-	P
C-Ox-FT	358 ± 112	-25.03	-	-	P

P: Pull-out, T: telescopic effect M:matrix breakage

the alkaline and saline solution is mainly governed by the high temperate and relative humidity of the curing environment rather than the concentration and chemical properties of the anions and cations dissolved in the aging solutions. Therefore, it can be assumed that regardless of the solution composition the ITZ undergoes similar chemical-physical modification over time. As discussed in section2.5 the fiber-matrix interface has been reported to play an important role in the degradation of the composite mechanical properties over time [51, 105, 143]. Although studies usually focus on composites reinforced with glass fibers, some degradation mechanism apply for all brittle fibers. Particularly the role of interface densening in the change of the flexural strength and toughness of carbon fibers reinforced cement composites have been deeply investigated by Katz and Bentur [144, 145]. The authors report an increase in the flexural strength and toughness of the composite with time up to a maximum at two-four weeks and then decrease thereafter, with a loss in up to 65 % of the maximum value. This is explained with an increase in the fiber-matrix bond, which in a first moment accounts for the increase in the composite properties, till a critical bond value is reached, and the failure mechanism of the composite is changed from fibers pull-out to fibers failure. According to Butler et al. the main causes for loss in toughness due to change in the ITZ is due to the accumulation between the filaments of thin-tabular fissile calcium hydroxide crystals, which can induced a premature failure of the composite subjected to tensile or flexural load

[105, 51]. The authors also report that this phenom is mitigated by pozzolanic additives since those are able to convert the CH crystals in CSH which forms a much more homogeneous and porous phase, providing an optimal fiber-matrix bond. Although the matrix employed in this work has a low content of Portland cement, it also does not contain pozzolanic addictive, so that the calcium hydroxide contained in the matrix as lime and that formed during the hydration process can not convert in CSH. Moreover, although CH can be consumed by reaction with CO_2 to form $Ca(CO_3)_2$, this reaction unlikely take place for samples immersed in aqueous solution, as discussed in chapter . As a consequence for sample C-Dry and C-Ox it can be assumed that the fibre-matrix interface is particularly reach in CH and sample with a higher hydration grade will also present a stiffer ITZ. For the C-Dry, that have a very pure bond with the matrix, the densening of the ITZ results meanly in an increase of the F_{max} thanks to the higher fibre-matrix bond. This would explain the increase in the pull-out load observed for C-Dry-NaOH, and the lower F_{max} value obtained for samples subjected to freeze-thaw cycles. Interesting the uncoated yarn aged in the saline solution show a decrease of the composite load-bearing capacity rather than an increase as in the case of the same samples immersed in the alkaline solution. A possible explanation is that in this case a stronger bond between the external filaments and the cementitious matrix is formed, which eventually lead to the decrease of the mechanical properties of the composite due to the premature failure of the fibers in direct contact with the matrix. This is also confirm by the change of the predominant failure mechanism of the specimens from pull-out to telescopic failure (Fig. 4.25b).

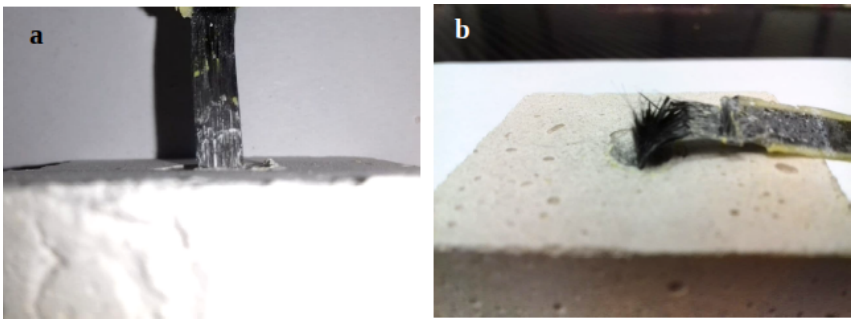

Figure 4.25: Failure mode observed for the pull-out test. a) Pull-out of the yarn without failure of the external filaments, observed mainly for specimens not subjected to accelerate aging b) Telescopic failure, observed mainly for the specimens after accelerate aging.

It could be supposed that the densening of the matrix in the saline solution is somehow increased by the accumulation of salt at the fibre-matrix interface, and therefore more detrimental for uncoated fibres. However, this can not be support on the base of the scientific literature available. Indeed, little information are available about the effect of salt accumulation in FRCM composite, and results are often difficult to compare because of the different materials and test methods employed.

Franzoni et al. extensively studies the effect of salt crystallization in FRCM systems using a galvanized steel fibres applied on masonery specimens with cement based and hydraulic-lime based mortar [111, 17]. They report a decrease of the 26 % of the bond capacities of the composites. However, they ascribed this reduction in the composite bearing capacities, only to the corrosion of the steel fibres in presence of chloride ions. Also Nobili observed a decrease of the tensile strength of impregnated ARG-FRCM composite subjected to aging in saline solution [106]. However, he also reports a marked reduction in the flexural strength of the matrix, which is not the case in this study. Donni reports a 29 % of the peak load in single-shear bond test performed on impregnated ARG-FRCM strips applied on clay brick respectively after immersion in NaCl solution at 60 °C [109]. However, the author also reports a remarkable decrease in the tensile strength of the yarns. Moreover, specimens subjected to saline exposure are reported to fail due to tensile rupture of the fabric out of the matrix or debonding at the matrix-substrate interface rather than at the matrix-fabric interface. Of course farther investigation on aging mechanism of FRCM composite expose to saline environment are need. For what it concerns the C-NS samples they do not show any decrease in the load-bearing capacities after aging in the aqueous solutions. On the contrary the F_{max} measured for the C-NS-NaOH and C-NS-S are respectively 41 % and 20 % higher than the reference. In this case the composite probably benefit of the presence of the nanosilica particles on the fibers surfaces which is reported to react with CH and forms a more delicate and uniform layer of CSH which enable a good a flawless bonding with the matrix [51]. However, farther analyses are certainly needed in order to confirm this hypothesis. Finally, it can be observed that the epoxy impregnated yarns show the highest increase in the pull-out load in saline and alkaline solution and the lowest change after exposure to freeze-thaw cycles. In this case the epoxy coating, which embedded the all filaments, can on one hand provide a better distribution of the shear stress at the yarn interface and between the filaments, and on the other hand it physically separates the fibers from the matrix, preventing them to be damaged from the portlandite crystals. As results the properties of the composite mainly results to vary with the compressive strength of the matrix. Indeed, the very high pull-out value reached by C-E-NaOH and C-E-S, respectively 925 and 939 N, correspond to the highest compressive strength obtained for the cementitious matrix (about 25 MPa, Table 4.8). The similar pull-out load obtained for the C-E pull-out specimens cured in laboratory condition and subjected to freeze-thaw cycles are in accordance with the similar compressive strength (about 22 MPa, Tab. 4.8) shown by the matrix aged in the same condition.

4.3.4 Remarks

According to the results obtained the following remarks can be made:

- Although a significant increase in the yarn tensile strength could be observed only by impregnation of the filaments with the epoxy resin, all the modification technique investigated lead to an increase in the pull-out load.
- For C-Ox and C-NS this could be attributed to a higher adhesion between fibre and matrix, due to the improved chemical compatibility of the yarn with the matrix. On the contrary for C-E the high pull-out load and much higher pull-out work were due mainly to a grate improvement of the friction developed during the pull-out at the fibre-matrix interface.
- No significant decrease in the tensile strength of the yarn could be observed after aging. On the contrary results of the pull-out test show that the properties of the composite change after exposure to different environment.
- The change in the mechanical properties of the composite is strongly influenced by the hydration grade of the cementitious matrix. For C-Dry and C-Ox in a earlier stage, the improved hydration of the matrix increases the bond between the matrix and the yarn and leads to higher pull-out value. However, a farther densening of the matrix leads to the premature failure of the external filaments and as a consequence of a reduction of the F_{max}. Aging in saline solution seams to increase this phenom, however farther investigation are need to clarify the causes of the results obtained.
- The stiffening of the fibre-matrix interface is partially mitigate by the nano-silica particle present on the fibres surface of C-NS.
- In C-E specimens, where the epoxy coating physically separate the filaments form the matrix, the difference in the F_{max} reached by the composite seams to depends mainly on the compressive strength of the matrix. The breakage of the matrix in to half observed for some sample after aging confirm the low adhesion of the C-E yarns with the matrix, and suggest that the impregnated yarn can act a separating layer in the matrix. Nevertheless, impregnation of the yarn with the epoxy coating results in the best mechanical performance and durability for the aging protocols investigated in this work.

4.4 IPF AR-glass Fibers

In this chapter is analyzed the effect of the experimental coatings on the mechanical properties on durability of the AR-glass fibers spun at the Leibniz-Institut für Polymerforschung of Dresden. First the coatings developed will be characterized, secondly the results obtained for the micro-mechanical tests will be presented. In the final part the aging test preformed on the single fibers, the rovings and the pull-out specimens will be presented.

4.4.1 Coating Characterization

FTIR Analysis

Figure 4.26 reports the IR spectrum obtained for the carboxylated self cross-linking styrene butadiene coating (SB).

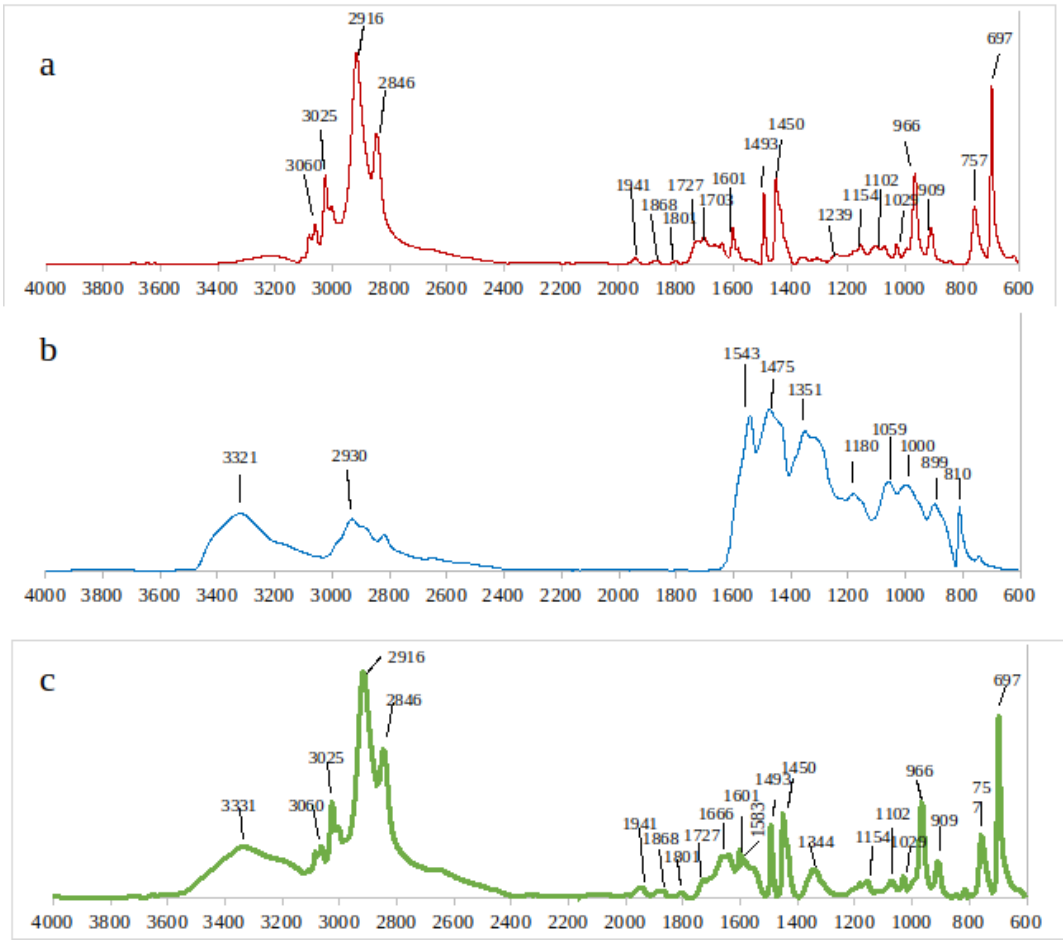

Figure 4.26: R spectrum of: a) the carboxylated self cross-linking styrene butadiene copolymer (SB), b) the methylolmelamine crosslinking agent and c) the SB copolymer with the crosslinking agent (CSB) cured at 160 °C.

The typical absorption of a styrene butadiene copolymer can be observed. The

band at 607 cm^{-1} and 757 cm^{-1} can be ascribed to the out of plan bending of the C-H on the phenil ring. Other styren absorption occurs at 3050 (aromatic C-H stretching). Absorption characteristic for the butadiene polymer are the bands at 909 and 966 cm^{-1} , which can be attributed to bending of the C-H on alkenes in the trans from, the scissoring of CH2 groups at 1450 the trans 1,4-C=C out of plane deformation (966 cm^{-1}) and the aromatic C-H stretching at 3025 cm^{-1} . The absorption at 1727 cm^{-1} (ascribed to C=O stretching) confirms the presence of carboxylated groups. For what it concerns the spectrum of the methylolmelamine this is found to be consistent with IR spectra reported in other works [146, 147, 148]. The absorption peaks at 810 and 1543 cm^{-1} are attributed rispectively to the C-H bending and C=C stretching of the triazine ring. The absorption at 1000 cm^{-1} is assigned to the hydroxymethyl groups. The bands at 1180 and 1475 cm^{-1} are attributed to the stretching of methylene (–CH2–) group. The peak at 1351 cm^{-1} occurs due to the vibration of the C–N bonds. The peaks at 2930 and 3321 cm^{-1} can be respectively assigned to the –N-H stretching of the secondary and primary amine groups. The two main absorption observed in the polymer after addition of the cross-linking agent are the peak at 1344 cm.1 and a broad band at 3331 cm^{-1} . Those can be attributed respectively to the C-N bonds in the methylene bridge an the primary amine N-H stretching. The absence of strong amide absorption suggest that the polymerization of the carboxylated styrene butadiene with the crosslinkg agent occurs via the formation of methylene ester linkages between the acid groups and the melamine as described in the litterateur [149, 150].

TGA and DSC Analysis

Figure 4.27 reports the TGA curves of the SB polymer with and without MMT particle performed in nitrogen atmosphere and oxidative condition (air). It can be observed that in nitrogen atmosphere the decomposition temperature of the polymer remains almost unchanged by addition of nanoclay. On the contrary measurements performed in oxidative condition display a great difference of stability. SB polymer presents a first weight loss at 336.59 °C followed by two great weight lost at 385.54 °C and 400,13 °C (respectively 36.43 % and 79.53 %) and to smaller residue at 440.37 °C and 543.68 °C (respectively 4.37 % and 15.39 %). By successive addition of nanoclay in the polymer the main degradation peaks are shifted to higher temperature ranging from 422.25 °C for 5 % nanoclay to 439.66°C for 80 % nanoclay. Zanetti et al. report similar results for the thermal analysis of PE blended with organomodified montmorillonite [151]. They attribute the improved thermal stability in oxidative condition to the formation of an organoclay shield that protect the polymer from oxygen. However, they observed a partial increment in thermal stability also for not exfoliated nanoclay composite, therefore the results obtained do not furnished clear information on the polymers nanostructure. Further information about the thermal behavior of the polymer were investigated by means of DSC analysis. The calculated

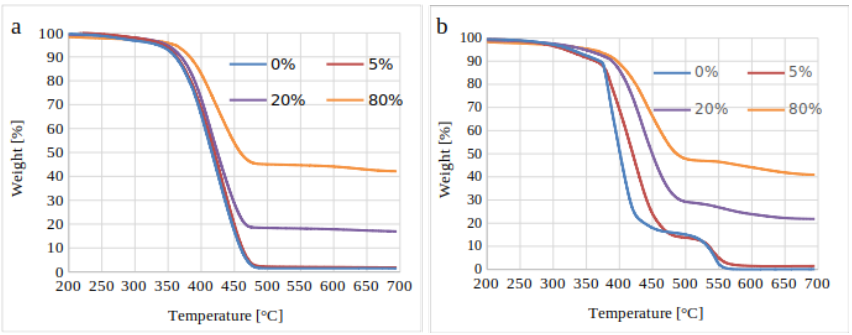

Figure 4.27: TGA curves of SB, SB5 SB20 and SB80 in nitrogen atmosphere (a) and in air (b).

T_g values were all found between -5,98 °C and -8,16 °C. No clear correlation between nanoclay content and T_g could be observed. It can be concluded that the addition of nanoclay had a beneficial effect on the thermal stability of the polymer but did not influence its glass transition temperature. Because of the not unambiguous results obtained no clear conclusion can be drawn about the structure of the nanoclay dispersed in the matrix on the base of thermal analysis.

X-Ray Diffraction

Figure 4.28 shows the diffractograms of the as received Cloisite®Na^+ powder, a nanoclay film obtained by drying the MMT disperion at 100 °C, and of the polymeric films. The layers spacing calculated from the diffraction peak of the as received Cloisite®Na^+. is equal to 1.21 nm which is in accordance with the information reported from the producer. Interestingly, it can be observed that after sonication in water the MMT sample displays a defraction peak that is shift to lower degrees, which suggests that the silicate layers have been distanced. Montmorillonite, as other smectite clay, is reported to swallow water molecules and form stable aqueous emulsion where the interlayer spacing can increase up to 40 Å for high water content [152]. Although, by successively drying of the emulsion the silicate interlayer spacing falls back to smaller distance value, Na^+ cations are reported to form hydrated complex with strongly bonded water molecules [153]. Therefore, it can be supposed that smaller difraction angle observed for the Cloisite®Na^+ after dispersion in distilled water, are due to the hydration of the montmorillonite interlayer cations. Figure 4.28 shows that the diffraction peaks of the SB5 and CSB5 film are further shift to smaller angles, with a corresponding d value of 1.46 nm.

Similar results have been reported for the intercalation of Alkylammonium ions and organosilae molecules [154, 87]. The results obtained suggest that the molecules intercalated between the silicate layer have smaller dimension than polymer chains. It is probable that the shift observed is due to the intercalation of surfactant agents typically employed for the formulation of coatings, rather than because of the intercalation of polymers chain. Therefor, according to the results obtained, the

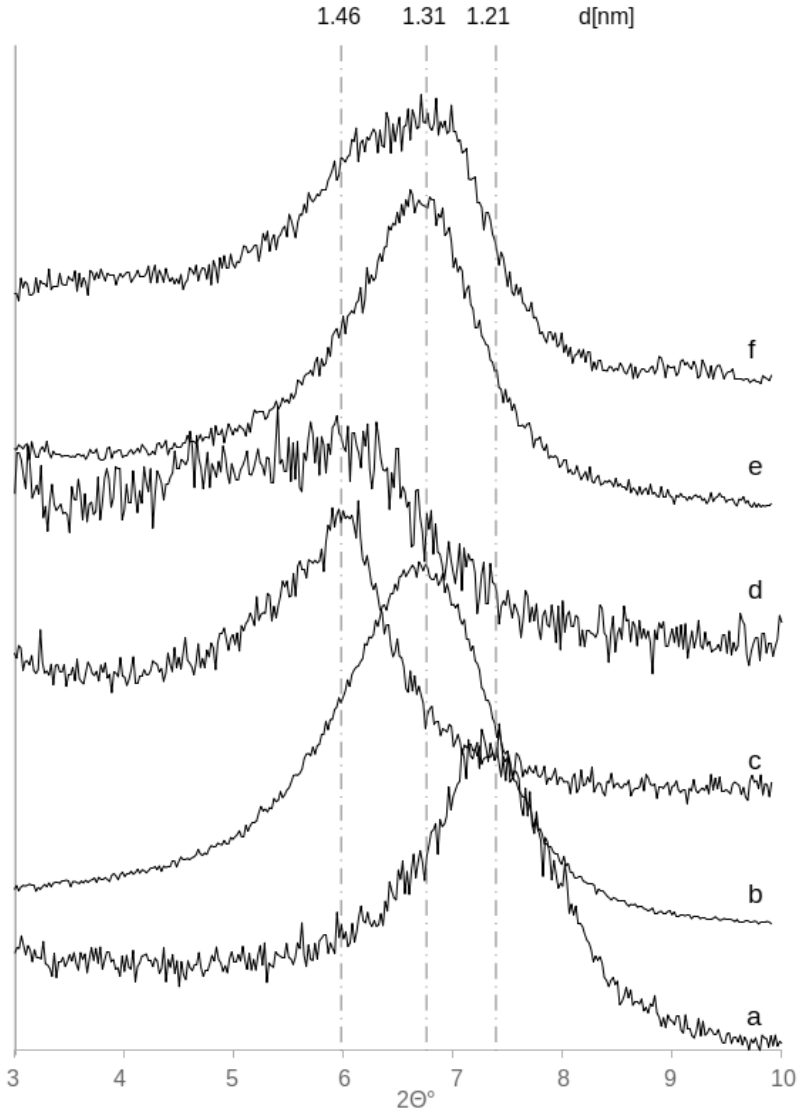

Figure 4.28: X-Ray difractogram of: Cloisite®Na^+ powder (a), MMT after sonication and stiring at 80°C in water (b), SB5 (c), CSB5 (d), SB20 (e) and SB 80(f).

formation of a nanostructured coating can not be confirmed. The flatter shape of the CSB5 diffraction peak (Fig.4.28d) can be attributed to a lower signal insensitivity due to the formation of many air bobbles in polymeric film, as can be observed from Figure 4.29c. On the contrary difracton peack of sample SB20 and SB80 correspond with that observed for the MMT dispersion. Therefore, it can be concluded that for a high amount of nanoclay the polymer obtained has no intercalated structure.

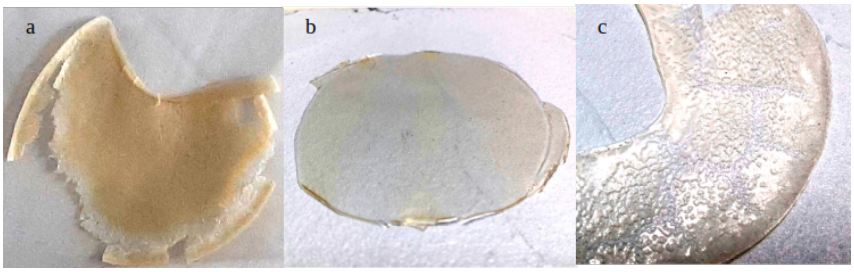

Figure 4.29: Film of MMT obtained from the MMT dispersion (a), SB5 (b) and CSB5 (c)

SEM-EDX

Results obtained from XRD diffraction give important infromation on the interlayer structure of the obtained polymers. However, this technique is not suitable to investigate the spatial distribution of silicate in the polymeric matrix. For this propose films of the cured polymer were analyzed by means of EDX spectroscopy. EDX analysis confirm the presence in both polymer SB5 And CSB5 of atoms typical of clay composition such as Mg, Al and Si. However, as it can be observed from the elemental distribution of silicium reported in Figure 4.30 , the nanoclay particles are differently distribute in polymer matrix SB and CSB. CSB5 presents agglomerates of more than 100 µm width while in SB5 the nanoclay particles form a kin of oriented strips of about 100 µm length and 5 to 50 µm width. Some difference can be observed also in the chemical composition of the polymeric films. Indeed, although as it could be expected the polymer consist mainly of carbon atoms, in the CSB5 nitrogen atoms were also detected. These can be attributed to the methyl melamine molecules of the cross-linking agent. Figure 4.30 shows that the nitrogen atoms do not present the same distribution of the carbon atoms in the polymeric matrix. On the contrary, they seam to be concentrated in the nanoclay agglomerate, as both the nanoclay particles and the cross-linking agent are both not uniformly dispersed in the polymeric film.

4.4.2 Fiber Surface Morphology

SEM

The non uniform distribution of the nanoclay particle observed in SEM-EDX immages of the CSB5 film (Fig. 4.30 also accounts for a non-homogenous surface of the IPF

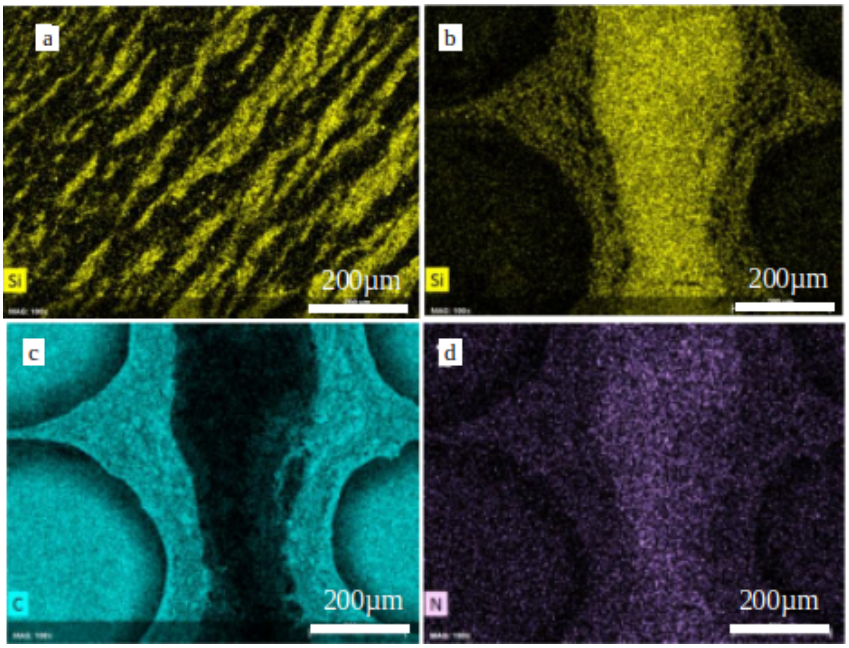

Figure 4.30: EDX analysis of the dried polymer films. (a) Si in SB5, (b) Si in CSB5, (c) C in CSB5 and (d) N in CSB5; magnification 100x.

CSB5 fibers. This can be clearly observe from the SEM images of the fibers (Fig. 4.31). It can be seen that although the fibers were coated with the same coating and following the same preocedure, they present a very different surface morpohology. This is not the case for fibers IPF SB, SB5 and CSB, that present and uniform polymer distribution on the surface (Fig. 4.32).

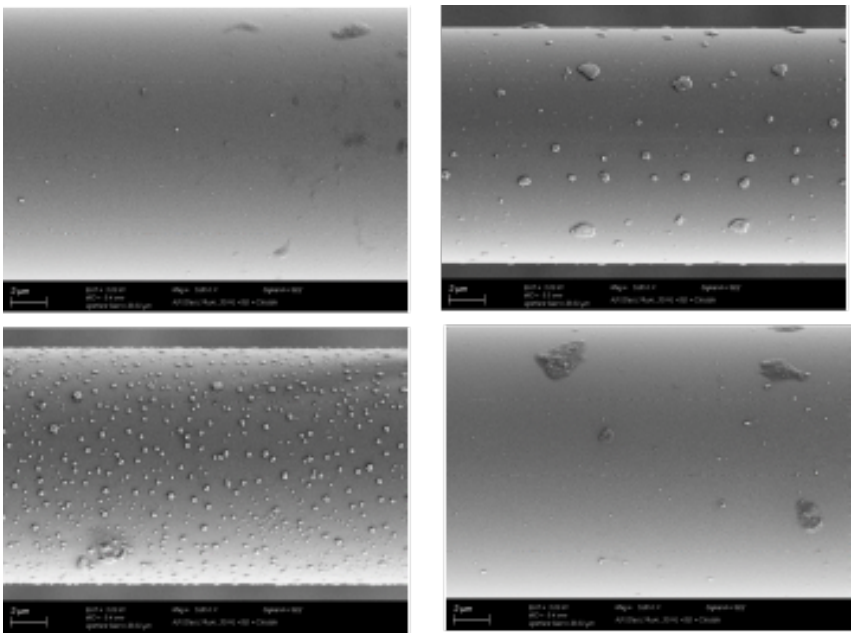

Figure 4.31: SEM immages of four different IPF CSB5 fibers.

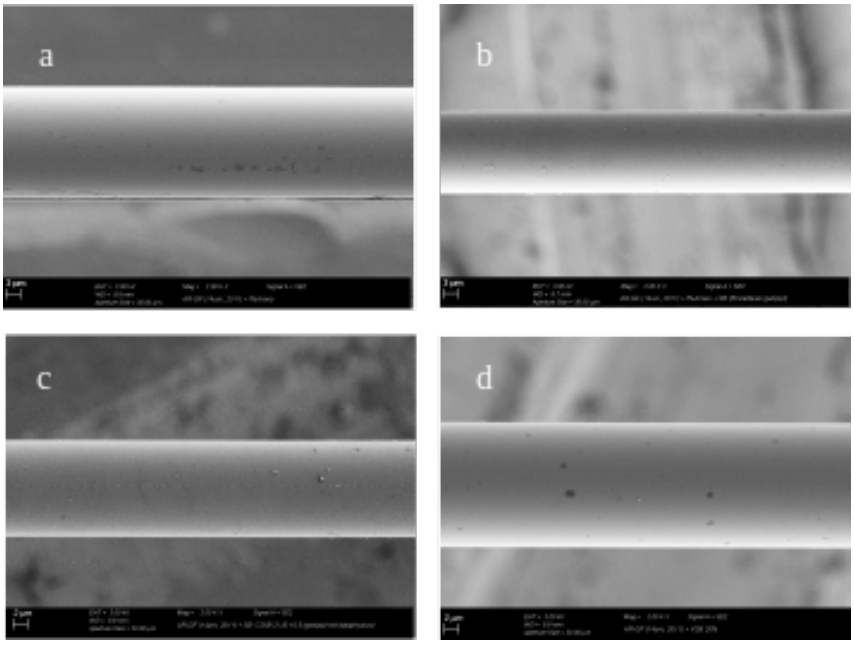

Figure 4.32: IPF fibers sized with AMEO (a) and coated with: SB (b), SB5 (c) and CSB (d).

AFM

Figure 4.33 reports the images of the coated fibers surface topography acquired with AFM. Average roughness Ra square roughness Rq and maximum roughness Rmax are reported in Table 4.9. Fibers IPF SB (Fig. 4.33a) exhibits a quite smooth surface, showing a rather homogeneous coating distribution in accordance with the SEM images (Fig.4.33b). IPF CSB also presents an homogeneous material distribution on the fiber surface, and a slight increase of the roughness, which is expected for the addition of a cross-linking agent in the polymer formulation. A far pronounced increase of the roughness parameters is observed by adding a 5wt % of MMT in the SB polymer. IPF SB5 displays the highest average roughness, square roughness and maximum roughness, which are three to four times higher than those obtained for the same polymer without nanoclay particles. An increase in the maximum roughness is observed also for IPF CSB5. However, any significant difference in the average and square roughness is observed compared to IPF CSB. On the contrary the Ra is the lowest obtained. This confirms the presence of nanoclay agglomerate in the CSB5 coating, rather than a uniform distribution of the MMT particles in the polymeric matrix.

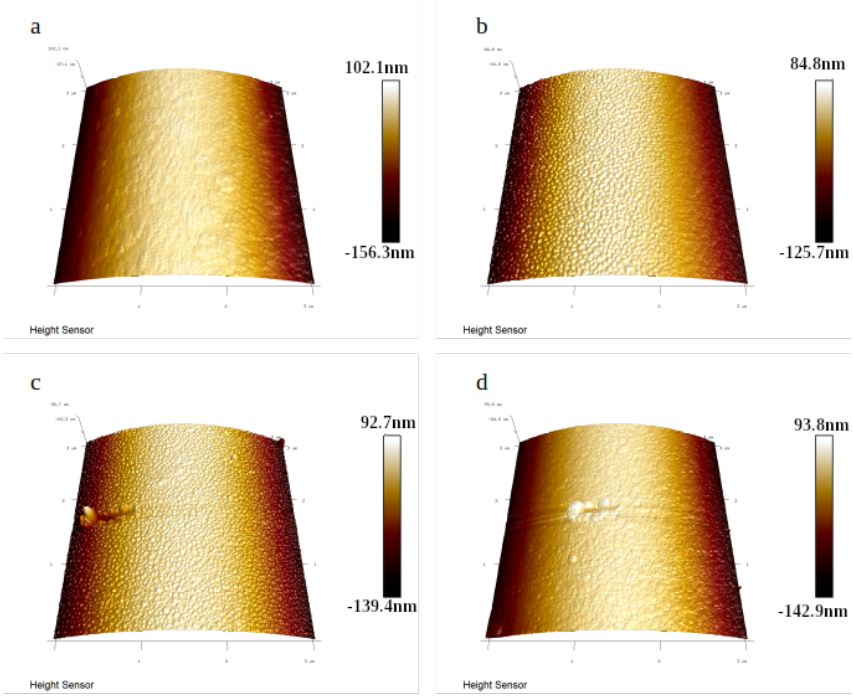

Figure 4.33: AFM images of fiber IPF a) SB, b) CSB c) SB5 and d) CSB5.

Table 4.9: Average roughness R_a square roughness R_q and maximum roughness R_{max} values of fibers with SB, SB_MMT, CSB and CSB_MMT coating, determined by AFM.

Fiber type	**R_a [nm]**	**R_q [nm]**	**R_{max} [nm]**
SB	2.27 ± 0.29	3.33 ± 0.4	38.88 ± 8.71
SB_MMT	11.90 ± 1.17	16.91 ± 1.61	160 ± 19.65
CSB	2.46 ± 1.03	3.66 ± 1.91	46.05 ± 31.56
CSB_MMT	1.92 ± 0.5	3.70 ± 1.22	107.20 ± 26.93

4.4.3 Hydration Products

Figure 4.34 shows the surface of roving and single fibers coated with SB and SB5. In both case the specimens containing nano-clay particles in the coating formulation display different crystals on the fiber surfaces. This could not be detected on the surface of IPF SB fibers. This confirms the ability of nanoclay particle to act as nucleation point of the formation of hydration products, as have been reported in other studies [62, 40].

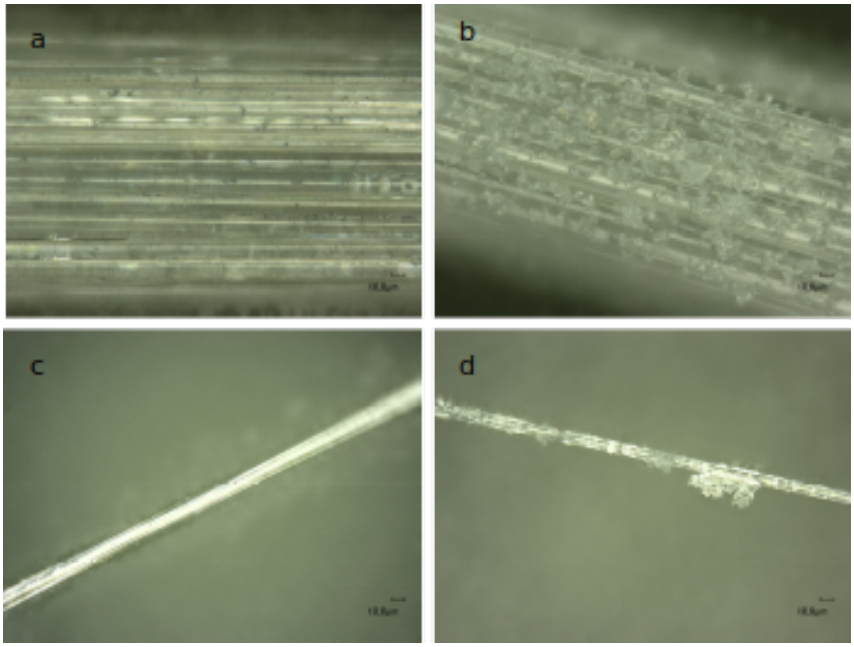

Figure 4.34: Single fibers and yarns coated with SB (a,c) and 5 % nanoclay SB (b,d) after 18 hours immersion in cement solution.

4.4.4 Micro-mechanical Tests

Single Fiber Tensile Test

Table 4.10 reports the mechanical properties obtained for the single fiber tensile test of the 14 μm IPF AR-glass fibers, unsized and after application of sizing and coating. It can be observed that the most significant increase in the tensile strength is obtained after application of the sizing. Compared to the uniszed fibers IPF PTMO fibers have a 50 % higher tensile strength and a 25 % higher scale parameter. As discussed in section 2.4.1 sizings are known to increase the fiber tensile strength by mitigating the effect of existing surface defect and preventing the formation of new surface flaws. The haling effect depend on the ability of the sizing to penetrate in the surface defect and is therefore correlated with the dimension of the sizing particles. Pure silanes dispersion have been proved to enable healing a great part of the defect content [155], which is in accordance to the results obtained for IPF and IPF PTMO. Howevere, the similar scale and shape parameters obtained for IPF PTMO, SB5 and CSB, suggests that the application of coatings on sized fibers does not lead to a further reduction of the number and severity of the surface flows.

Table 4.10: Mechanical properties of the 14 µm IPF AR-glass fibers, unsized, sized with PTMO and coated with SB5 and CSB, CoV % in brackets.

Sample	**Young's modulus [MPa]**	**Tensile strength [MPa]**	**Strain at break [%]**	σ_0 **[MPa]**	**m**	$\mathbf{R_2}$
IPF	76.14 (3.39%)	1018.48 (37.23%)	1.51 (38.40 %)	1352	3.27	0.99
IPF PTMO	76.16 (1.32%)	1534.47 (28.28%)	2.35 (30.11%)	1712	3,56	0.97
IPF SB5	76.34 (1.11%)	1560.11 (24.02%)	2.29 (27.00%)	1702	4.03	0.98
IPF CSB	77.06 (1.03%)	1578.88 (23.55%)	2.35 (24.73 %)	1724	4.81	0.98

Single Fiber Pull-out Test

Figure 4.35 and Figure 4.36 present the load displacement curves obtained for the QSFPO tests conducted on glass fibres with different surface modification embedded within the cementitious matrix. As discussed in chapter usually the force-displacement curved obtained for QSFPO test are characterized by a linear elastic deformation till start of interfacial debonding, were usually an abrupt slope-change of the curve is observed which manifests as a "kink" in the graph. However, as has been observed in other studies and already discussed in chapter due to the similar elastic moduli of fibres and matrix, glass fibres embedded in cementitous matrix do not display the typicall "kink" which can be observed for example for low modulus polymer matrices. After reaching the maximum load peak (F_{max}), a force drop is observed. This is due to the loss in equilibrium between interfacila and frictional adhesion, that causes an uncontrolled debonding until the frictional bond is reached. For now on, the fibre is completely debonded, and the load measured is determined only by the fibre-matrix friction. Some qualitative information on the fiber-matrix interaction of the different

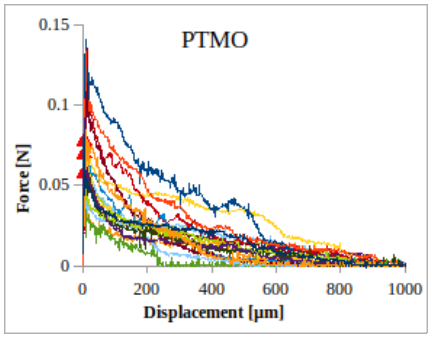

Figure 4.35: Force-displacement curves of single fiber pull-out tests of ARG fibers treated with PTMO sizing.

IPF fibers can be obtained observing the graph shape. All the fibres reach the

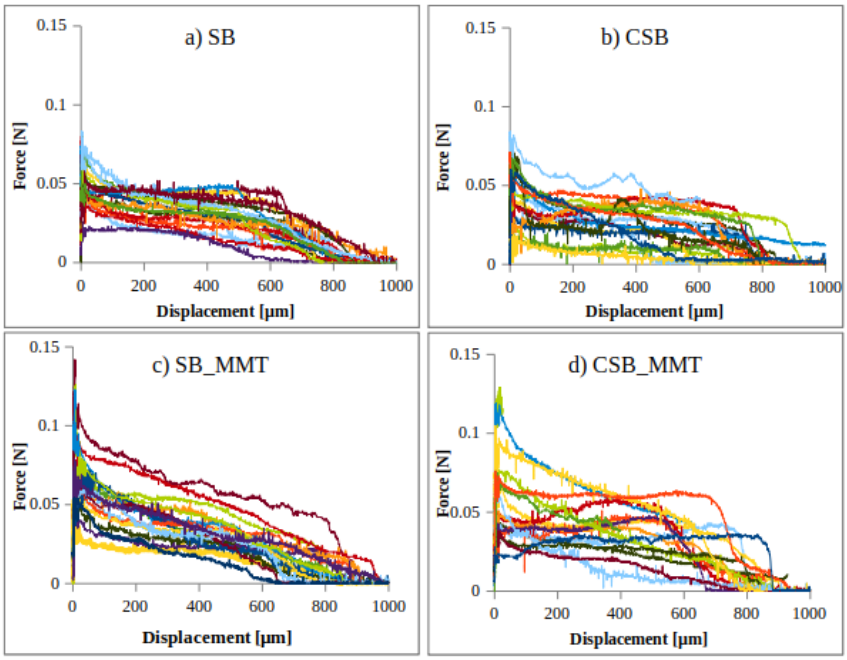

Figure 4.36: Force-displacement curves of single fiber pull-out tests of ARG fibers with different coatings.

maximum force at low displacement levels due to the brittle nature of the fiber-matrix combination. After reaching the F_{max} IPF PTMO curves are characterized by a pronounced load drop, which suggest a higher chemical fibre-matrix bonding compared to the coated fibres. On the contrary the fiber-matrix interaction of the coated fibres is dominated by the pull-out of the fibres after debonding, and the load decrease occurs much slower than in the PTMO curves. This can be attributes to the mechanical interlocking caused by the coating which is removed from the fibre surface and accumulates between the fibre and the matrix. A more detailed discussion of the fibre-matrix interaction can be conducted analysing the IFSS and pull-out work W_{tot} , reported in Table 4.11 IPF PTMO displays the highest F_{max} and IFSS values due to the high chemical bond at the fibre-matrix interface promoted by the ability of silane groups to react with the OH-groups present on both the fibres surface and the cementitous matrix.

Table 4.11: Results of SFPO depending on the surface treatment of the ARG fibers.

Sample name	**IFSS [MPa]**	**W_{total}[mN*mm]**	**l_e** [mm]
PTMO	4.2 ± 2.4	15.2 ± 7.6	663 ± 245
SB	1.9 ± 0.3	25.3 ± 5.6	894 ± 163
CSB	1.5 ± 0.5	20.3 ± 7.5	847 ± 106
SB_MMT	2.2 ± 0.5	28.8 ± 10.1	782 ± 117
CSB_MMT	1.9 ± 0.5	34.4 ± 11.3	883 ± 62

The SB coating account on one hand for a reduction of the IFSS (-55 %), but on the other hand for an increase in the pull-out work (+40 %). The IFSS and W_{tot} of IPF CSB are both lower than the values obtained for IPF SB. The slight increase of the surface roughness observed for IPF CSB (Tab. 4.9) does not seem to improve neither the adhesion with the matrix nor the pull-out work. On the contrary a significant increase of the F_{max} peak can be observed for SB5 and CSB5 compared to the fibres with the same coating. This support the hypothesis that nanoclay particles promote the chemical interaction between the organic coating and the cementitous matrix, and confirm the results obtained by immersing the fibres in the cement solution (Fig. 4.34).

Remarks

The results obtained can be summarized as follows:

- The maximum load reached by the coated fibers is always lower compared with PTMO fibers. However, after fiber debonding and for larger displacement values, the pull-out load is higher for the coated fibers resulting in higher pull-out work.
- For both SB and CSB coating the addition of MMT particles produced an increase in the maximum force reached. This can be attributed to a better interaction with the cementitious matrix and to the ability of nanoclay particles to work as nucleating species for the formation of hydration products.
- Increase of the polymer roughness did not lead to an increase of the pull-out load, suggesting that the modification of the chemical characteristics has a major impact on the interaction with the cementitious matrix.

4.4.5 Macro-mechanical Tests

Roving Tensile Test

Figure 4.37a and 4.37b report respectively the maximum tensile strength and the elastic modulus of the IPF glass yarns with sizing and polymeric coatings SB, SB5, SB20 and SB80. The highest load value are obtained for the yarns with the SB coating, that reached a maximum tensile strength of 719 MPa, which is about 48 % higher than the tensile strength obtained for the uncoted samples (487 MPa). By gradually decreasing the polymeric amount of the coatings lower tensile strength value are obtained. This is particularly evident for sample IPF SB80 whose tensile strength value are in the range of that obtained for the uncoated yarns.

Figure 4.38 clearly shows that in the yarns IPF SB80 the low amount of polymer (3.53 % of the total yarn weight) is not sufficient to build a continuous film that embed all the single filaments. By higher amount of polymer in the coating the filaments are tightly bound to each other, so that a better stress distribution is obtained resulting

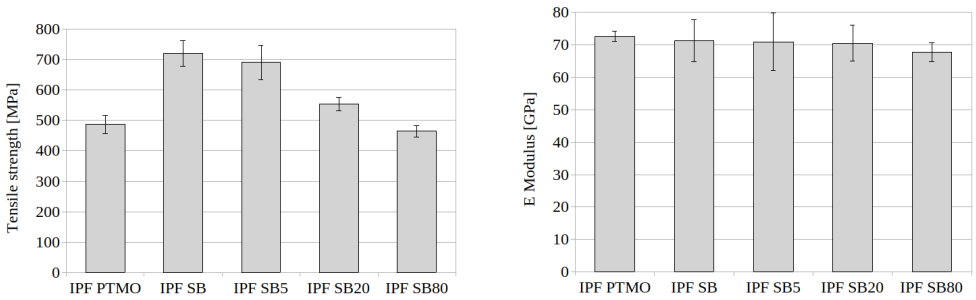

(a) Maximum tensile strength of IPF yarns PTMO, SB, SB5, SB20 and SB80.

(b) Elastic modulus of IPF yarns PTMO, SB, SB5, SB20 and SB80.

Figure 4.37: Carbon yarns tensile strength and E modulus.

in a higher yarn tensile strength. However, also for the coated yarns, the maximum tensile strength obtained is well below that of the single filaments (1534 MPa).This is probably due to the fact that also the coatings SB, SB5 and SB20, were not able to fully impregnate the multi-filament yarns. This is in accordance with the failure mode observed for the coated samples. Indeed, as it can be seen in Figure 4.39 also yarns with a higher polymer amount display a progressive failure of the filaments.

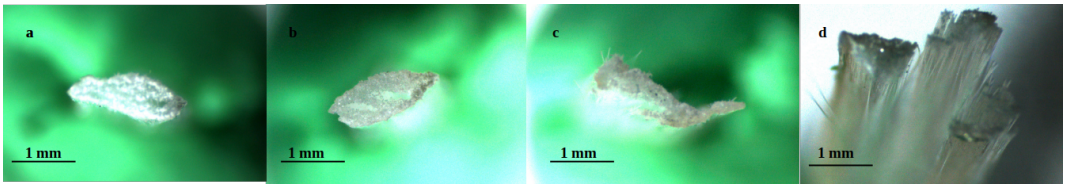

Figure 4.38: Macroscope image of the cross-section of the IPF yarns with coating SB (a), SB5 (b), SB20 (c) and SB80 (d).

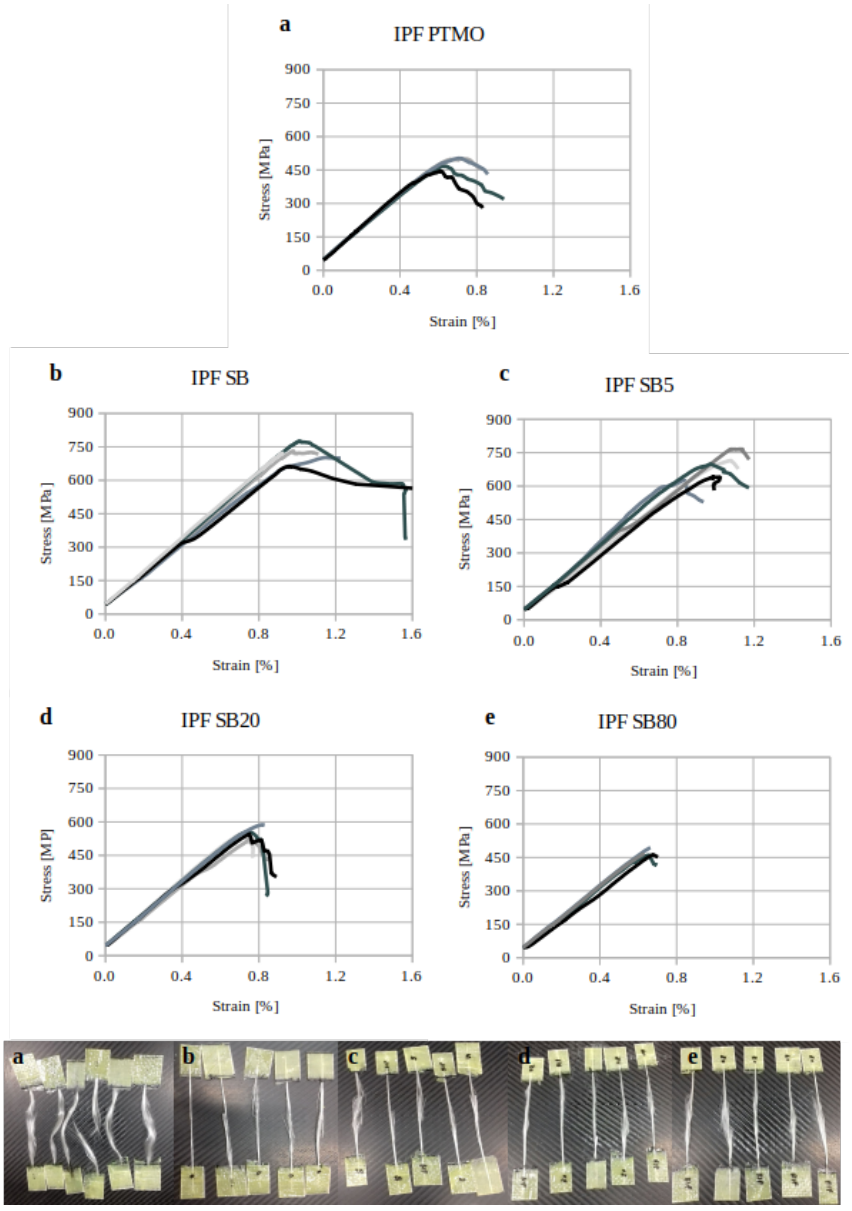

Figure 4.39: Stress-strain curve and failure mode of yarn IPF PTMO (a), SB (b), SB5 (c), SB20 (d) and SB80(e).

Roving Pull-out Test

Figure 4.40 shows the load-displacement curves obtained for the IPF rovings with and without coatings. The maximum pull-out load (F_{max}) and the pull-out work W_3 are reported in Table 4.12. The pull-out behavior of IPF PTMO is characterized by a first linear increase of the load, followed by a pronounced load decrease after reaching the maximum load F_{max}. Figure 4.41a shows that the cementitious matrix wasn't able to penetrate in the core of the roving. However, during the pull out test PTMO rovings reached higher loading vale than during the tensile test, which suggest that the matrix could provide in some extent a good stress distribution between the filaments. This is confirmed by the complete failure of the roving during the test observed for some samples. As discussed in the previous chapters, uncoated multifilament yarns are usually reported exhibiting a telescopic failure due to the inability of the matrix to involve all the filament in the stress distribution. However, in this case this phenom can be partially reduced due to the relatively small diameter of the rovings employed. Moreover, as shown in Figure 3.13 in some PTMO specimens the roving were found to be completely spread out in the matrix, which accounts for a higher number of filaments in direct contact with the matrix.

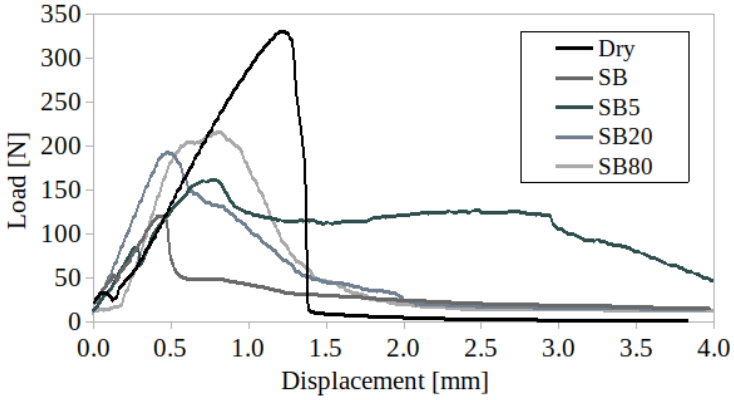

Figure 4.40: Typical load-displacement curve obtained for the pull out of IPF rovings PTMO, SB, SB5, SB20 and SB80.

In general the coated roving reached lower pull-out load than the PTMO samples. However, by considering the different geometry of the samples it can be observed that a significant decrease of the shear stress is observed only for SB sample. With the 5 % addition of nanoclay the maximum pull-out load observed increase form 104 N to 159 N (+53 %), and it farther increases at 179 N for SB20 (+73 %) and 201 N (+94 %) for SB80. The lower pull-out value obtained for the SB polymer can be explained by the partial dissolution of the coating in the cementitious matrix. Indeed, Styrene-acrylate latexs have been reported to slow down the hydration process of the cementitious matrix [**?**], which would explained the lower bond with the matrix. When nanoclays are dispersed in the coating this effect is mitigated by the ability of the nanoclay to act as nucleating point for hydration products [40].The modification

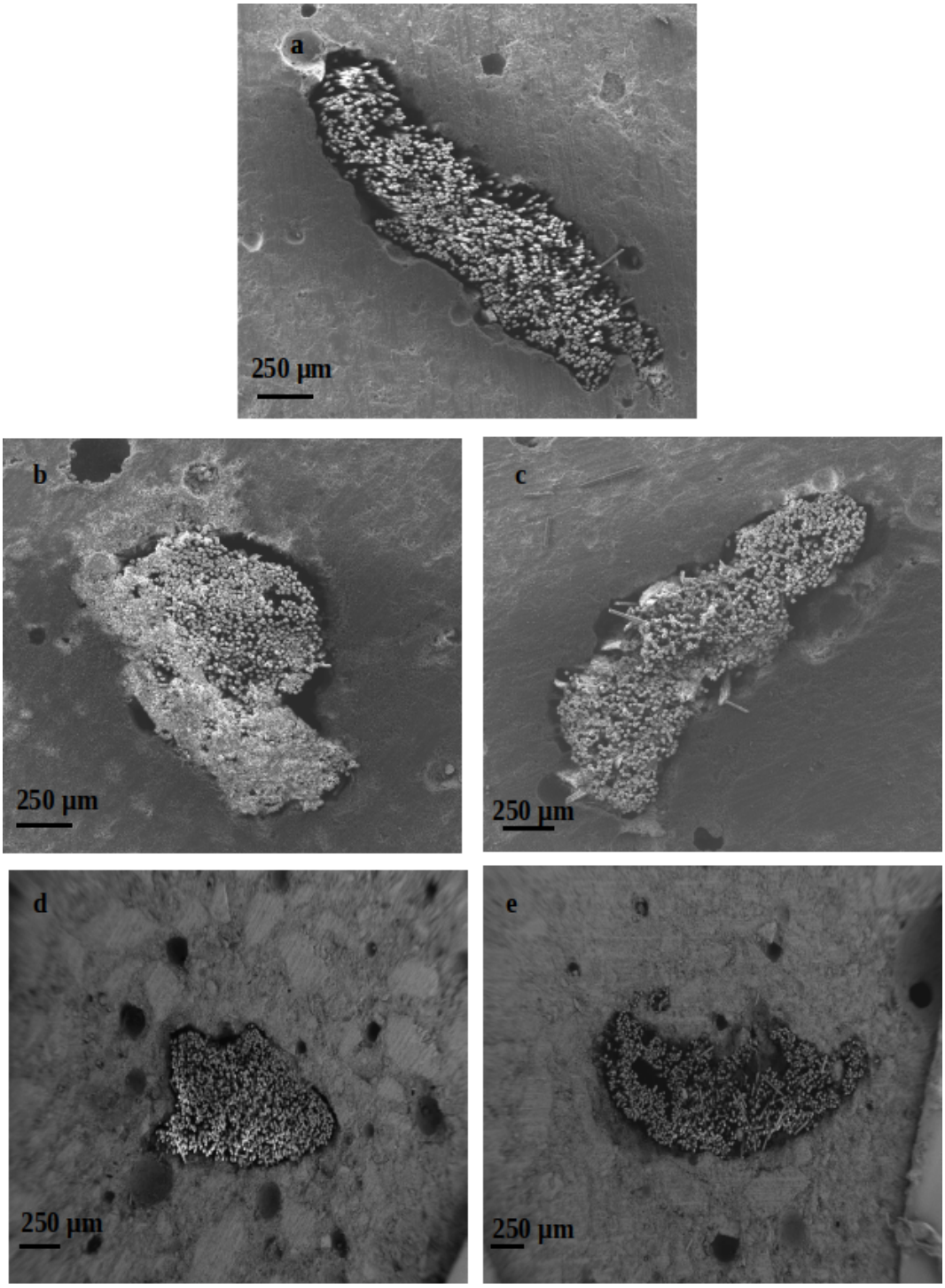

Figure 4.41: Cross section of specimens a) PTMO, b) SB, c) SB5, d) SB20 and e)cSB80 after pull-out.

Table 4.12: Pull out value obtained for IPF roving after 111 days aging at laboratory condition.

Sample	$\mathbf{S}_e$ **[mm]**	$\mathbf{F}_{max}$ **[N]**	τ_{max} **[MPa]**	$\mathbf{W}_3$	**Failure mode**
IPF	1.35 ±	312 ±	0.77 ±	334 ±	T/R
PTMO	0.10	42	0.10	102	
IPF SB	0.52 ±	104 ±	0.53 ±	115 ±	P
	0.11	25	0.13	25	
IPF SB5	0.67 ±	159 ±	0.82 ±	264 ±	P
	0.11	52	0.27	90	
IPF SB20	0.75 ±	179 ±	0.92 ±	214 ±	T/P
	0.24	43	0.22	63	
IPF SB80	0.70 ±	201 ±	1.04 ±	260 ±	T/P
	0.14	24	0.12	92	

P: Pull-out, T: telescopic effect, R: roving breakage

of the roving with a polymeric coating has also a strong influence on the shape of the graph in the debonded zone. For all the coated roving the drop of the load after reaching the F_{max} is less pronounced. Particularly some curved obtained for SB5 maintained relatively high pull-out value also at high displacement as shown in Figure 5.6.5. This can be attributed to the friction developed at the yarn-matrix interface during the pull-out of the yarn from the matrix after debonding. By decreasing the amount of polymer in the coating the graph shape gradually displace a more pronounced load drop in the debonding zone. However, it can be noted that despite the smaller amount of polymer coating SB5 is much more efficient than coating SB in preventing the pull-out load to drop after the debonding of the yarn.

4.4.6 Remarks

From the results obtained the following conclusions can be drawn:

- The tensile strength of the roving is in general increase by the modification of the roving with a coating. The higher the polymer content in the coating the higher the improvement of the load-bearing capacity.
- For the pull-out test the opposite results are obtained, with the PTMO rovings showing the highest F_{max} and W_3 and the SB the lowest pull-out load and pull-out work.
- Coated roving show a more ductile behavior compared to the PTMO samples.
- The addition of nanoclay particles in the coating formulation sensibility increase the interaction with the cementitious matrix. Samples SB80 show the highest shear stress followed by sample SB20 and SB5.

4.4.7 Accelerate Aging

Singel Fiber Tensile Test

Unsized

Figure 4.42 shows the surface of the unsized IPF fibers after aging in different solutions. For the fibers immersed in the saline solution no sign of corrosion can be observed, while sample subjected to the NaOH and 3 ions protocols both display signs of chemical attack. Interesting it can be observed that the corrosion profile shown by the fibers is different for the two alkaline solutions. Fibers storaged in the NaOH solutions show a brittle shell-like layer on their surfaces, but the surface of the fiber underneath the corrosion shell, which emerged where the layer is partially peeled off, seams intact. On the contrary fibers aged in the 3 ions solution displays a uniform net like corrosion pattern.

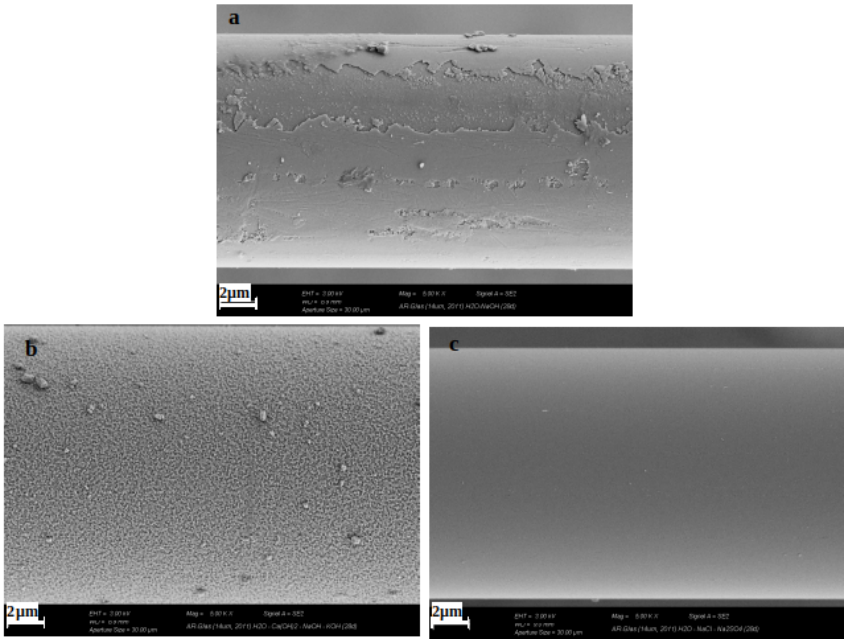

Figure 4.42: Surface of unsized IPF fibers after aging in a) NaOH , b) 3 ions and c) saline solution for 1000 hours at 40°C.

Tabel 4.13 reports the Weibull parameters calculated for the specimens subjected to different aging protocols. For specimens immersed in NaOH solution a unimodal distribution was observed while the specimens immersed in the three ions and saline solution display a bimodal distribution. For samples subjected to saline exposure a clear increase of the scale parameter σ_{01} is observed, while the σ_{01} of the specimens 3 Ions decreases from 1352 to 864 MPa. Despite the high pH value of the NaOH solution also specimens NaOH report a light increment of the scale parameter σ_{01}. This is in accordance to the corrosion mechanism proposed by Scheffler et al., which supposed that at some state of the corrosion process in NaOH solution the filament

experiment an increase of the failure stress as discussed in section . On the contrary the marked decrease of the filaments stress failure as well as the occurrence of a bimodal distribution for low failure stress value observed for sample 3 Ions has a closer resemblance with the degradation mechanism observed for glass filaments immersed in cement solution. This can be attributed to the high percentage of $Ca(OH)_2$ dissolved in the 3 Ions solution. Indeed, the corrosion mechanisms of glass fibers in cement solution is reported to be influence by the formation of a low soluble $Ca(OH)_2$ layer.

Table 4.13: Values of the two-parameter Weibull distribution function of unsized IPF fiber after aging protocols.

Aging	**Distribution I**				**Distribution II**			
protocol	σ_{01} **[MPa]**	$\mathbf{m_1}$	$\mathbf{R_2}$	**n**	σ_{02} **[MPa]**	$\mathbf{m_2}$	$\mathbf{R_2}$	**n**
Rif	1352	3.27	0.99	50				
NaOH	1529	3.19	0.95	50				
3 Ions	864	3.00	0.93	39	59	4.20	0.93	11
Saline	2253	12.41	0.95	32	1110	4.10	0.95	18

A remarkable increase of the scale parameter σ_{01} and the relative shape parameter m_1 is observed after aging in the saline solution. An increase in the characteristic failure stress of glass fibers immersed in NaOH solution has been attributed by Scheffler et al. to the peeling of the external layer of glass fibers and the consequent removal of flaws from the filament surface. SEM images obtained for the filament immersed in the saline solution do not reveal any external sheet detaching from the filament surface. However, glass immersed in aqueous solution are known to slowly dissolve due to the degradation of siloxane bond, forming a gel like phase of extracted silica on the fiber surface. Since at pH=7 this process is far slower than at high pH value it can be assumed that the layer of the filament attacked by the saline solution has a relatively small thickness. In this case small defect on the fiber surface may have been removed accounting for the higher failure stress obtained in Distribution I. On the contrary, filaments presenting more sever flaw are rather affect by the dissolution of the external layer of the fiber. This would explain the occurrence of a second distribution with a lower scale parameter.

AMEO

Figure 4.43 shows the surface of the AMEO IPF fibers after aging in different solutions. Significant difference can be observed in the change of the fiber surface after aging between the sized and unsized fibers. Storage of AMEO IPF fibers in the NaOH solution causes a diffuse blistering and splitting of the fibers surface. This was also partially observed on the surface of AMEO IPF fibers aged in the 3 Ions solution, but to a much lesser extent. In some case crystal agglomerate attached to

the fibers surface could be detected. Different results have been obtained for the AMEO IPF fibers immersed in the saline solution. Some fibers display a smooth homogeneous surface (Fig.4.43), other present diffuse encrustation on their surface. This difference can be the result of the non homogeneous distribution of the sizing on the fiber surface (Fig. 3.4), since filaments employed for durability test were not single dip coated in the sizing, but immersed in the 1 % AMEO solution as a bundle.

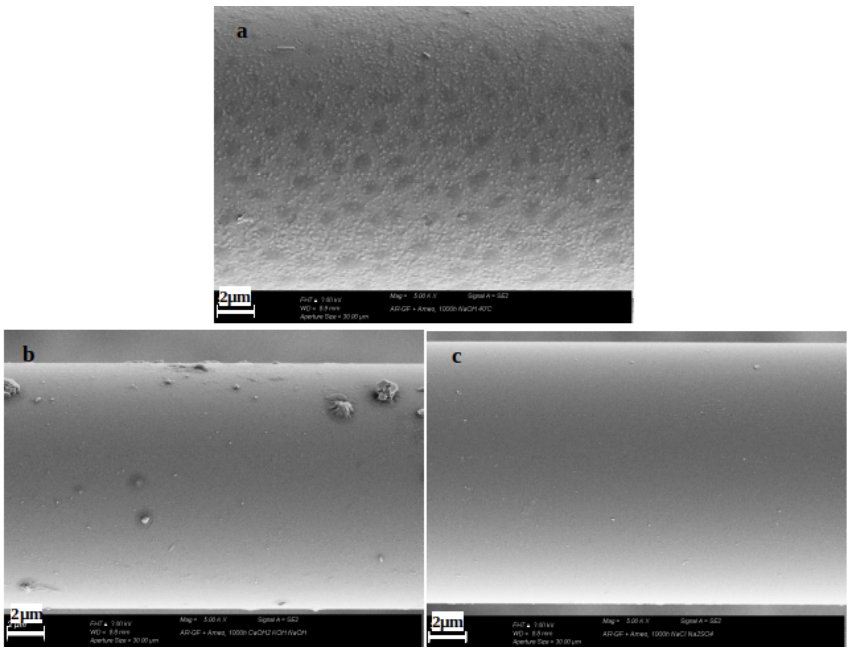

Figure 4.43: Surface of AMEO IPF fibers after aging in a) NaOH , b) 3 ions and c) saline solution for 1000 hours at 40°C.

Table 4.14 reports the scale and shape parameters for the Weibull distribution of the filament stress failure. First of all it can be observed that the scale parameter of the sized filaments is considerably higher than that obtained for the unszied fiber, which confirm the ability of the sizing to mitigate the surface defect of the fibers. The AMEO sizing results event more efficient than the PTMO sizing to improve the tensile strength of the filament. However, it could not be employed in combination with the Carboxylated-Styrene Butadyen film former because the amino group on the Ethoxysilane reacted with the carboxylic group on the polymer, resulting in an unstable sizing formulation.

A mixed failure stress distribution is observed for filaments aged in the NaOH solution. The scale parameter σ_{01} is barely affected by the aging protocols, but the scale parameter σ_{02} reveal that some filaments fail at the same stress value of unsized filament. This suggests that the sizing has been partially removed form the fiber surface. The high shape parameter obtained for Distribution I m1=14.34 indicates that where the sizing is still attached on the filaments it maintains its ability to mitigate the size and distribution of defects. A significant decrease of the scale parameter σ_{01} is observed for the filaments storaged in the 3 Ions solution. However,

Table 4.14: Values of the two-parameter Weibull distribution function of AMEO IPF fibers before and after aging in NaOH and 3 Ions solution.

Aging	**Distribution I**				**Distribution II**			
protocol	σ_{01} **[MPa]**	$\mathbf{m_1}$	$\mathbf{R_2}$	**n**	σ_{02} **[MPa]**	$\mathbf{m_2}$	$\mathbf{R_2}$	**n**
Rif	1889	4.20	0.97	50				
NaOH	1809	14.34	0.97	36	1364	2.50	0.95	14
3 Ions	1576	4.20	0.98	50				

the characteristic failure stress remain far above that obtained for the unsized fibers before aging, suggesting that the alkaline corrosion is considerably slow down by the sizing.

Rovings tensile test

Table 4.15, 4.16, 4.17 reports the mechanical properties of the IPF roving before and after aging protocols. For all the environment the IPF SB presents the highest tensile strength, immediately followed by the IPF SB5. This seams to confirm that the amount of polymeric coating plays a predominant role in the load-bearing capacity of the yarns. However, also the coated yarns experiment a significant decrease of the maximum tensile strength after 2000 hours immersion in the alkaline solution. After alkaline exposure IPF SB and SB5 have a maximum tensile strength of 398 MPa and 386 MPa respectively, which correspond to a decrease of the 44 % of the original tensile strength of the yarns. Figure 4.44 shows that after immersion in the alkaline solution grate part of the coatings is removed form the fibers surface, which indicate a low resistance of the polymer to alkaline exposure. Therefore, the decrease of the tensile strength observed can be partially attributed to a compromise stress transfer between the single fibers due to the partial dissolution of the polymeric coating. However, the tensile strength value of IPF SB and SB5 after aging are inferior than the maximum tensile strength of IPF PTMO before accelerate aging (487 Mpa), and the decrease in the tensile strength of the roving is much sever than that observed for the single fibers. Figure 4.45 shows that the surfaces of the coated fibers after aging do not display any evident sign of corrosion, which is in accordance with the results obtained for the IPF AMEO fibers storaged in the same solution for 1000 hours. However, it can be observed that different hydroxide crystals agglomerate has deposited between the filaments (Fig. 4.44 and 4.44).

Table 4.15: Mechanical properties of the IPF roving before environmental exposure (CoV in round brackets)

Roving	**Maximum tensile strength** $\sigma_{max,yarn}$ **[MPa]**	**Tensile strength increase/ decrease [%]**	**Elastic modulus Eyarn (GPa)**	**Ultimate strain** $\varepsilon_{max,yarn}$ **[%]**
PTMO	486.64 (6.07%)	-	72.55 *(1.60%)*	0.67 *(8.15%)*
SB	718.57 (5.82%)	-	71.23 *(6.55%)*	1.00 *(8.11%)*
SB5	689.52 (8.25%)	-	*70.89 (8.95%)*	*1.00 (11.19%)*
SB20	552.94 (4.02%)	-	*70.49 (5.54%)*	*0.76 (5.21%)*
SB80	*464.13 (4.13%)*	-	*67.61*	*0.64*

Table 4.16: Mechanical properties of the IPF roving after aging in 3 Ions solution (CoV in round brackets)

Roving	**Maximum tensile strength** $\sigma_{max,yarn}$ **[MPa]**	**Tensile strength increase/ decrease [%]**	**Elastic modulus Eyarn (GPa)**	**Ultimate strain** $\varepsilon_{max,yarn}$ **[%]**
PTMO	301.89 (4.78%)	-37.96	68.26 *(6281%)*	0.43 *(8.42%)*
SB	397.84 (10.45%)	-44.63	61.38 *(10.89%)*	0.59 *(15.94%)*
SB5	385.84 (7.70%)	-44.04	68.63 *(2.07%)*	*0.53 (13.64%)*
SB20	337.92 (9.77%)	-38.89	69.03 *(8.25%)*	*0.48 (6.68%)*
SB80	344.33 (3.50%)	-25.81	68.67 *(3.01%)*	*0.45 (7.67%)*

Table 4.17: Mechanical properties of the IPF roving after aging in saline solution (CoV in round brackets)

Roving	**Maximum tensile strength** $\sigma_{max,yarn}$ **[MPa]**	**Tensile strength increase/ decrease [%]**	**Elastic modulus Eyarn (GPa)**	**Ultimate strain** $\varepsilon_{max,yarn}$ **[%]**
PTMO	619.34 (3.92%)	+27.27	69.78 *(6.80%)*	*0.95 (2.97%)*
SB	818.38 (9.76%)	+13.86	76.21 *(6.86%)*	1.17 *(9.14%)*
SB5	701.71 (6.97%)	+1.77	75.71 *(3.53%)*	*0.94 (10.06%)*
SB20	660.43 (5.82%)	+19.44	69.02 *(17.85%)*	*0.90 (17.35%)*
SB80	*538.18* (7.88%)	+15.95	70.11 *(1.42%)*	*0.75 (14.85%)*

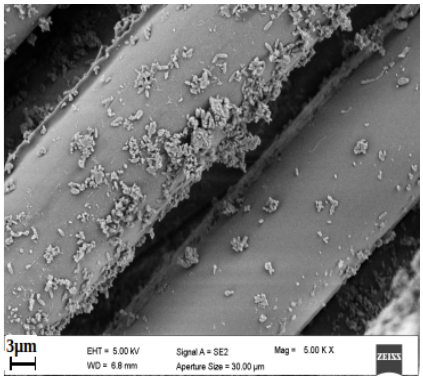

Figure 4.44: SEM images of the tensile test specimens PTMO immersed in the 3 Ions solution.

When the filaments are tightened during the tensile strength the presence of thin-tabular crystal as $Ca(OH_2$ between the filaments can induce lateral punctual pressure on the fibers surface, leading to a premature failure of the roving. This would be confirmed by the presence of scratches observed on the surface of some fibers after tensile test 4.46, and would also explaine why the roving 3 Ions failed in the proximity of the epoxy tabs (where the filaments are brought closer to each other), rather than in the middle of the roving as observed for sample Ref and Saline. Te lowest decrease of the yarn tensile strength is observed for the IPF SB80 (-26 % compared to the reference). Before immersion in the alkaline solution no relevant influence on the yarn tensile strength was observed between the IPF PTMO and IPF SB80. However, after accelerate aging the SB80 coated yarn have a maximum tensile strength of 344 MPa which is 14 % higher than the IPF PTMO. Indeed,

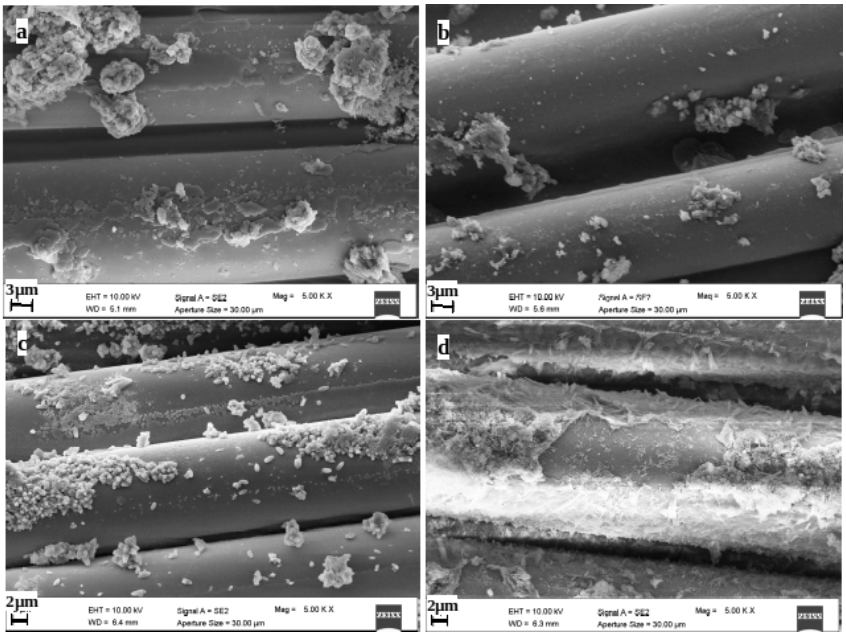

Figure 4.45: SEM images of the tensile test specimens a) SB, b) SB5, c) SB40 and d) SB80 immersed in the 3 Ions solution.

the IPF PTMO are more severely affected by the immersion in alkaline solution. This suggests that the small amount of polymer contained in the SB80 coating is not sufficient to considerably improve the stress distribution between the filaments compared to the PTMO sizing. However, an increase in the yarn durability to alkaline attack is observed. For what it concerns the other coated fibers, the results obtained suggest that the tensile strength degradation is due to a combination of polymer degradation and fiber alkaline corrosion. For what it concerns the aging of yarns in saline environment it can be observed that all samples experiment an increase of the maximum tensile strength. This confirms the results obtained for the unsized single filaments. Interesting it can be observed that tensile strength of the SB5 roving is almost unchanged. As discussed in the previous chapter the mechanism responsible for the increase of the fiber tensile strength after immersion in the saline solution involves the diffusion of water molecules and ions at the fiber interface. Therefore, the results obtained for roving SB5 after aging in the saline solution seams to confirm that the intercalated nanoclay particles provide a superior barrier to molecules diffusion.

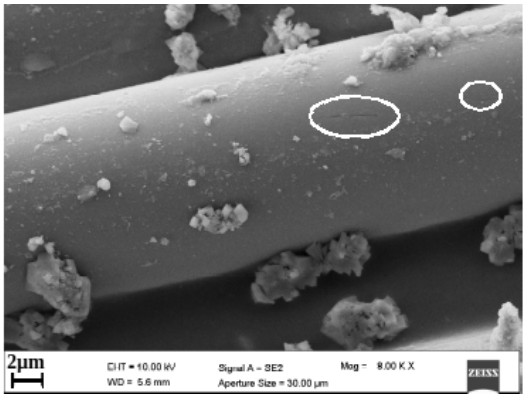

Figure 4.46: SEM images SB5 the tensile test specimens ages in the 3 Ions solution.

Pull-out

Figure 4.47 shows the load-displacement curves obtained for the pull-out of the IPF rovings with and without coatings after aging in the 3 Ions solution. In general the shape of the pull-out graph reassemble that obtained for the samples aged in laboratory condition. However, for all specimens a significant decrease of the maximum pull-out load was observed (Tab. 4.18). The SB sample presents the highest decrease of the F_{max} which confirm the very low stability of the SB polymer to alkaline attack. However, the failure mode for the SB does not change after aging in alkaline solution, and the pull-out of the roving from the matrix without failure of the external filaments remains the only failure mode observed. Also in Figure 4.48b no accumulation of hydration products could be observed between the filaments. Therefore, the reduced pull-out load observed is probably due to the partial dissolution of the polymeric coating causing a reduction of the friction developed at the fiber-matrix interface. On the contrary the loss in performance observed for PTMO sample is to attribute with the densining of the ITZ as can be observed in Figure4.48a. This is also confirm by the reduction in the pull-out work and the higher number of specimens where all the filaments of the roving failed. It can be observed in Figure 4.48a that the cementitious matrix has almost reached the core of the multi-filament roving. Sample SB20 and SB80 show a similar decrease of the pull-out load. SB80 still presents the highest shear stress (0.78 MPa) followed by the coating SB20 (0.69 MPa) and the SB5 (0.66 MPa). However, the lowest decrease of the composite mechanical properties is observed for the roving modified with the coating SB5.

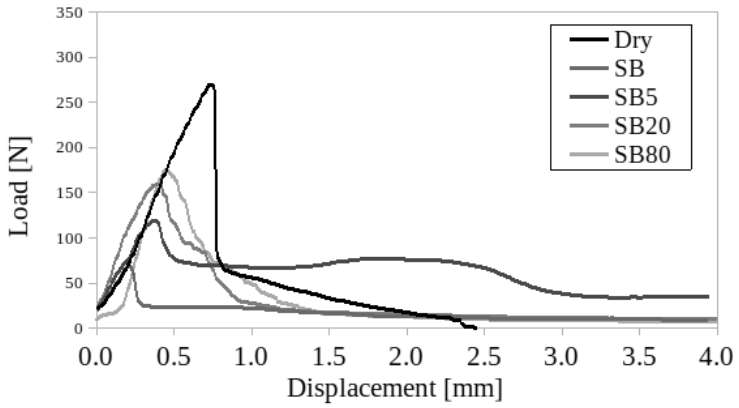

Figure 4.47: Typical load-displacement curve obtained for the pull out of IPF rovings PTMO, SB, SB5, SB20 and SB80, after aging in alkaline solution.

Table 4.18: Pull out value obtained for samples aged in alkaline solution.

Sample	**Se [mm]**	**F_{max} [N]**	**τ_{max} [MPa]**	**F_{max} variation [%]**	**W_3**	**W_3 variation [%]**	**Failure mode**
PTMO	0.82 ± 0.39	210 ± 56	0.52 ± 0.14	-32.90	138 ± 52	-60.97	R
SB	0.32 ± 0.12	67 ± 6	0.35 ± 0.03	-35.15	118 ± 78	-5.05	P
SB5	0.48 ± 0.08	128 ± 31	0.66 ± 0.16	-19.55	259 ± 81	-1.82	P
SB20	0.51 ± 0.21	134 ± 30	0.69 ± 0.15	-25.41	131± 98	-38.74	R/T/P
SB80	0.63 ± 0.11	152 ± 51	0.78 ± 0.26	-24.58	122±48	-53.00	T

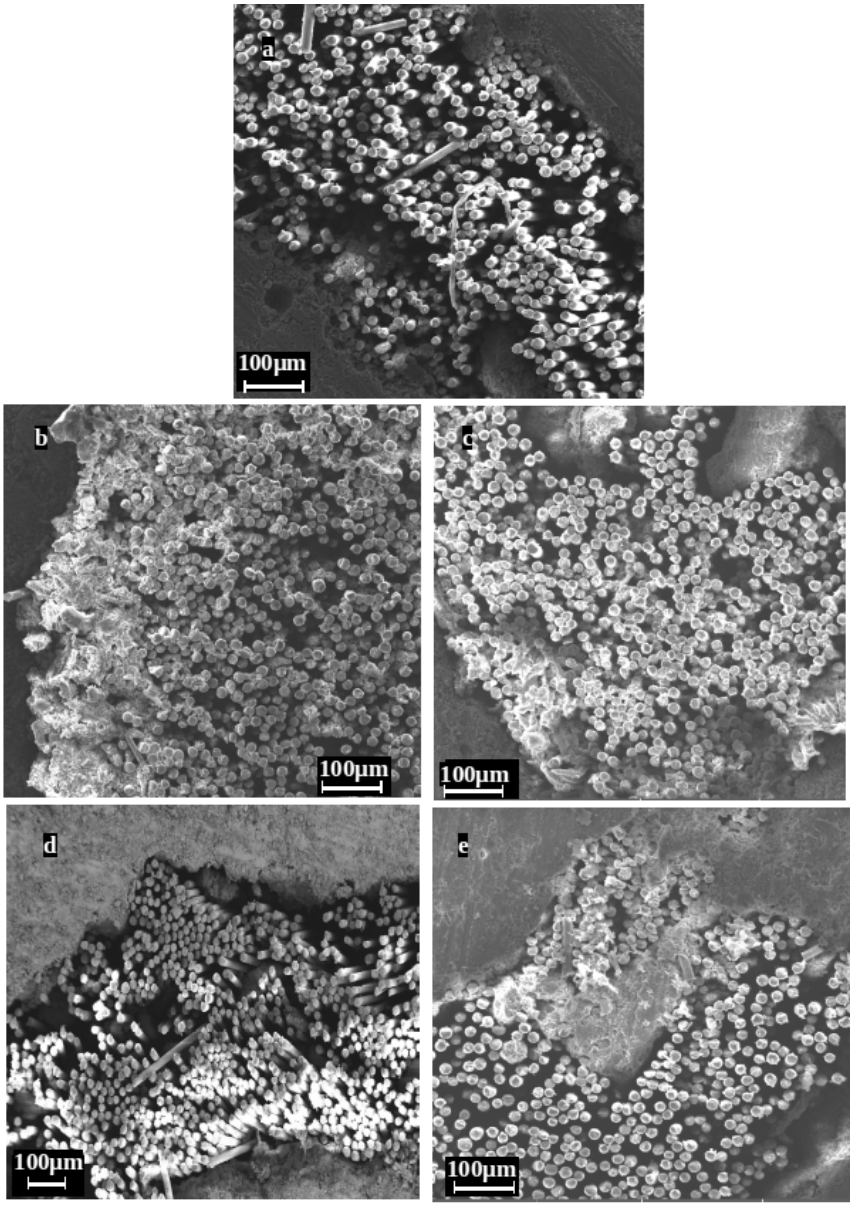

Figure 4.48: Cross section of specimens aged in the 3 ions solution after pull-out a) PTMO, b) SB, c) SB5, d) SB20 and e) SB80.

Different results are obtained for the specimens aged in the saline solution, which pull-out curves are reported in Figure 4.49.

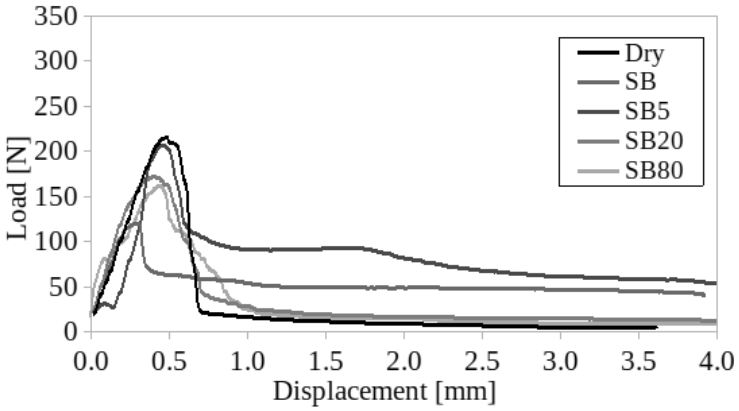

Figure 4.49: Typical load-displacement curve obtained for the pull out of IPF rovings PTMO, SB, SB5, SB20 and SB80, after aging in saline solution.

The decrease of the maximum pull-out load and pull-out work (Tab. 4.19) observed for the PTMO samples immersed in the saline solution is similar to that observed after aging in the alkaline solution (Tab. 4.18). This support the hypothesis that the loss in the composite performance is mainly due to the densining of the ITZ rather than to the chemical corrosion of the glass fibers. Also IPF SB80 aged in the saline solution experiments a similar decrease of the F_{max} and W_3 as the same sample immersed in the alkaline solution. Nevertheless the decrease of the mechanical properties of the composite is less sever than for samples PTMO which suggest that the small amount of polymer was able to partially prevent the formation of a stiff ITZ. This can be observed comparing Figure 4.50a and 4.50e. It can be seen that the external filaments of the PTMO specimens are tightly embedded in the cementitious matrix, which is not the case in sample SB80. This is in accordance with results presents in other studies conducted on the effect of polymeric coatings on the ITZ [71][60][105].

For roving IPF SB20 the F_{max} remains unchanged, however the composite display a less ductile behavior as can be observed in Figure 4.49. This also account for a reduction of the pull-out work in the face of the unaffected maximum pull-out load. SB_S shows a light increase of the maximum pull-out load, while the pull-out work does not experience any evident change. This confirms the high dependence of the coating stability with the pH value of the matrix. Indeed, as discussed in section the pH of the matrix immersed in the alkaline solution after 2000h retain a higher alkalinity than the same matrix aged in the saline solution. As can be seen in Figure 4.50b after exposure to the saline protocols the filaments are still embedded in the polymeric coating which prevent the hydration products to accumulate between the filaments. The change in the F_{max} of the coated roving highlight the superior ability of the coating SB5 to simultaneously provided a good interaction with

Table 4.19: Pull out value obtained for samples aged in saline solution.

Sample	**Se [mm]**	**F_{max} [N]**	τ_{max} **[MPa]**	**F_{max} variation [%]**	**W_3**	**W_3 variation [%]**	**Failure mode**
PTMO	0.63 ± 0.10	218 ± 52	-30.16	0.54 ± 0.13	159 ± 75	-54.98	R
SB	0.70 ± 0.35	114 ± 14	10.41	0.59 ± 0.07	121 ± 68	-3.37	P
SB5	0.50 ± 0.05	196 ± 25	23.56	1.01 ± 0.13	262 ± 46	-0.80	P
SB20	0.48 ± 0.22	184 ± 36	2.92	0.95 ± 0.18	163 ± 105	-23.86	T/R
SB80	0.57 ± 0.17	158 ± 6	-21.21	0.82 ± 0.03	102± 18	-60.66	T/R

cementitious matrix and a high durability of the composite. The results obtained for sample PTMO, SB80, SB20 and SB suggest that the ability of the composite to withstand a loss in performance over time is mainly related to the amount of polymer that cover the glass filaments. However, despite a lower amount of polymer content sample SB5 show the highest durability, with an increase of the pull-out load of the 24 %. As can be observed in Figure 4.50c the external filaments of the SB5 roving are protected by a thin layer of polymer which forms a very homogeneous interface with the cementitious matrix, but prevent the accumulation of hydration products between the filaments. The same can be observed for SB_S. In both case the increase of the pull-out load is due to the stronger bond formed with the cementitious matrix thanks to its improved hydration in the high humidity of the aging environment. However, this effect is more marked for the coating SB5 thanks to the addition of the nanoclay particles. For what it concerns the behavior of the composite in the post debonding region, it can be observed that for both SB_S and SB5_S, despite the increase of the pull-out load, no significant change in the pull-out work could be observed. This suggests a tendency of the composite to gain a more brittle behavior over time. However, at the aging condition investigated both systems maintain a certain ductility. Interesting the addition of the nanoclay particles does not seems to increase the brittleness of the composite over time as has been reported in other studies [62][40]. This can be attributed on one hand to the relatively low alkalinity of the cementitious matrix employed and on the other hand to the optimal dispersion of the MMT particles in the polymeric coating.

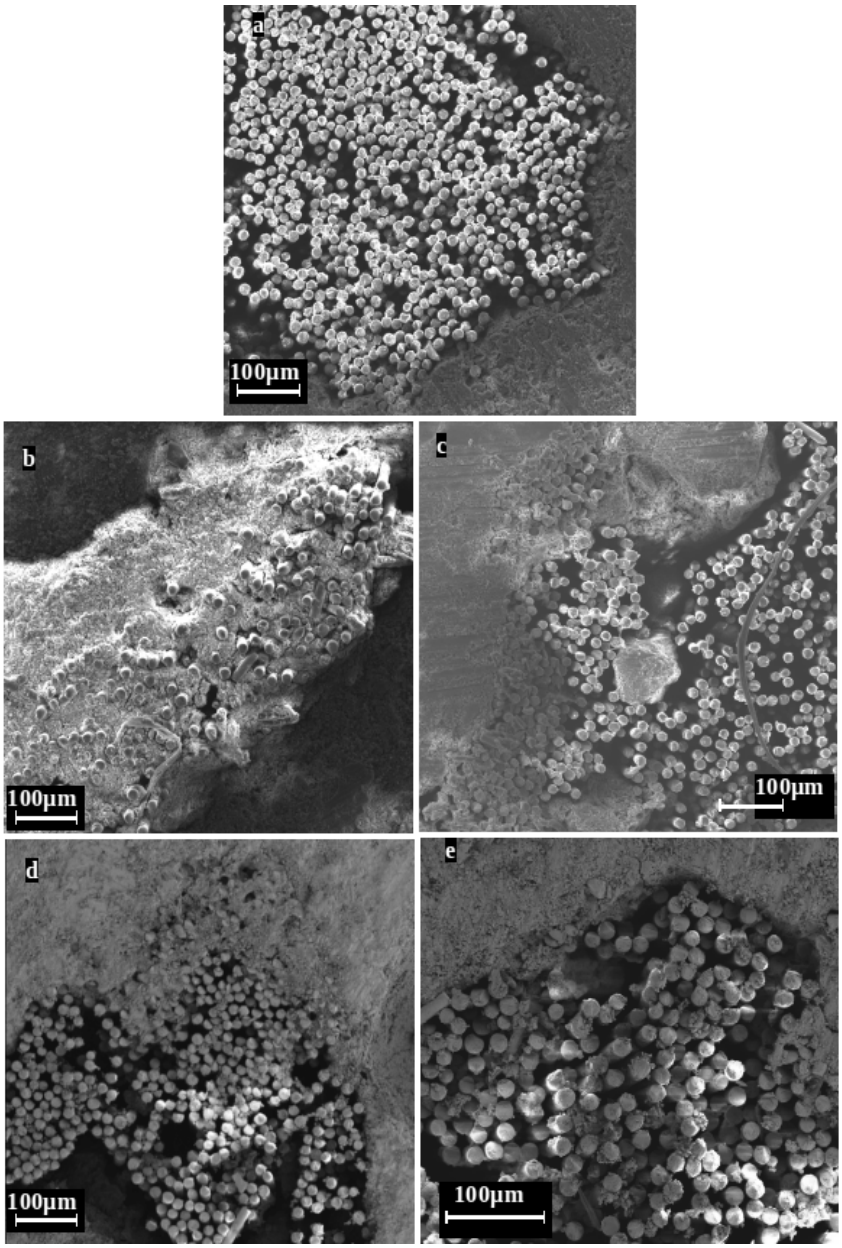

Figure 4.50: Cross section of specimens aged in the saline solution after pull-out a) PTMO, b) SB, c) SB5, d) SB20 and e) SB80.

Remarks

From the results obtained the following conclusions can be drawn:

- Regardless of the application of sizing or coating on the fibers surface the 3 Ions solution is the most aggressive for the glass-fibers. Despite presenting some clear sign of corrosion the unsized filament storaged in the NaOH solution did not experiment a decrease of the tensile strength. For some unclear reason the saline solution have a beneficial effect on the tensile strength of the filaments.

- Despite the small thickness of the sizing a sensible improvement of the fibers' durability was observed in the 3 Ions solution. On the contrary a significant decrease of the scale parameter was observed for AMEO filaments immersed in the NaOH solution, which was attributed to the removal of the sizing from the fibers surface.

- For all rovings a sensible decrease of the roving tensile strength is observed after 2000 hours aging in the 3 Ions solution. Roving SB and SB5 maintain the highest tensile strength but experiment the highest loss in performance which suggest that the polymer has a low stability in alkaline envioronments.

- For what it concerns the pull-out behavior the uncoated roving display a similar decrease of the mechanical properties regardless of the aging protocols. Both PTMO_3 and PTMO_S display a decrease of the maxium pull-out load of about the 30% and of the pull-out work between the 55 and 61 %. The loss in mechanical properties of the composite immersed in the saline solution is not in accordance with the results obtained for the durability test performed on the rovign and the cementitious matrix. This confirm that the change in the mechanical properties of the composite over timer are mainly governed by the change of the ITZ. Particulary for the PTMO_3 and PTMO_S the exposure to high humidity environment determine a stiffening of the ITZ which causes the premature failure of the glass filaments.

- With the exception of SB_3 the sample with the coated roving are always less severely effected by the aging protocols than the uncoated one. In both environment sample SB5 show the highest durability.

- The beneficial effect, observed for the pull-out samples aged at laboratory condition, of adding an high amount (20 and 80%) of nanoclay particles to the coating formulation is less marked for samples immersed in the 3 Ions solution, and becomes detrimental for specimens aged in the saline solution.

- The best results in terms of increase of polymer-matrix interaction and durability, are obtained with the addition of 5% of MMT in the polymeric coatings.

This can be attributede on one hand to the optimal balance between polymer content and nanocaly particle and on the other hand to the particular nanostructure obtained for the coating SB5.

Chapter 5

Conclusions and outlooks

5.1 Conclusions

The main objective of this work was to study the effect of different surface modification techniques on the durability of FRCM (Fabric Reinforced Cementitious Matrix) composites. Secondly the employment of nanoclay particles for the development of an hybrid inorganic-polymer coating was investigated as technique for the modification of the ARG fiber-matrix interface in order to obtain a composite with improved mechanical properties and durability. Aging protocols were chosen according to the AC 434-13 and the Italian guideline proposed by the CSLPP and on the basis of literature available. Chemically stable carbon fibers as well as AR-glass fibers, which are known to be sensitive to high pH value, have been used. Different coating has been employed which include: epoxy resin, nanosilica coating, commercial SB, carboxylated SB with and without addition of Montmorillonite nano particles in different percentages. Studies were conducted on both the composite and the components in order to better understand the mechanism responsible for the change of the FRCM mechanical properties exposed to different environments. Particularly the studies conducted with the AR glass fibers spun at the IPF enable a systematic investigation on the effect of the aging protocols also on the unsized filaments. Change in the chemical-physical structure of the materials in the different phases of the studies where investigated by means of different analytical methods which include: Furier Transformed Infrared-spectroscopy (FTIR)-analysis, Scanning Electron Microscopy (SEM), Electronic Microscopy, X-Ray diffraction and Ion Chromatography analysis. For the characterization of the nanoclay modified coating Thermogravimetric Anlysis and Differential Scanning Calorimetry (TGA and DSC) where employed as well as X-Ray diffraction and SEM-EDX-analysis, which enable to determine whether the polymer was intercaleted between the layer silicates or not, and if the nano silicates were uniformly dispersed in the polymeric matrix. The characterization of the fiber surface after modification with different coating was conducted with SEM and Atomic Force Microscopy (AFM)-analysis. The effect of the coatings on the fiber-matrix interface was than investigated performing Quasi static single fiber pull-out test. The results were than compared with those obtained form the pull-out of single roving coated with the same polymer and embedded in the same cementitious matrix.

According to the results obtained from the durability tests performed the following conclusion can be drawn. The change of the matrix mechanical properties over time are mainly influenced by the relative humidity and the temperature of the environment, with sample immersed in aqueous solution displaying higher compressive and flexural strength and those subjected to freeze-thaw cycle having slightly lower mechanical properties than the reference. Although the chemical composition of the aging solution has no significant impact on the mechanical properties of the matrix, sample immersed in the alkaline solution maintain higher pH values over time, and Ion Chromatography analysis proved that NaCl salt has penetrated in the matrix when samples where immersed in the saline solution. The effect of the aging protocols on the reinforcement depend on the kind of fibers used (AR-glass or carbon) and the different coating and sizing employed. No significant change in the tensile strength of the carbon yarns subjected to accelerate aging was observed, regardless of the possible modification conducted. This confirms the high chemical stability of the carbon fibers as well as the resistance to chemical attack of the epoxy coating employed. On the contrary, significant change in the mechanical properties of the BM ARG-fabric and IPF fibers where observed depending on the aging protocols and the application of sizing or coatings. On one hand the application of sizing and coating increase the tensile strength of the reinforcement and slow down the corrosion of the glass fibers. On the other hand both the commercial SB coating and the different coating formulations developed in this study show a low resistance to high temperature and pH values, so that the partial dissolution of the coatings results in a sever decrease of the yarn and roving tensile strength after aging in alkaline solutions at 40 °C. For some unknown reason, after aging in the saline solution, an increase of the tensile strength is observed for both unsized IPF ARG fibers and IPF roving regardless of the application of a coating. A beneficial effect in the addition of salts to the aging solution was also observed for the BM-ARG yarns. Yarns aged in the saline solution were substantially less effected than the same yarns immersed in NaOH solution and tap water. For the Pull-out test conducted on the carbon roving the highest pull-out load and pull-out work were always obtained for the epoxy impregnated yarn, regardless of the aging protocols adopted. Good results in terms of both enhancement of the fiber-matrix interaction and durability were also obtained with the nanosilica coating. The carbon yarns treated with an oxidative solution show a better interaction with the cementitious matrix, but eventually a loss in performance is obtained with the strengthening of the cementitious matrix over time. The same is observed also for the unmodified fibers. This highlights that the chemical stability of the reinforcement is a necessary but not sufficient prerequisite to obtain composite materials which can maintain their performance over time. Regardless of the fibers and coatings employed, in general the change in the yarns tensile strength after application of some kind of coating does not reflect the change of the composite properties observed in the pull-out test. In case of carbon fibers a significant increase in the yarn tensile strength was observed only by impregnating the filaments with

the epoxy resin, but all the modification techniques investigated lead to an increase in the pull-out load. On the contrary for the IPF ARG the SB rovings display the highest tensile strength but the lowest pull-out load and pull-out work were observed. Moreover, while the tensile strength of the roving is mainly influenced by the polymer content in the coating, the mechanical properties of the composite increases by increasing the amount of MMT particles in the coating formulation. The same discrepancy was also obtained for the durability test conducted on the reinforcement and the composite. For the carbon fibers no significant difference can be found on the yarn tensile strength after accelerate aging, but the mechanical properties of the pull-out specimens, realized with the same yarns, display significant change in the pull-out load and pull-out work after exposure to different aging protocols. Similar results are obtained for the BM and IPF ARG-fibers. Despite the tensile strength of the BM ARG yarn decreases, particularly after immersion in the NaOH solution, no significant loss in performance could be observed for the tensile strength of the FRCM coupons immersed in the saline and alkaline solution. For the IPF rovings significant difference in the durability of the composite were observed according to the coatings employed. Rovings with a low polymer content (PTMO and SB80), display a similar decrease of the F_{max} and W_3 regardless of the aging protocols. This is strongly in contrast to the increase in tensile strength observed for the IPF rovings immersed in the saline solution. According to the durability test conducted on the IPF roving sample SB5 are the second most affected by the aging in alkaline solution and display the lowest increase of tensile strength after immersion in the saline solution. On the contrary durability test conducted on the pull-out show that sample SB5 have the highest resistance to the alkaline environment and the highest increase in pull-out load after aging in the saline solution. Those results confirm the crucial role played by the ITZ in the determining the mechanical properties of the composite, and confirm that the ability of the systems to maintain its function over time does not only depend on the durability of its components. For what it concerns the effect of nanoclay addition on the mechanical properties and the durability of the composite material studied, following conclusion can be drawn: for a percentage of 5% of MMT nanoparticles a coating with an intercaleted structure could be obtained, however by increasing the percentage of nanoclay this nanostructure was loss; the addition of nanoclay does not affect the T_g of the polymer but an increase in the thermal stability of the polymer was observed for TGA analyses conducted in oxidative condition. AFM analyses reveal an increase in the polymer roughness, however QSFPO results suggest that this plays a minor role in the pull-out behavior of the composite. Nevertheless, a significant increase in maximum pull-out load was observed in both QSPO and roving pull-out test by adding 5 % of MMT nanoparticles in the SB coating. The macro mechanical pull-out tests conducted on roving SB20 and SB80 show that in the early phase of the composite life coatings with higher percentage of nanoclay particles provide composite with higher mechanical properties. However, both coating formulations reveal a low ability to prevent a

loss in the composite mechanical properties over time. On the contrary, the coating obtained with 5 % of nanoclay shows a superior resistance than the other coating formulations in the pull-out specimens subjected to accelerate aging. Nevertheless, the low resistance of the SB5 coating in an environment with high pH value highlights that the intercalation of nanoclay can only slow down the degradation of the coating, and therefore a certain chemical resistance of the polymeric matrix is an essential prerequisite.

5.2 Outlooks

The study conducted highlights that the ability of FRCM composite to maintain high performance level over time not only depends on the durability of its components. Therefore, accelerate aging tests used for the prediction of the long term performance, should be performed on the complete FRCM system. This is in accordance with methods recommended by the american and italian guidelines. However, the results obtained also question the efficiency of some of the aging protocols adopted. Particularly, it has been proved that the immersion of the composite in alkaline solution keeps the pH of the matrix at high alkaline value, while over the real life service of the material this would actually decrease. Also for the aging in saline solution alternative methods could be taken in consideration. Indeed, despite the penetration of salt ions in the matrix could be proved, no accumulation of the salt crystals could be observed, neither on the matrix surface nor at the fiber-matrix interface. Comparison with other aging protocols, such as wet dry cycles, could be conducted in order to reproduce as close as possible the real degradation mechanisms, that the composite undergoes during its life service. Organic coatings with a good stability in alkaline condition have been proved to increase the durability of the composite subjected to high humidity environment, however some studies have shown that the impregnation of the reinforcement with a polymeric coating can compromise the mechanical properties of the composite when exposed to high temperate. Since polymer-layered silicate nanocomposites are known to have a higher thermal stability compared to normal polymer, the modification of polymeric coating with nanoclay particles could also be investigated as a possible technique to overcome this issue. Finally, it could be observed that also the SB5 coating was not immune to chemical degradation in high alkaline environment, proving that a certain chemical stability of the polymeric matrix is an essential prerequisite for the development of coatings to be employed for the modification of FRCM textiles. In the future, other polymeric matrices could be investigated for this application.

Bibliography

[1] ACI 549.4R. Design and construction of externally bonded Fabric-Reinforced Cementitious Matrix (FRCM) systems for repair and strengthening concrete and masonry Structures. Technical report, 2013.

[2] R. Fangueiro and F. Soutinho. 3 - textile structures. In R. Fangueiro, editor, *Fibrous and Composite Materials for Civil Engineering Applications*, Woodhead Publishing Series in Textiles, pages 62–91. Woodhead Publishing, 2011.

[3] A Gries, T; Offermann P.; Peled. 3-textile. In W Brameshuber, editor, *Textile Reinforced Concrete - State-of-the-Art Report of RILEM TC 201-TRC*. RILEM Publications SARL, 2006.

[4] H. Hu and Y. Liu. 11 - high modulus, high tenacity yarns. In R. Alagirusamy and A. Das, editors, *Technical Textile Yarns*, Woodhead Publishing Series in Textiles, pages 329–386. Woodhead Publishing, 2010.

[5] Elizaveta Martynova and Holger Cebulla. Chapter 7 - glass fibers. In Boris Mahltig and Yordan Kyosev, editors, *Inorganic and Composite Fibers*, The Textile Institute Book Series, pages 131 – 163. Woodhead Publishing, 2018.

[6] A. Paul. Chemical durability of glasses; a thermodynamic approach. *Journal of Materials Science*, 12(11):2246–2268, 1977.

[7] Boris Mahltig. Chapter 9 - Basalt Fibers. In Boris Mahltig and Yordan Kyosev, editors, *Inorganic and Composite Fibers*, The Textile Institute Book Series, pages 195–217. Woodhead Publishing, 2018.

[8] Kunal Singha. A Short Review on Basalt Fiber. *International Journal of Textile Science*, 1(4):19–28, 2012.

[9] Jiří Militký, Rajesh Mishra, and Hafsa Jamshaid. 20-Basalt fibers. In Anthony R. Bunsell, editor, *Handbook of Properties of Textile and Technical Fibres (Second Edition)*, The Textile Institute Book Series, pages 805–840. Woodhead Publishing, 2018.

[10] Arnon; Bentur and Sidney Mindess. *Fiber Reinfroced Cementitious Composites*. Taylor & Francis, second edition, 2007.

[11] S. Tiwari and J. Bijwe. Surface Treatment of Carbon Fibers - A Review. *Procedia Technology*, 14:505–512, 2014.

[12] Alessandro Pegoretti and Matteo Traina. 17 - Liquid crystalline organic fibers and their mechanical behavior. In Anthony R. Bunsell, editor, *Handbook of Properties of Textile and Technical Fibres*, The Textile Institute Book Series, pages 621–697. Woodhead Publishing, second edition edition, 2018.

[13] W. Brameshuber, Tanja Brockmann, J. Wastiels, Manfred Curbach, C. Meyer, G. Vilkner, B. Mobasher, A. Peled, H.W. Reinhardt, and M. Krüger. *4 Concrete/Matrix*, pages 29–56. RILEM Publications SARL, 2006.

[14] D. D. L. Chung. Use of polymers for cement-based structural materials. *Journal of Materials Science*, 39(9):2973–2978, 2004.

[15] Bernd Walk-Lauffer, Jeanette Orlowsky, and Michael Raupach. Verstärkung des inneren Roving-Verbundes im textilbewehrten Beton. In *Verstärkung Des Inneren Roving-Verbundes Im Textilbewehrten Beton.*, pages 281–290, Weimar, 24. Bauhaus-Univ.

[16] Consiglio Superiore dei Lavori Pubblici. Linea Guida per la identificazione, la qualificazione ed il controllo di accettazione di compositi fibrorinforzati a matrice inorganica (FRCM) da utilizzarsi per il consolidamento strutturale di costruzioni esistenti. pages 1–5, 2018.

[17] Elisa Franzoni, Mattia Santandrea, Cristina Gentilini, Alberto Fregni, and Christian Carloni. The role of mortar matrix in the bond behavior and salt crystallization resistance of FRCM applied to masonry. *Construction and Building Materials*, 209:592–605, 2019.

[18] Fulvio Parisi, Costantino Menna, and Andrea Prota. 10 - fabric-reinforced cementitious matrix (frcm) composites: Mechanical behavior and application to masonry walls. In Mohammad Jawaid, Mohamed Thariq, and Naheed Saba, editors, *Failure Analysis in Biocomposites, Fibre-Reinforced Composites and Hybrid Composites*, Woodhead Publishing Series in Composites Science and Engineering, pages 199 – 227. Woodhead Publishing, 2019.

[19] Leonidas Alexandros S. Kouris and Thanasis C. Triantafillou. State-of-the-art on strengthening of masonry structures with textile reinforced mortar (TRM). *Construction and Building Materials*, 188:1221–1233, November 2018.

[20] Ali Dalalbashi, Bahman Ghiassi, and Daniel V. Oliveira. Textile-to-mortar bond behaviour in lime-based textile reinforced mortars. *Construction and Building Materials*, 227:116682, 2019.

[21] Jacopo Donnini, Giovanni Lancioni, Tiziano Bellezze, and Valeria Corinaldesi. Bond Behavior of FRCM Carbon Yarns Embedded in a Cementitious Matrix: Experimental and Numerical Results. *Key Engineering Materials*, 747:305–312, 2017.

[22] Jacopo Donnini. *STUDY OF ENHANCED FIBER REINFORCED CEMENTITIOUS MATRIX (FRCM) SYSTEMS FOR STRUCTURAL REHABILITATION*. PhD thesis, Università Politecnica delle Marche, 2016.

[23] Diana Arboleda. *Fabric Reinforced Cementitious Matrix (FRCM) Composites for Infrastructure Strengthening and Rehabilitation : Characterization Methods*. PhD thesis, University of Miami, 2014.

[24] Natalie Williams Portal. *Usability of Textile Reinforced Concrete: Structural Performance, Durability and Sustainability*. PhD thesis, Chalmers University of Technology, 2015.

[25] Saad M. Raoof, Lampros N. Koutas, and Dionysios A. Bournas. Bond between textile-reinforced mortar (TRM) and concrete substrates: Experimental investigation. *Composites Part B: Engineering*, 98(May):350–361, 2016.

[26] Stefano De Santis, Francesca Giulia Carozzi, Gianmarco de Felice, and Carlo Poggi. Test methods for Textile Reinforced Mortar systems. *Composites Part B: Engineering*, 127:121–132, 2017.

[27] Luciano Ombres. Analysis of the bond between fabric reinforced cementitious mortar (frcm) strengthening systems and concrete. *Composites Part B: Engineering*, 69:418–426, 2015.

[28] J Hegger, N Will, A Bentur, M Curbach, F Jesse, B Mobasher, A Peled, and J Wastiels. 6.2 Mechanical behaviour of textile reinforced concrete. In Wolfgang Brameshuber, editor, *Textile Reinforced Concrete - State-of-the-Art Report of RILEM TC 201-TRC*. 2006.

[29] RILEM Technical Committee 232-TDT (Wolfgang Brameshuber), W. Brameshuber, M. Hinzen, A. Dubey, A. Peled, B. Mobasher, A. Bentur, C. Aldea, F. Silva, J. Hegger, T. Gries, J. Wastiels, K. Malaga, C. Papanicolaou, L. Taerwe, M. Curbach, V. Mechtcherine, A. Naaman, J. Orlowsky, P. Hamelin, H. W. Reinhardt, S. Shah, R. Toledo, T. Triantafillou, Amir Si Larbi, D. Garcia, L. Garmendia, S. Gopinath, and F. Jesse. Recommendation of RILEM TC 232-TDT: Test methods and design of textile reinforced concrete: Uniaxial tensile test: Test method to determine the load bearing behavior of tensile specimens made of textile reinforced concrete. *Materials and Structures/Materiaux et Constructions*, 49(12):4923–4927, 2016.

[30] ICC-ES. AC434.13 - Acceptance criteria for masonry and concrete strengthening using fabric reinforced cementitious matrix (FRCM) composite systems. 2013.

[31] Diana Arboleda, Francesca Giulia Carozzi, Antonio Nanni, and Carlo Poggi. Testing procedures for the uniaxial tensile characterization of fabric-reinforced cementitious matrix composites. *Journal of Composites for Construction*, 2016.

[32] Jacopo Donnini, Giovanni Lancioni, and Valeria Corinaldesi. Failure modes in FRCM systems with dry and pre-impregnated carbon yarns: Experiments and modeling. *Composites Part B: Engineering*, 140:57–67, May 2018.

[33] P. Di Maida, E. Radi, C. Sciancalepore, and F. Bondioli. Pullout behavior of polypropylene macro-synthetic fibers treated with nano-silica. *Construction and Building Materials*, 82:39–44, 2015.

[34] Björn Banholzer. *Bond Behaviour of a Multi-Filament Yarn Embedded in a Cementitious Matrix; 1. Aufl.* PhD thesis, Aachen, 2004. Druckausgabe: 2004. - Onlineausgabe: 2005; Zugl.: Aachen, Techn. Hochsch., Diss., 2004.

[35] B. Banholzer, W. Brameshuber, and W. Jung. Analytical simulation of pull-out tests - The direct problem. *Cement and Concrete Composites*, 27(1):93–101, 2005.

[36] Edith Mäder, Rosemarie Plonka, Michael Schiekel, and Rainer Hempel. Coatings on alkali-resistant glass fibres for the improvement of concrete. *Journal of Industrial Textiles*, 33(3):191–207, 2004.

[37] Alva Peled and Arnon; Bentur. Quantitative Description of Pull-out Behavior of Crimped Yarns from Cement Matrix. *Journal of materials in civil engineering*, 15(November/December 2003):537–544, 2003.

[38] Sachiko Sueki, Chote Soranakom, Barzin Mobasher, and Alv Peled. Pullout-slip response of fabrics embedded in a cement paste matrix. *Journal of Materials in Civil Engineering*, 19(9):718–727, 2007.

[39] Roey Nadiv, Alva Peled, Viktor Mechtcherine, Simone Hempel, and Christof Schroefl. Micro- and nanoparticle mineral coating for enhanced properties of carbon multifilament yarn cement-based composites. *Composites Part B: Engineering*, 111:179–189, 2017.

[40] Simone Hempel, Marko Butler, Mirella Kratz, Christina Scheffler, and Rosemarie Plonka. Improvement of bond behaviour and durability of AR-glassfibre-reinforced concrete by polymer-fibre coatings. In *15th Congress of the Glassfibre Reinforced Concrete Association Internationa*, pages 225–233, Prague, Czech Republic, 20.

[41] Ting Gong, Ali A. Heravi, Ghaith Alsous, Iurie Curosu, and Viktor Mechtcherine. The impact-tensile behavior of cementitious composites reinforced with carbon textile and short polymer fibers. *Applied Sciences (Switzerland)*, 9(19), 2019.

[42] Christina Scheffler, Serge Zhandarov, Wolfgang Jenschke, and Edith Mäder. Poly (vinyl alcohol) fiber reinforced concrete: Investigation of strain rate

dependent interphase behavior with single fiber pullout test under quasi-static and high rate loading. *Journal of Adhesion Science and Technology*, 27(4):385–402, 2013.

[43] Christina Scheffler, Serge Zhandarov, Enrico Wölfel, and Edith Mäder. Interphases in Cementitious Matrix: Effect of Fibers, Sizings, and Loading Rates. In Viktor Mechtcherine, Volker Slowik, and Petr Kabele, editors, *Strain-Hardening Cement-Based Composites*, volume 15 of *RILEM*, pages 275–283. 2018.

[44] Francois De Luca, Giorgio Sernicola, Milo S. P. Shaffer, and Alexander Bismarck. "brick-and-Mortar" Nanostructured Interphase for Glass-Fiber-Reinforced Polymer Composites. *ACS Applied Materials and Interfaces*, 10(8):7352–7361, 2018.

[45] Serge Zhandarov and Edith Mäder. An alternative method of determining the local interfacial shear strength from force-displacement curves in the pull-out and microbond tests. *International Journal of Adhesion and Adhesives*, 55:37–42, 2014.

[46] Victor C. Li and Henrik Stang. Interface property characterization and strengthening mechanisms in fiber reinforced cement based composites. *Advanced Cement Based Materials*, 6(1):1–20, 1997.

[47] Serge Zhandarov and Edith Mäder. Characterization of fiber/matrix interface strength: Applicability of different tests, approaches and parameters. *Composites Science and Technology*, 65(1):149–160, 2005.

[48] C. L. Page. Microstructural features of interfaces in fibre cement composites. *Composites*, 13(2):140–144, 1982.

[49] H. W; Reinhardt, M; Krüger, A. Bentur, W; Brameshuber, B; Banholzer, M; Curbach, F; Jesse, B; Mambasher, A; Peled, and H; Schorn. Composite materials - 6.1 Bond. In W Brameshuber, editor, *Textile Reinforced Concrete - State-of-the-Art Report of RILEM TC 201-TRC*. RILEM Publications SARL, 2006.

[50] Andrej Ivanic, Samo Lubej, Rebeka Rudolf, and Ivan Anzel. Bond behavior of carbon-fiber yarn embedded in cement mortar. *Science and Engineering of Composite Materials*, 18(September):181–186, 2011.

[51] Marko Butler, Viktor Mechtcherine, and Simone Hempel. Experimental investigations on the durability of fibre-matrix interfaces in textile-reinforced concrete. *Cement and Concrete Composites*, 31(4):221–231, 2009.

[52] Massimo Messori, Andrea Nobili, Cesare Signorini, and Antonella Sola. Mechanical performance of epoxy coated AR-glass fabric Textile Reinforced Mortar:

Influence of coating thickness and formulation. *Composites Part B: Engineering*, 149:135–143, September 2018.

[53] J. Donnini, V. Corinaldesi, and A. Nanni. Mechanical properties of FRCM using carbon fabrics with different coating treatments. *Composites Part B: Engineering*, 88, 2016.

[54] Michael Raupach, Jeanette Orlowsky, Till Büttner, U. Dilthey, and M. Schleser. Epoxy-impregnated textiles in concrete. Load bearing capacity and durability. In W. Brameshuber J. Hegger and N. Will, editors, *ICTRC'2006 - 1st International RILEM Conference on Textile Reinforced Concret*, pages 77–88. RILEM Publications SARL, 2006.

[55] M. Schleser, B. Walk-Lauffer, M. Raupach, and U. Dilthey. Application of polymers to textile-reinforced concrete. *Journal of Materials in Civil Engineering*, 18(5):670–676, 2006.

[56] Cesare Signorini, Andrea Nobili, Antonella Sola, and Massimo Messori. Designing epoxy viscosity for optimal mechanical performance of coated Glass Textile Reinforced Mortar (GTRM) composites. *Construction and Building Materials*, 233:117325, February 2020.

[57] U. Dilthey, Markus Schleser, Martin Möller, and Oliver Weichold. Application of polymers in textile reinforced concrete From the interface to construction elements. In W. Brameshuber J. Hegger and N. Will, editors, *ICTRC'2006 - 1st International RILEM Conference on Textile Reinforced Concret*, pages 77–88. RILEM Publications SARL, 2006.

[58] J. Hegger and S. Voss. Investigations on the bearing behaviour and application potential of textile reinforced concrete. *Engineering Structures*, 30(7):2050–2056, July 2008.

[59] Eliyahu Adiel Sasi and Alva Peled. Three dimensional (3D) fabrics as reinforcements for cement-based composites. *Composites Part A: Applied Science and Manufacturing*, 74:153–165, July 2015.

[60] T. Büttner, A. Keil, and Michael Raupach. Improvement of the load- bearing capacity and durability of textile-reinforced concrete due to the use of polymers. *Proceedings of the 16th International Conference on Soil Mechanics and Geotechnical Engineering*, (6):1–11, 2008.

[61] S. P. Yin, S. L. Xu, and F. Wang. Investigation on the flexural behavior of concrete members reinforced with epoxy resin-impregnated textiles. *Materials and Structures*, 48(1-2):153–166, January 2015.

[62] Christina; Scheffler, S. L. Gao, R. Plonka, E. Mäder, S. Hempel, M. Butler, and V. Mechtcherine. Interphase modification of alkali-resistant glass fibres and carbon fibres for textile reinforced concrete II: Water adsorption and composite interphases. *Composites Science and Technology*, 69(7-8):905–912, 2009.

[63] Marcos Labronici and Hatsuo Ishida. Toughening composites by fiber coating: a review. *Composite Interfaces*, 2(3):199–234, 1994.

[64] K. Grundke, Edith Mäder, K. Grundke, H. J. Jacobasch, and G. Wachinger. Surface, interphase and composite property relations in fibre-reinforced composites. *Composites*, 25:739–744, 1994.

[65] J. L. Thomason. Glass fibre sizing: A review. *Composites Part A: Applied Science and Manufacturing*, 127(September), 2019.

[66] E. Wölfel, Christina; Scheffler, I. Curosu, and V. Mechtcherine. Single fibre pull-out tests of polypropylene and glass fibres in cement-based matrices at high loading rates. *ECCM 2018 - 18th European Conference on Composite Materials*, (June):24–28, 2020.

[67] Heike Hund and Rolf-Dieter Hund. *Textile Finishing and Finishing Technologies*, pages 427–477. Springer Berlin Heidelberg, Berlin, Heidelberg, 2016.

[68] Christiane Freudenberg. Textile fiber materials. In Chokri Cherif, editor, *Textile Materials for Lightweight Constructions: Technologies - Methods - Materials - Properties*, pages 37–101. Springer Berlin Heidelberg, Berlin, Heidelberg, 2016.

[69] Shang Lin Gao, Edith Mäder, Anwar Abdkader, and Peter Offermann. Sizings on alkali-resistant glass fibers: Environmental effects on mechanical properties. *Langmuir*, 19(6):2496–2506, 2003.

[70] P. Zinck, M. F. Pay, R. Rezakhanlou, and J. F. Gerard. Mechanical characterisation of glass fibres as an indirect analysis of the effect of surface treatment. *Journal of Materials Science*, 34(9):2121–2133, 1999.

[71] Shin-ichi; Igarashi and Kawamura Mitsunori. Effect of Sizing in Bundled Fibers on the Interfacial Zond Between the Fibers and the Cement Past Matrix. *Cement and Concrete research24*, 24(4):695–703, 1994.

[72] Christina; Scheffler, T. Förster, E. Mäder, G. Heinrich, S. Hempel, and V. Mechtcherine. Aging of alkali-resistant glass and basalt fibers in alkaline solutions: Evaluation of the failure stress by Weibull distribution function. *Journal of Non-Crystalline Solids*, 355(52-54):2588–2595, 2009.

[73] Till Quadflieg, Sebastian Leimbrink, Thomas Gries, and Oleg Stolyarov. Effect of coating type on the mechanical performance of warp-knitted fabrics and

cement-based composites. *Journal of Composite Materials*, 52(19):2563–2576, 2018.

[74] T. Büttner and M. Raupach. Polymer Impregnation of Textile Reinforced Concrete to Enhance Durability – Laboratory Testing and Long-Term Modelling. *Restoration of Buildings and Monuments*, 18(3-4):185–194, August 2012.

[75] Christina; Scheffler, S. L. Gao, R. Plonka, E. Mäder, S. Hempel, M. Butler, and V. Mechtcherine. Interphase modification of alkali-resistant glass fibres and carbon fibres for textile reinforced concrete I: Fibre properties and durability. *Composites Science and Technology*, 69(3-4):531–538, 2009.

[76] S. L. Gao, E. Mäder, and R. Plonka. Coatings for glass fibers in a cementitious matrix. *Acta Materialia*, 52(16):4745–4755, 2004.

[77] Christina Scheffler. *Zur Beurteilunf von AR-Glasfasern in Alkalischer Umgebung*. PhD thesis, Technischen Universität Dresden, 2009.

[78] Kai Schneider, Albert Michel, Marco Liebscher, Lucas Terreri, Simone Hempel, and Viktor Mechtcherine. Mineral-impregnated carbon fibre reinforcement for high temperature resistance of thin-walled concrete structures. *Cement and Concrete Composites*, 97:68 – 77, 2019.

[79] Z. Cohen and A. Peled. Effect of nanofillers and production methods to control the interfacial characteristics of glass bundles in textile fabric cement-based composites. *Composites Part A: Applied Science and Manufacturing*, 43(6):962–972, 2012.

[80] O. Homoro, M. Michel, and T. N. Baranger. Improvement of the mechanical properties of a glass multifilament yarn reinforced ettringitic matrix using an innovative pre-impregnation process. *European Journal of Environmental and Civil Engineering*, pages 1–16, March 2020.

[81] Cesare Signorini, Antonella Sola, Andrea Nobili, and Cristina Siligardi. Lime-cement textile reinforced mortar (TRM) with modified interphase. *Journal of Applied Biomaterials and Functional Materials*, 17(1), 2019.

[82] C. Signorini, A. Nobili, E. I. Cedillo González, and C. Siligardi. Silica coating for interphase bond enhancement of carbon and AR-glass Textile Reinforced Mortar (TRM). *Composites Part B: Engineering*, 141(July 2017):191–202, 2018.

[83] Oliver Weichold and Martin Möller. A cement-in-poly(vinyl alcohol) dispersion for improved fibre-matrix adhesion in continuous glass-fibre reinforced concrete. *Advanced Engineering Materials*, 9(8):712–715, 2007.

[84] Oliver Weichold. Advanced coatings to improve the durability in continuous glass-fibre reinforced concrete. *Key Engineering Materials*, 466:175–182, 2011.

[85] Meni Zamir, Raghu Sripada, and Alva Peled. Hybrid fillers in carbon-fabric-reinforced cement-based composites. *Cement and Concrete Composites*, 98(July 2018):113–124, 2019.

[86] S. L. Gao, E. Mäder, and R. Plonka. Nanostructured coatings of glass fibers: Improvement of alkali resistance and mechanical properties. *Acta Materialia*, 2007.

[87] S. Pavlidou and C. D. Papaspyrides. A review on polymer-layered silicate nanocomposites. *Progress in Polymer Science (Oxford)*, 33(12):1119–1198, 2008.

[88] Jyongsik Jang and Hojung Yang. The effect of surface treatment on the performance improvement of carbon fiber/polybenzoxazine composites. *Journal of Materials Science*, 35:2297–2303, 2000.

[89] Xinrui Zhang, Xianqiang Pei, Qian Jia, and Qihua Wang. Effects of carbon fiber surface treatment on the tribological properties of 2D woven carbon fabric/polyimide composites. *Applied Physics A*, 95(3):793–799, June 2009.

[90] Mohammad Andideh and Masoud Esfandeh. Statistical optimization of treatment conditions for the electrochemical oxidation of PAN-based carbon fiber by response surface methodology: Application to carbon fiber/epoxy composite. *Composites Science and Technology*, 134:132–143, October 2016.

[91] Panayiotis Kainourgios. Electrochemical surface functionalization of carbon fibers for chemical affinity improvement with epoxy resins. *Applied Surface Science*, page 12, 2017.

[92] Li Rongzhi, Li Ye, and Yiu-Wing Mai. Application of plasma technologies in fibre-reinforced polymer composites: A review of recent developments. Composite Part A:73–86, 1997.

[93] Xuli Fu, Weiming Lu, and D. D. L. Chung. Improving the bond strength between carbon fiber and cement by fiber surface treatment and polymer addition to cement mix. *Cement and Concrete Research*, 26(7):1007–1012, 1997.

[94] Luca Lavagna, Simone Musso, Giuseppe Ferro, and Matteo Pavese. Cement-based composites containing functionalized carbon fibers. *Cement and Concrete Composites*, 88:165–171, 2018.

[95] Kai Schneider, Matthias Lieboldt, Marco Liebscher, Maik Fröhlich, Simone Hempel, Marko Butler, Christof Schröfl, and Viktor Mechtcherine. Mineral-Based Coating of Plasma-Treated Carbon Fibre Rovings for Carbon Concrete Composites with Enhanced Mechanical Performance. *Materials*, 10(4):360, March 2017.

[96] Huanyu Li, Marco Liebscher, Albert Michel, Antje Quade, Rüdiger Foest, and Viktor Mechtcherine. Oxygen plasma modification of carbon fiber rovings for enhanced interaction toward mineral-based impregnation materials and concrete matrices. *Construction and Building Materials*, 273:121950, March 2021.

[97] Huanyu Li, Marco Liebscher, Majid Ranjbarian, Simone Hempel, Lazaros Tzounis, Christof Schröfl, and Viktor Mechtcherine. Electrochemical modification of carbon fiber yarns in cementitious pore solution for an enhanced interaction towards concrete matrices. *Applied Surface Science*, 487:52–58, September 2019.

[98] P. Purnell, A Bentur, M Raupach, Rainer Hempel, J Orlowsky, and Michael Schiekel. 6.3 Durability. In *Textile Reinforced Concrete - State-of-the-Art Report of RILEM TC 201-TRC*, pages 187–209. RILEM Publications SARL, 2006.

[99] Francesco Micelli and Maria Antonietta Aiello. Residual tensile strength of dry and impregnated reinforcement fibres after exposure to alkaline environments. *Composites Part B: Engineering*, 159:490–501, February 2019.

[100] Consiglio Superiore dei Lavori Pubblici-Servizio Tecnico Centrale. Linea Guida per la identificazione, la qualificazione ed il controllo di accettazione di compositi fibrorinforzati a matrice inorganica (FRCM) da utilizzarsi per il consolidamento strutturale di costruzioni esistenti. 2018.

[101] Viktor Mechtcherine. Towards a durability framework for structural elements and structures made of or strengthened with high-performance fibre-reinforced composites. *Construction and Building Materials*, 31:94–104, 2012.

[102] Karrar Al-Lami, Tommaso D'Antino, and Pierluigi Colombi. Durability of Fabric - Reinforced Cementitious Matrix (FRCM) Composites : A Review. *Applied Sciences*, pages 1–25, 2020.

[103] Natalie Williams Portal, Mathias Flansbjer, Pär Johannesson, Katarina Malaga, and Karin Lundgren. Tensile behaviour of textile reinforcement under accelerated ageing conditions. *Journal of Building Engineering*, 5(May 2016):57–66, 2016.

[104] M. De Munck, M. El Kadi, E. Tsangouri, J. Vervloet, S. Verbruggen, J. Wastiels, T. Tysmans, and O. Remy. Influence of environmental loading on the tensile and cracking behaviour of textile reinforced cementitious composites. *Construction and Building Materials*, 181:325–334, 2018.

[105] Marko Butler, Viktor Mechtcherine, and Simone Hempel. Durability of textile reinforced concrete made with AR glass fibre: Effect of the matrix composition. *Materials and Structures/Materiaux et Constructions*, 43(10):1351–1368, 2010.

[106] A. Nobili. Durability assessment of impregnated Glass Fabric Reinforced Cementitious Matrix (GFRCM) composites in the alkaline and saline environments. *Construction and Building Materials*, 105:465–471, 2016.

[107] K. De Weerdt, A. Colombo, L. Coppola, H. Justnes, and M. R. Geiker. Impact of the associated cation on chloride binding of Portland cement paste. *Cement and Concrete Research*, 68:196–202, 2015.

[108] Isabella Giorgia Colombo, Matteo Colombo, and Marco Di Prisco. Tensile behavior of textile reinforced concrete subjected to freezing-thawing cycles in un-cracked and cracked regimes. *Cement and Concrete Research*, 73:169–183, 2015.

[109] Jacopo Donnini. Durability of glass FRCM systems: Effects of different environments on mechanical properties. *Composites Part B: Engineering*, 174(April), 2019.

[110] Shiping Yin, Lei Jing, Mengti Yin, and Bo Wang. Mechanical properties of textile reinforced concrete under chloride wet-dry and freeze-thaw cycle environments. *Cement and Concrete Composites*, 96:118–127, February 2019.

[111] Elisa Franzoni, Cristina Gentilini, Mattia Santandrea, and Christian Carloni. Effects of rising damp and salt crystallization cycles in FRCM-masonry interfacial debonding: Towards an accelerated laboratory test method. *Construction and Building Materials*, 175:225–238, 2018.

[112] Mario Collepardi. *Il Nuovo Calcestruzzo*. Iv edition, 2006.

[113] M. D. A. Thomas and K. J. Folliard. Concrete aggregates and the durability of concrete. *Durability of Concrete and Cement Composites*, pages 247–281, 2007.

[114] J. Lanas, R. Sirera, and J. I. Alvarez. Study of the mechanical behavior of masonry repair lime-based mortars cured and exposed under different conditions. *Cement and Concrete Research*, 36(5):961–970, 2006.

[115] Thomas R. Dulki. Determination of Acid Concentration in Specialty Alloy Pickling Baths by Ion Chromatography. *Analytical Chemestry*, 51:1439–1443, 1979.

[116] R. W. Douglas and T. M. M. El-Shamy. Reactions of Glasses with Aqueous Solutions. *Journal of the American Ceramic Society*, 50(1):1–8, January 1967.

[117] Reinhard Conradt. Chemical Durability of Oxide Glasses in Aqueous Solutions: A Review. *Journal of the American Ceramic Society*, 91(3):728–735, March 2008.

[118] Marcela Fridrichová, Karel Dvořák, and Dominik Gazdič. Method for the Accelerated Testing of the Durability of a Construction Binder using the Arrhenius Approach. *Slovak Journal of Civil Engineering*, 24(1):24–33, 2017.

[119] B. A. Proctor, D. R. Oakley, and K. L. Litherland. Developments in the assessment and performance of grc over 10 years. *Composites*, 13(2):173–179, 1982.

[120] K. L. ; Litherland, D. R. ; Oakley, and B. A. Proctor. The Use of Accelerated Ageing Procedures to Predict the Long Term Strength of GRC Composites. *Cement and Concrete Research*, 11(c):455–466, 1981.

[121] P. Purnell and J. Beddows. Durability and simulated ageing of new matrix glass fibre reinforced concrete. *Cement and Concrete Composites*, 27(9-10):875–884, 2005.

[122] Francesca Ceroni, Antonio Bonati, Vittorio Galimberti, and Antonio Occhiuzzi. Effects of environmental conditioning on the bond behavior of FRP and FRCM systems applied to concrete elements. *Journal of Engineering Mechanics*, 144(1):1–15, 2018.

[123] G. L. Kalousek, L. C. Porter, and E. J. Benton. Concrete for long-term service in sulfate environment. *Cement and Concrete Research*, 2(1):79–89, 1972.

[124] Peter Bekker, Greg Borchelt, Norman Bright, Frieder Emrich, Mike Forde, Hector Gallegos, Caspar Groot, Ed Hedstrom, Steve Lawrence, Paul Maurenbrecher, Claudio Modena, Adrian Page, Felicita Pires, Dimitri Pumd, Czech Republic, John Roberts, Stephan Schmidt, Peter Schubert, Mike Schuller, J. Schwartz, Siegfried Sttckl, and Timber West. MS-A.1 Determination of the resistance of wallettes against sulphates and chlorides. *Materials and Structures*, 31(1):2–9, 1998.

[125] American Society For Testing and Materials-ASTM D1141. Standard Practice for the Preparation of Substitute Ocean Water. *ASTM International*, 98(Reapproved 2013):1–3, 2013.

[126] D7705. Alkali Resistance of Fiber Reinforced Polymer (FRP) Matrix Composite Bars used in Concrete Construction 1. *ASTM Standards*, i(Reapproved):1–5, 2012.

[127] Le Thi Mai Hoa. Characterization of multi-walled carbon nanotubes functionalized by a mixture of HNO3/H2SO4. *Diamond and Related Materials*, 89:43–51, October 2018.

[128] W. Ehrentraut, R. Plonka, E. Mäder, and S. Gao. Pilot equipment for continuous spinning of alkaline resistant glass fibers. *Technische Textilien*, 48(1), 2005.

[129] D. M. Wilson. Fiber Strength. *Encyclopedia of Materials: Science and Technology*, pages 3138–3142, 2001.

[130] ISO 10406-1:2015 - Fibre-reinforced polymer (FRP) reinforcement of concrete – Test methods – Part 1: FRP bars and grids.

[131] S. Zwaag. The concept of filament strength and weibull modulus. *Journal of Testing and Evaluation 17(5), 292-298. (1989)*, 17, 09 1989.

[132] Christina Scheffler, Serge Zhandarov, and Edith Mäder. Alkali resistant glass fiber reinforced concrete: Pull-out investigation of interphase behavior under quasi-static and high rate loading. *Cement and Concrete Composites*, 84:19–27, 2017.

[133] Serge Zhandarov, Edith Mäder, Christina Scheffler, Gerhard Kalinka, Claudia Poitzsch, and Stefan Fliescher. Investigation of interfacial strength parameters in polymer matrix composites: Compatibility and reproducibility. *Advanced Industrial and Engineering Polymer Research*, 1(1):82–92, 2018.

[134] E. Mäder, K. Grundke, H.-J. Jacobasch, and G. Wachinger. Surface, interphase and composite property relations in fibre-reinforced polymers. *Composites*, 25(7):739–744, January 1994.

[135] M. A. López-Manchado, B. Herrero, and M. Arroyo. Preparation and characterization of organoclay nanocomposites based on natural rubber. *Polymer International*, 52(7):1070–1077, 2003.

[136] Lucía Garijo, Xiaoxin Zhang, Gonzalo Ruiz, and José J Ortega. Age effect on the mechanical properties of natural hydraulic and aerial lime mortars. *Construction and Building Materials*, page 12, 2020.

[137] J. Lanas, J.L. Pérez Bernal, M.A. Bello, and J.I. Alvarez Galindo. Mechanical properties of natural hydraulic lime-based mortars. *Cement and Concrete Research*, 34(12):2191–2201, December 2004.

[138] James Beaudoin and Ivan Odler. Hydration, Setting and Hardening of Portland Cement. In *Lea's Chemistry of Cement and Concrete*, pages 157–250. Elsevier, 2019.

[139] B. Johannesson, K. Yamada, L. O. Nilsson, and Y. Hosokawa. Multi-species ionic diffusion in concrete with account to interaction between ions in the pore solution and the cement hydrates. *Materials and Structures/Materiaux et Constructions*, 40(7):651–665, 2007.

[140] Björn Johannesson. *Transport and sorption phenomena in concrete and other porous media*. PhD thesis, Division of Building Materials, 2000. Defence details Date: 2000-11-10 Time: 10:15 Place: John Ericssons väg 1, V:A External reviewer(s) Name: Jonasson, Jan-Erik Title: Docent Affiliation: Division of Structural Engineering, LTU —.

[141] Jacopo Donnini and Valeria Corinaldesi. Mechanical characterization of different FRCM systems for structural reinforcement. *Construction and Building Materials*, 145:565–575, August 2017.

[142] Mengyuan Lu, Huigang Xiao, Min Liu, Xiaojiao Li, Hui Li, and Li Sun. Improved interfacial strength of SiO2 coated carbon fiber in cement matrix. *Cement and Concrete Composites*, 91(January):21–28, 2018.

[143] Arnon; Bentur. Role of Interfaces in Controlling Durability of Fiber-Reinforced Cements. *Journal of Materials in Civil Engineering*, 12:2–7, 2000.

[144] Amnon Katz and Arnon Bentur. Effect of matrix composition on the aging of CFRC. *Cement and Concrete Composites*, 17(2):87–97, January 1995.

[145] Amnon Katz and Arnon Bentur. Mechanisms and Processes Leading to Changes in Time in the Properties of CFRC. 3:1–13, 1996.

[146] Yuki Nakanishi, Yosuke Hara, Wataru Sakuma, Tsuguyuki Saito, Kazuki Nakanishi, and Kazuyoshi Kanamori. Colorless transparent Melamine–Formaldehyde aerogels for thermal insulation. *ACS Applied Nano Materials*, 3(1):49–54, 2020.

[147] Qinying Li, Jun-jun Liu, Xiao Sun, and Li Xu. Hierarchically Porous Melamine-Formaldehyde Resin Microspheres for the Removal of Nanoparticles and Simultaneously As the Nanoparticle Immobilized Carrier for Catalysis. *ACS Sustainable Chemistry & Engineering*, 7(1):867–876, January 2019.

[148] Yuhong Song, Ruiyang Ma, Caina Jiao, Lin Hao, Chun Wang, Qiuhua Wu, and Zhi Wang. Magnetic mesoporous polymelamine-formaldehyde resin as an adsorbent for endocrine disrupting chemicals. *Microchimica Acta*, 185(1):19, January 2018.

[149] Robert Saxon and Firmin C. Lestienne. Curing relations of hexakis(methoxymethyl)melamine and its combinations with acrylic polymers. *Journal of Applied Polymer Science*, 8(1):475–488, January 1964.

[150] Richard C Wilson and William F Pfohl. Study of cross-linking reactions of melaminerformaldehyde resin with hydroxyl functional polyester by generalized 2-D infrared spectroscopy q. page 10, 2000.

[151] Marco Zanetti, Pierangiola Bracco, and Luigi Costa. Thermal degradation behaviour of PE/clay nanocomposites. *Polymer Degradation and Stability*, 85(1):657–665, 2004.

[152] Yoshiaki Fukushima. X-Ray Diffraction Study of Aqueous Montmorillonite Emulsions. *Clays and Clay Minerals*, 32(4):320–326, 1984.

[153] Abhijit Chatterjee, Fujio Mizukami, and Akira Miyamoto. Effect of exchangeable cation and hydration layer on the swelling property of 2:1 dioctahedral smectite clay - A periodic density functional study. *Studies in Surface Science and Catalysis*, 156:335–342, 2005.

[154] Mohammad Asgari. Silane functionalization of sodium montmorillonite nanoclay The effect of dispersing media on intercalation and chemical grafting. *Applied Clay Science*, page 11, 2018.

[155] P. Zinck, E. Mäder, and J. F. Gerard. Role of silane coupling agent and polymeric film former for tailoring glass fiber sizings from tensile strength measurements. *Journal of Materials Science*, 36(21):5245–5252, 2001.